Palaeontologia Electronica
palaeo-electronica.org

A new member of a large and archaic balaenid from the Late Miocene of Sapporo, Hokkaido, Japan partly fills a gap of right whale evolution

Yoshihiro Tanaka, Toshiyuki Kimura, Tatsuya Shinmura, Hiroto Ohira, and Hitoshi Furusawa

ABSTRACT

The family Balaenidae (right whales) includes two genera and four extant species, all of which are endangered and giant animals measuring approximately 17 to 20 m in length. The history of the Balaenidae spans about 20 million years. Several small sized extinct balaenids from the Pliocene have been identified. However, half of this history remains unknown owing to a 9-million-year gap from 15.2 to 6.1 m.y.a. in the fossil record. A well-preserved fossil balaenid skeleton, designated SMAC 2731, from the Late Miocene approximately 9 m.y.a. in Sapporo, Hokkaido, Japan, is named as *Megabalaena sapporoensis* gen. et sp. nov. This specimen preserves the skull, periotics in situ, tympanic bullae, right mandible, basihyal-thyrohyal, right stylohyal, sternum, seven cervical vertebrae, nine thoracic vertebrae, and 16 more posterior vertebrae, rib fragments, scapulae, and left forelimb elements. All preserved vertebral epiphyses are fused, indicating that SMAC 2731 was physically mature. Notably, *M. sapporoensis* can be distinguished from other balaenids by its excavated orbit in dorsal view with a large postorbital process, dorsoventrally high anterior part of the involucrum of the tympanic bulla, long compound posterior process, high coronoid process and deeper subcondylar furrow of the mandible, incipient cervical fusion (C2+C3 only), and its slender forelimb bones, including the humerus, radius and ulna. Based on a bizygomatic width of 2.2 m, the estimated total length of the holotype of *M. sapporoensis* is 12.7 m. Overall, *M. sapporoensis* indicates that balaenids diversified prior to the Late Miocene.

Yoshihiro Tanaka. Sapporo Museum Activity Center, 5-15-1-6, Hiragishi, Toyohira-ku, Sapporo, Hokkaido 062-0935 Japan; Division of Academic Resources and Specimens, Hokkaido University Museum, Kita 10, Nishi 8, Kita-ku, Sapporo, Hokkaido, 060-0810 Japan; and Numata Fossil Museumm 6-493 Nishi Machi, Numata Town, Hokkaido 078-2204, Japan (corresponding author). yoshi.tanaka.research@gmail.com
Toshiyuki Kimura. Gunma Museum of Natural History, 1674-1 Kamikuroiwa, Tomioka, Gunma, 370-2345

https://zoobank.org/EA2A31AC-7125-4F3A-9E47-66418F5CDDDD

Final citation: Tanaka, Yoshihiro, Kimura, Toshiyuki, Shinmura, Tatsuya, Ohira, Hiroto, and Furusawa, Hitoshi. 2025. A new member of a large and archaic balaenid from the Late Miocene of Sapporo, Hokkaido, Japan partly fills a gap of right whale evolution. Palaeontologia Electronica, 28(2):a37.
https://doi.org/10.26879/1549
palaeo-electronica.org/content/2025/5581-archaic-balaenid-from-japan

Japan. kimura@gmnh.pref.gunma.jp
Tatsuya Shinmura. Division of Academic Resources and Specimens, Hokkaido University Museum Kita 10, Nishi 8, Kita-ku, Sapporo, Hokkaido, 060-0810 Japan and Ashoro Museum of Paleontology, 29-25, Konan 1, Ashoro Hokkaido 089-3727, Japan. shinmura@ashoromuseum.com
Hiroto Ohira. Shimane University, Matsue, Shimane 690-8504, Japan. ohira@riko.shimane-u.ac.jp
Hitoshi Furusawa. Sapporo Museum Activity Center, 5-15-1-6, Hiragishi, Toyohira-ku, Sapporo, Hokkaido 062-0935 Japan

Keywords: Balaenidae; new genus; new species; Tortonian; gigantism; Japan

Submission: 7 March 2025. Acceptance: 12 July 2025.

INTRODUCTION

The family Balaenidae (right whales) includes two genera and four extant species (Committee on Taxonomy, 2022), which are endangered and large animals measuring about 17-20 m in length (Jefferson et al., 2008). Modern right whales have robust bodies and swim slowly and efficiently perform skim feeding (Woodward et al., 2006).

The history of the Balaenidae spans approximately 20 million years. The oldest known record of this family is *Morenocetus parvus* from Patagonia, Argentina (Cabrera, 1926; Buono et al., 2017) dating to the Early Miocene (19.8–18.2 m.y.a. [Ma]) (Marx and Fordyce, 2015). Another primitive named balaenid *Peripolocetus vexillifer* (16.0–15.2 Ma) from California has need for a modern redescription and reinterpretation (Kellogg, 1931; Marx and Fordyce, 2015). Another named balaenid *Eubalaena shinshuensis* (6.1–5.9 Ma) is known from Japan (Kimura et al., 2007). There is a about 9 million years gap of balaenid fossils, which can be identified into species level between the two records 15.2 to 6.1 Ma as above. Marx and Lambert (2021) call it as “the Miocene gap” of balaenids.

Previously, the diversity of the Balaenidae was thought to be low during the Miocene (Buono et al., 2017) and to have suddenly increased during the Early Pliocene (Kimura, 2009). Early members of balaenids from the Early to Middle Miocene are known to have been small, around 4–6 m in length (Bisconti et al., 2003, 2005, 2021). In a previous study, Bisconti et al. (2021) estimated body lengths of extinct balaenids and proposed a hypothesis regarding the evolution of body size: (1) the origin of gigantic body size in the genus *Eubalaena* including *E. shinshuensis*, occurred as early as the latest Miocene, likely coinciding with pulses of nutrients sustaining large zooplankton populations; (2) a reduction in total body length occurred in some linages independently during the Pliocene; (3) the origin of gigantic body size in *Balaena mysticetus* is likely related to the invasion of the Arctic Ocean in the last 3 million years.

In summary, the history of the Balaenidae has a major gap in the Miocene, spanning about 9 million years between 15.2–6.1 Ma (Marx and Lambert, 2021). Specifically, only a few specimens are known from the Miocene specimens are known. The question remains, what occurred during this long unknown interval? A well-preserved fossil balaenid skeleton discovered from the Late Miocene (approximately 9 Ma evaluated by fission track analysis of zircon crystals, Table 1) in Sapporo, Hokkaido, Japan (Figures 1 and 2), has a body length as 12.7 m, including the skull, and a mandible is reported here for the first time. This skeleton has an estimated body length of 12.7 m. and preserves the skull, mandible, and postcranial

TABLE 1. Fission-track dating result. Dating was carried out by the external detector method and internal crystal surface was used. Ages were calculated using dosimeter glass NIST-SRM612 and samples were irradiated at pneumatic tube of graphite facility (Tc-pn) of Kyoto University Reactor (KUR). Zeta value 367.1±4.1 (Ohira, 2004) was used. ρ=track density; N=total number of tracks counted; s for spontaneous, i for induced and d for dosimeter; P(χ^2)=probability of obtaining χ^2 value for v degrees of freedom (where v=number of crystals-1) (Galbraith 1981); r=correlation coefficient between ρ_s and ρ_i; U=average uranium content.

Sample Name	No. Crys.	ρs (Ns) (×10^6/cm^2)	ρi (Ni) (×10^6/cm^2)	P(χ^2) %	ρd (Nd) (×10^5/cm^2)	r	U ppm	Age (Ma) (±1σ)
KG2018	34	1.1791(836)	5.1396(3644)	23.7	2.1417(7173)	0.85	328	9.0±0.4

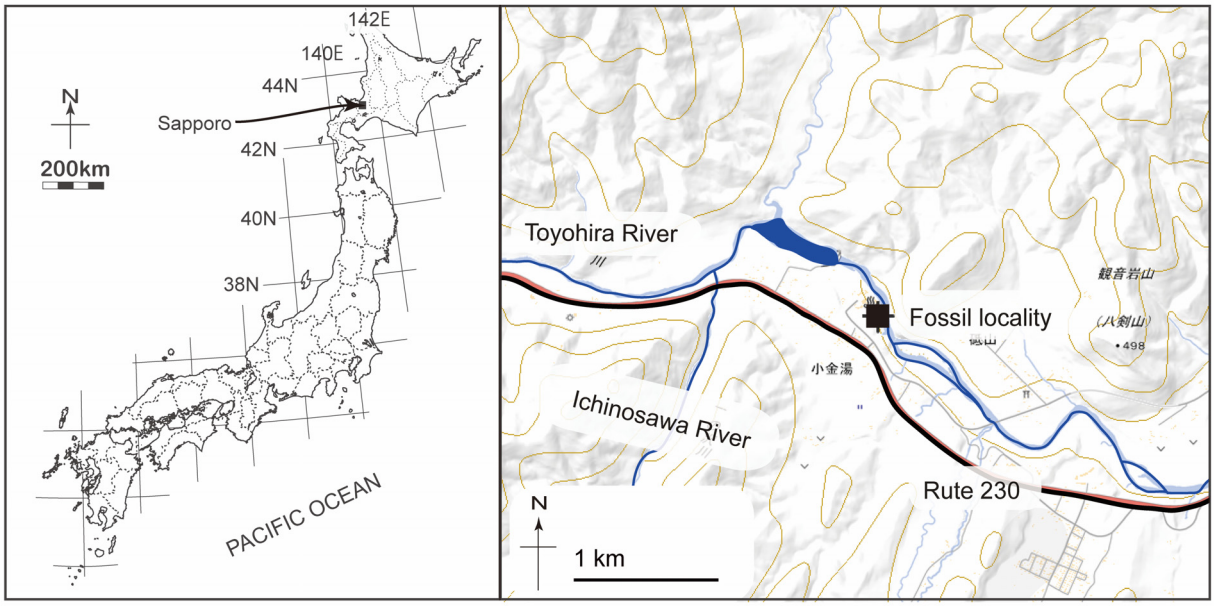

FIGURE 1. Maps showing the fossil locality (black square) of SMAC 2731, *Megabalaena sapporoensis.* The base maps (left and right) are modified from Tanaka and Kohno (2015) and the topographic map published by the Geospatial Information Authority of Japan respectively.

elements, and partly fills the gap in right whale evolution. This is a large balaenid, which is approximately a size three times larger than those of early balaenids. Regarding body size diversity, this new fossil enhances our understanding of balaenid diversity, which appears to have expanded earlier than the Late Miocene.

MATERIALS AND METHODS

Morphological terminology follows Mead and Fordyce (2009) mainly, Flower (1885) for postcranial skeleton, and Tanaka (2024) for the basihyalthyrohyal. Because of the difficulty in examining heavy fossils, we used a 3D scanner (Artec Spider/Eva, Artec Group, Luxembourg) to generate 3D models. Such models were used for producing figures and life restoration.

The phylogenetic position of *Megabalaena sapporoensis* gen. et sp. nov. (SMAC 2731) was analyzed using the matrix of Tanaka et al (2020), which was derived from the matrix of Buono et al. (2017). This study added codings of *M. sapporoensis* and recently established balaenids *Antwerpibalaena liberatlas* and *Charadrobalaena valentinae* (Duboys de Lavigerie et al., 2020; Bisconti et al., 2023). In the phylogenetic analysis, character 226 on cervical vertebrae was added a state, and was changed several codings (Appendix 4). The matrix contains 257 morphological characters and 46 taxa (Appendices 1–9). The percentage of coded characters for *M. sapporoensis* is 56% (including soft tissue characters) and 59% (excluding soft tissue).

The matrix was managed using the software MESQUITE 3.81 (Maddison and Maddison, 2021). Analysis was performed using TNT v. 1.5 (Goloboff and Catalano, 2016). All the characters were treated as unordered, equal, and implied weights (K=1 and 3) with backbone constraint of extant taxa, based on the topology of the molecular tree by McGowen et al. (2009). The analysis used New Technology Search with recover minimum length trees equal to 1000 times. The random seed value was 1. The resulting most parsimonious trees were summarized using strict and 50% majority consensus trees.

Institutional Abbreviations

CAS, California Academy of Sciences, San Francisco, USA. FCCP, Fukagawa City Cultural Properties, Hokkaido, Japan. IRSNB, Institut Royal des Sciences Naturelles de Belgique, Brussels, Belgium. KMNH, Kitakyushu Museum of Natural History, Fukuoka, Japan. MCMV, Museo Civico, Montopoli Valdarno (Pisa), Italy. MCRE, Musei Civici di Reggio Emilia, Reggio Emilia, Italy. MLP, Museo de La Plata, La Plata, Argentina. MNHNP, Museum National d'Histoire Naturelle, Centre National d'Etude des Mammiferes Marins, Paris, France. MSNTUP, Museo di Storia Naturale e del

FIGURE 2. Photos taken during digging up SMAC 2731, *Megabalaena sapporoensis.* A photo taken at a very beginning of excavation in 2008 showing several associated vertebrae (A). A green field note is 16.5 cm long and 9.5 cm wide. A photo taken in 2009 showing the locality of SMAC 2731, *Megabalaena sapporoensis*, just beside Toyohira River (B).

Territorio, Università di Pisa, Pisa, Italy. MTUF, Museum of Marine Science, Tokyo University of Marine Science and Technology, Tokyo, Japan. NMB, Natuurmuseum Brabant, Tilburg, The Netherlands. NMNS, National Museum of Nature and Science, Tsukuba, Japan. NMNZ, Museum of New Zealand Te Papa Tongarewa, Wellington, New Zealand. SDSNH, San Diego Natural History Museum, San Diego, California, USA. SFM, Shinshushinmachi Fossil Museum, Shinshushinmachi, Japan. SMAC, Sapporo Museum Activity Center, Hokkaido, Japan. USNM, National Museum of Natural History, Smithsonian Institution, Washington D.C., USA. ZMUC, Zoological Museum of the University of Copenhagen, Denmark.

SYSTEMATIC PALEONTOLOGY

CETACEA Brisson, 1762
NEOCETI Fordyce and de Muizon, 2001
MYSTICETI Gray, 1864
CHAEOMYSTICETI Mitchell, 1989
BALAENIDAE Gray, 1825
Megabalaena gen. nov

zoobank.org/E011831E-D47F-4A06-938A-E27A8D5330A9

Type species. *Megabalaena sapporoensis* sp. nov.

Etymology. The generic name, *Megabalaena*, is named derived from ancient Greek megas meaning great, large and mighty, and the type genus name of the family Balaenidae.

Diagnosis. As for the holotype and only species.

TABLE 2. Measurements in mm of *Megabalaena sapporoensis* (SMAC 2731) skull and mandible following Buono et al. (2017), and Tanaka and Taruno (2019). For skull and mandible, distances are either horizontal or vertical, unless identified as point to point. + shows an incomplete measurement, because of erosion.

Skull	
Bizygomatic width	2232
Width of the skull at the level of the exoccipitals	1350
Supraoccipital width anterior to foramen magnum	900
Transverse diameter of left occipital condyle	130
Dorsoventral diameter of left occipital condyle	150+
Transverse diameter of foramen magnum	100
Distance between lateral border of left occipital condyle and lateral border of left exoccipital	550
Width of the occipital condyles and foramen magnum	310
Anteroposterior diameter of the supraorbital process of the frontal of the distal edge	290
Transverse diameter of the supraorbital process of the frontal	870+
Width of the optic canal in its medial portion	20
Width of the optic canal in its lateral portion	220
Length of the optic canal	680+
Orbit length (between preorbital and postorbital process)	200
Mandible	
Height of mandible, from coronoid process to ventral margin	350
Maximum preserved width of mandible	290+
Height of body just anterior to coronoid process	320

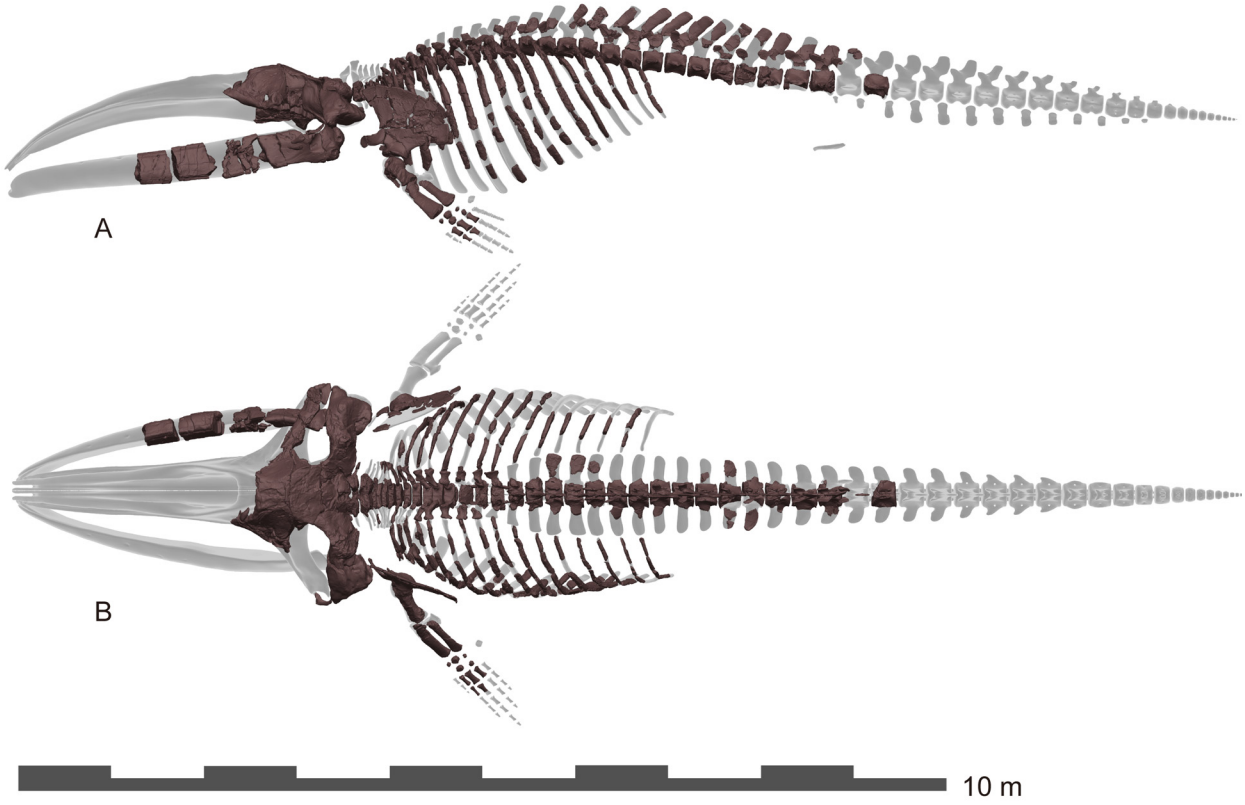

FIGURE 3. Images based on a 3D model showing preserved elements in brown of SMAC 2731, *Megabalaena sapporoensis* in dorsal view (A) and left lateral view (B). Missing parts were created by T. Shinmura refer to extant balaenids NMNS-M55028 and MTUF-M061A both *Eubalaena japonica*. The vertebrae posterior to the ninth thoracic vertebra are difficult to identify because of their limited preservation. Ribs separated into over 100 fragments. These elements' original positions are uncertain and roughly estimated based on their morphologies and the extant species *Eubalaena glacialis*.

Megabalaena sapporoensis sp. nov.
(Figures 3 to 22, Tables 2 to 5)

zoobank.org/BB19FDAE-EEA2-44A2-86DD-EC9530CF30FA

Holotype. SMAC 2731, the skull consists of the posterior half, missing all but the base of the rostrum, including the posterior ends of the maxillae, premaxillae, nasals, frontals, jugals, palatines, vomer, parietals, pterygoids, squamosals, exoccipitals, supraoccipital, exoccipitals, basioccipital, basisphenoid, periotics in situ, tympanic bullae, right posterior mandible, basihyal-thyrohyal, right stylohyal, sternum, seven cervical vertebrae including a fused axis and third cervical vertebra, nine thoracic vertebrae, and 16 more posterior vertebrae, rib fragments, scapulae, and left forelimb elements including humerus, ulna, radius, five carpals, three metacarpals, and two phalanges.

Locality and horizon. SMAC 2731 was found at a riverbed of Toyohira River in Sapporo City, Hokkaido, Japan, by Kazuhisa Mori on 10 October 2008: Latitude 42°58'1.24"N, longitude 141°13'18.01"E (Figures 1 and 2). SMAC 2731 was found from the upper part of the Toyama Formation. At the fossil area, the diatomaceous siltstone Toyama Formation is distributed. Diatomaceous siltstone of the Toyama Formation is exposed at the type locality (Ozaki and Komatsubara, 2014). A 5–6 cm thick layer of tuff is deposited approximately 1 m below the type stratum of SMAC 2731. The geochronologic age of the tuff was evaluated by fission track analysis of zircon crystals. Euhedral zircon crystals were successfully extracted by magnetic and heavy liquid separation and subsequent experimental procedures followed Ohira (2004). Fission track analysis resulted in a date of 9.0 ± 0.4 Ma (Table 1). The chi-square test (P(χ2): 23.3%) passed 5% significance level, which assures the general absence of extra-Poissonian errors in the analysis, suggesting an identical

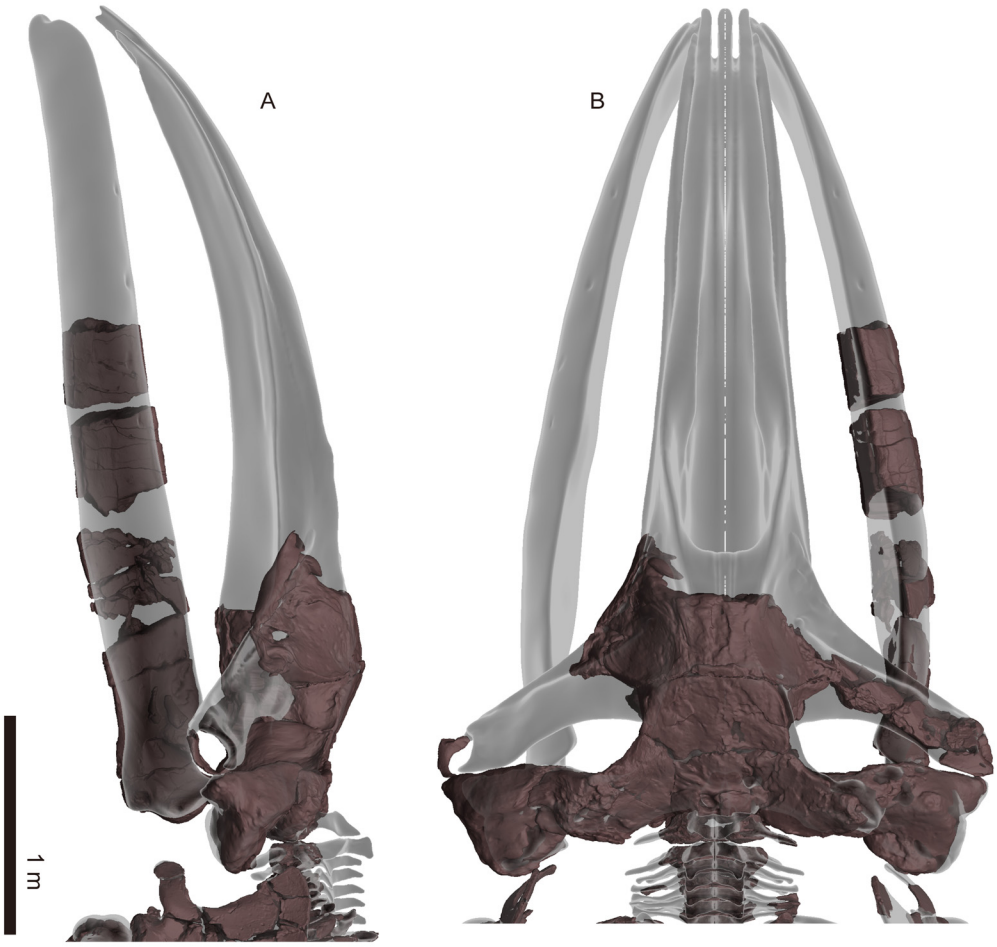

FIGURE 4. Images based on a 3D model showing skull elements of SMAC 2731, *Megabalaena sapporoensis* in left lateral view (A) and dorsal view (B). Deformations are restored using 3D model editor by T. Shinmura. Settings are the same to Figure 3.

grain-age population in the sample. Thus, the age of SMAC 2731 is approximately 8.6–9.4 Ma (Tortonian, early Late Miocene). About 200 m downstream from the locality of SMAC 2731, four ribs and the sternum of a sirenian *Hydrodamalis* sp. was discovered from the Toyama Formation too, and diatom zone and fission track analysis indicated an age of about 8 Ma (Furusawa 2007). The Toyama Formation provides molluskan fossils *Lucinoma* and *Conchocele*, which live at bathyal to deep cold waters (Suzuki, 2007).

Etymology. Named after the fossil locality, Sapporo City.

Diagnosis. *Megabalaena sapporoensis* is a member of the Balaenidae because it has a combination of these character states such as a posteriorly pointed anterior edge of the supraorbital process lateral to the ascending process of the maxilla with the skull in dorsal view (Character 31, state 0), laterally oriented postorbital process in dorsal view (Character 38, state 1), confluent posterior border of the zygomatic process of the squamosal and exoccipital in dorsal view (Character 67, state 1), dorsoventrally higher than long parietal in lateral view (Character 76, state 1), anterolaterally directed zygomatic process of the squamosal in dorsal view (Character 86, state 2), distinctly higher than long squamosal including the zygomatic and postglenoid processes (Character 92, state 1), short squamosal fossa (Character 96, state 1), foramen pseudovale opening posteriorly between the squamosal and pterygoid (Character 118, state 1), and posteriorly diverging basioccipital crests in ventral view (Character 125, state 0).

Among the Balaenidae, *Megabalaena sapporoensis* uniquely has an excavated orbit in dorsal view with a large postorbital process, dorsoventrally high anterior part of the involucrum of the

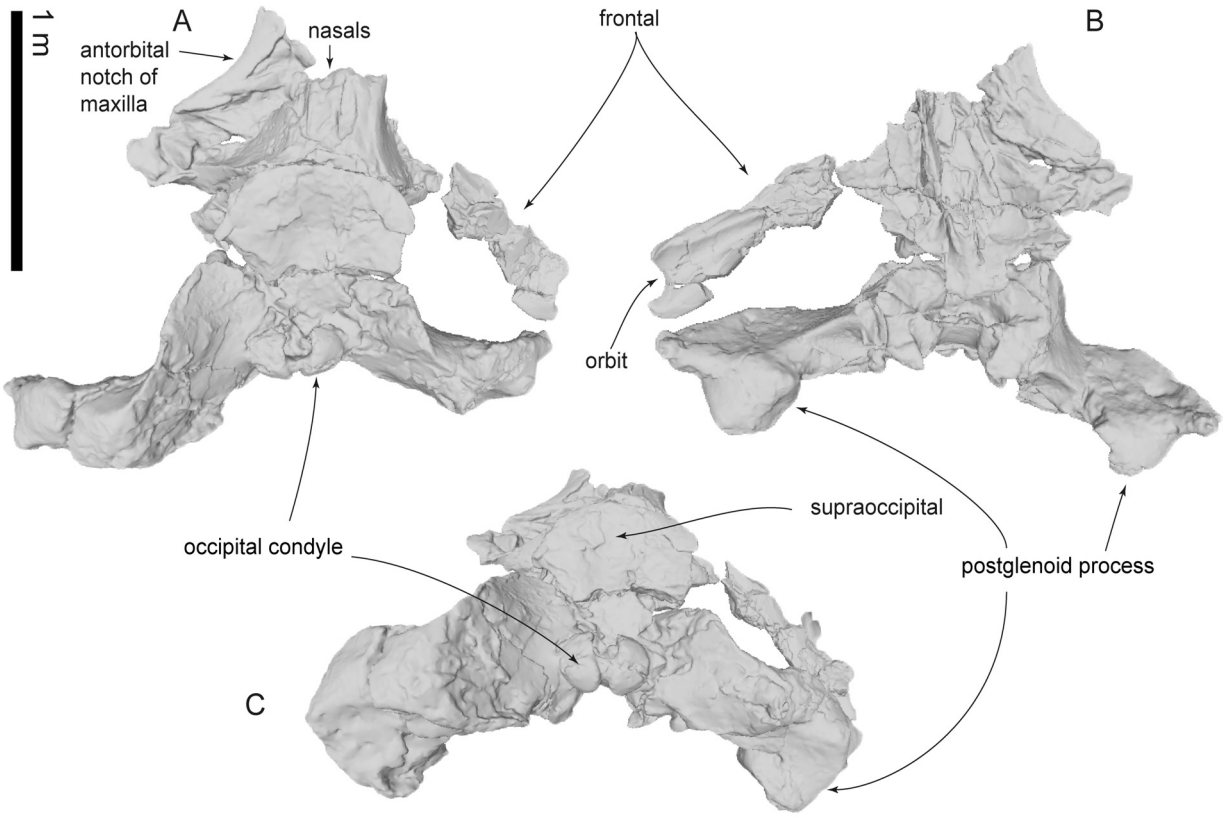

FIGURE 5. Images based on a 3D model showing preserved skull elements of SMAC 2731, *Megabalaena sapporoensis* in dorsal view (A), ventral view (B), and posterior view (C). Deformations are not restored.

tympanic bulla, long compound posterior process, high coronoid process and deeper subcondylar furrow of the mandible. *M. sapporoensis* uniquely has an autapomorphic combination of characters among the Balaenidae: a posterolaterally projected lateral process of the maxilla at the base of the rostrum (Character 15, state 0), overlapped jugal with the zygomatic process of the squamosal (Character 44, state 0), an anteroposteriorly compressed exposure of the frontal on the skull vertex (Character 73, state 1), more posteriorly located posterior apex of nuchal crest than the occipital condyle (Character 80, state 0), a confluent medial border of postglenoid process in ventral view with more medial portion of squamosal (Character 111, state 0), an anteroposteriorly flattened compound posterior process (Character 171, state 2), indistinct medial lobe of the tympanic bulla (Character 187, state 1), lack of the transverse crease on the dorsal surface of the involucrum of the tympanic bulla (Character 191, state 0), a subcondylar furrow extended across the posterior surface of the mandibular condyle, separating it from the angular process both medially and laterally (Character 212, state 3). *M. sapporoensis* also uniquely has unfused cervical vertebrae except the axis and third cervical vertebra (Character 226, state 1), and slender forelimb long bones including the humerus with a low and proximodistally short deltoid ridge, radius, and ulna (see discussion).

Compared to modern balaenids *(Balaena mysticetus, Eubalaena australis, E. glacialis,* and *E. japonica)* and some fossil species *(Peripolocetus vexillifer, Balaenella brachyrhynus, Balaenula astensis,* and *Antwerpibalaena liberatlas), M. sapporoensis* can be differentiated by having a ventrally oriented lateral furrow of the tympanic bulla in lateral view (Character 178, state 0). Compared to more earlier branching balaenids *(Morenocetus parvus* and *P. vexillifer)* and some other fossil species *(B. brachyrhynus* and *B. astensis), M. sapporoensis* can be differentiated by having a poorly exposed compound posterior process of the tympanoperiotic on lateral skull wall (Character 172, state 0). Compared to *Eubalaena shinshuensis* from Nagano, Japan, *M. sapporoensis* has a low anterolateral part of the nuchal crest. *E. shinshuensis* has a strong and laterally projected anterior part

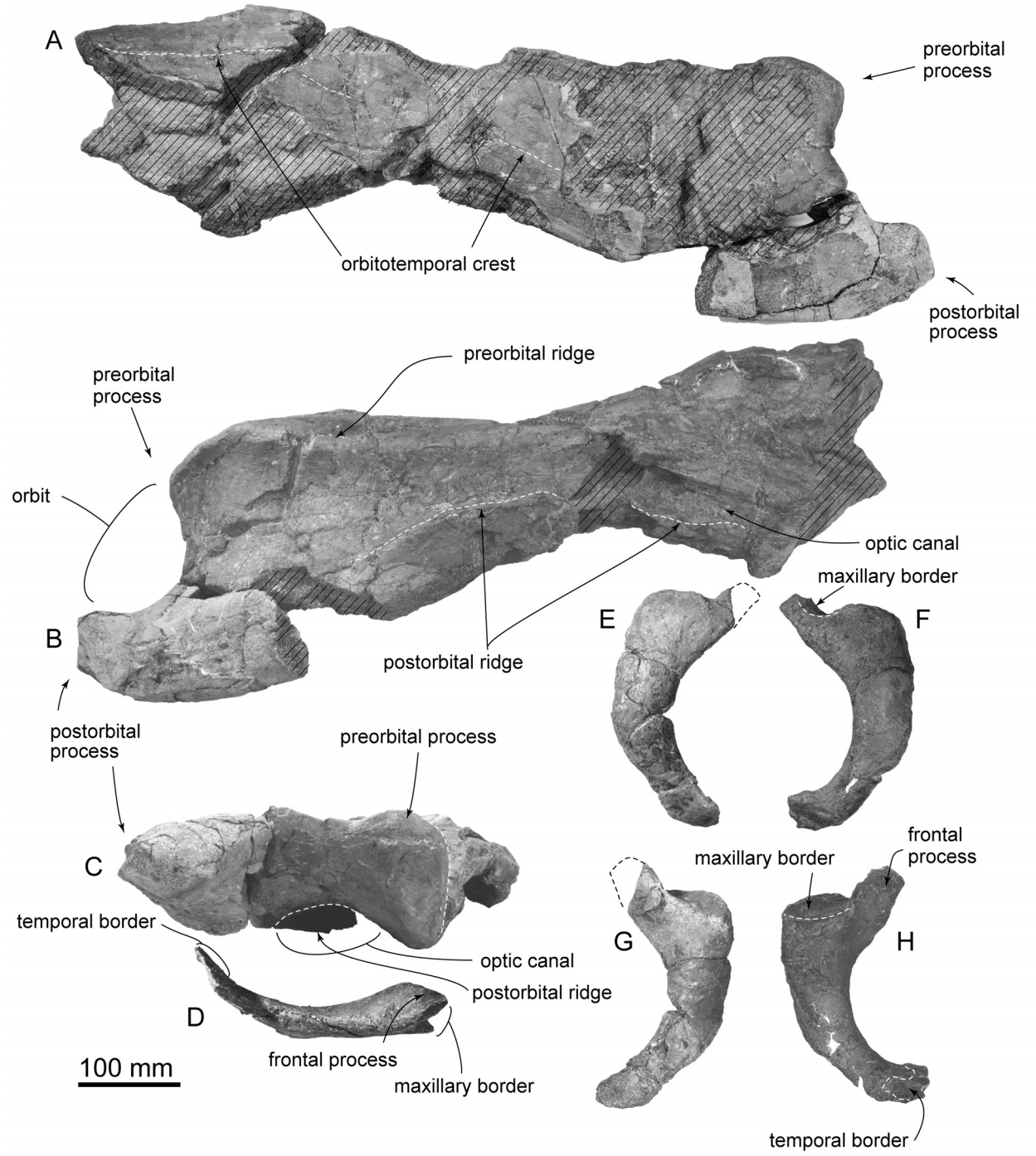

FIGURE 6. Frontal and jugals of SMAC 2731, *Megabalaena sapporoensis.* Right frontal in dorsal view (A, ventral view (B), and lateral view (C). Left jugal in lateral view (D). Right (E) and left jugals (F) in ventral view. Right (G) and left jugals (H) in dorsal view.

of the nuchal crest. Compared to *Archaeobalaena dosanko* from Hokkaido Japan, and some other balaenids *(Morenocetus parvus, Eubalaena ianitrix,* and *B. astensis), M. sapporoensis* can be differentiated by having the supramastoid crest of zygomatic process of the squamosal. Compared to fossil balaenids *(M. parvus, B. brachyrhynus, Eubalaena ianitrix, A. dosanko,* and *B. astensis), M. sapporoensis* can be differentiated by having strongly laterally projected pre- and postorbital pro-

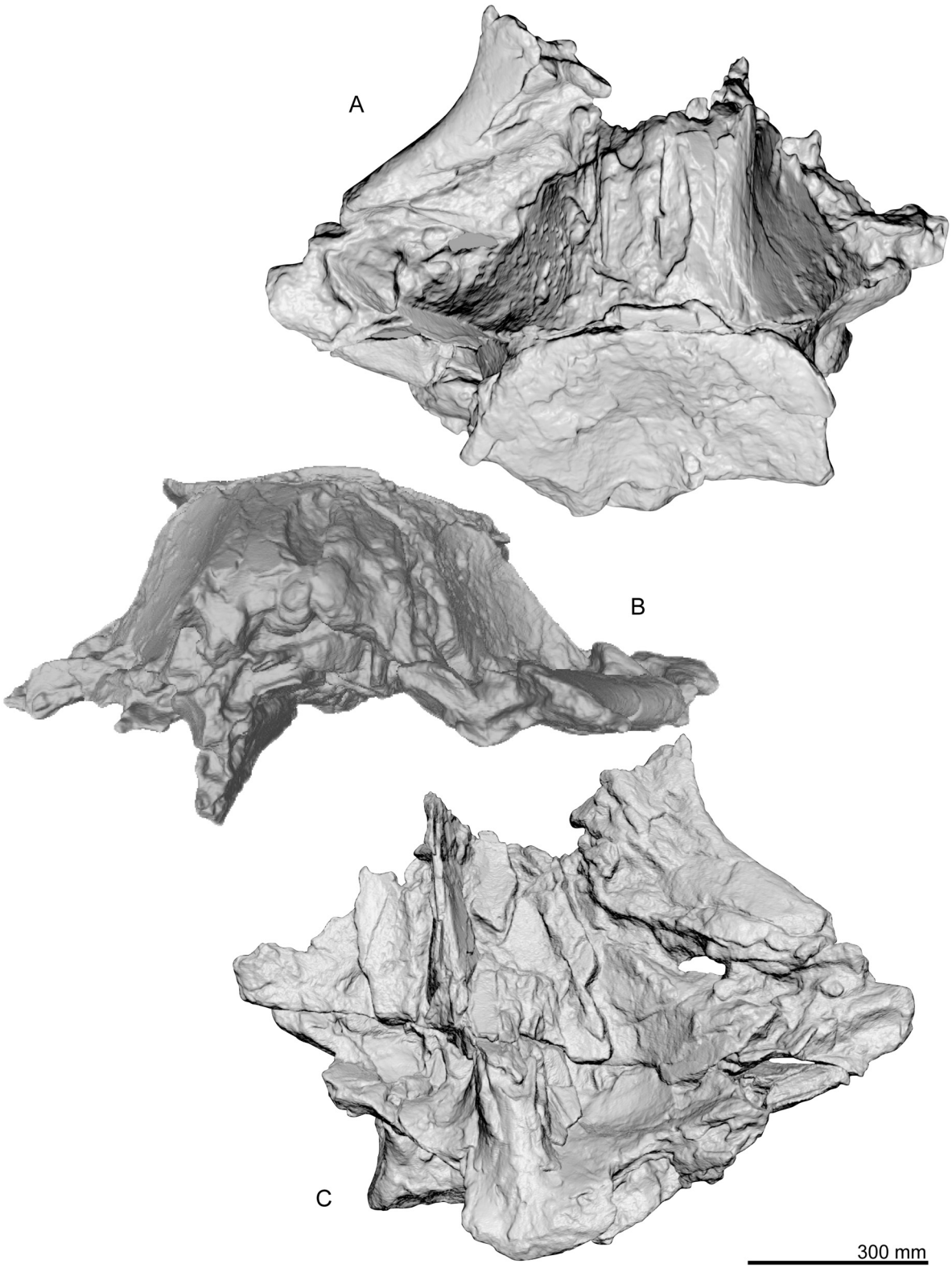

FIGURE 7. Vertex area of skull, SMAC 2731, *Megabalaena sapporoensis* in dorsal view (A), anterior view (B), and ventral view (C). These images are based on a 3D model.

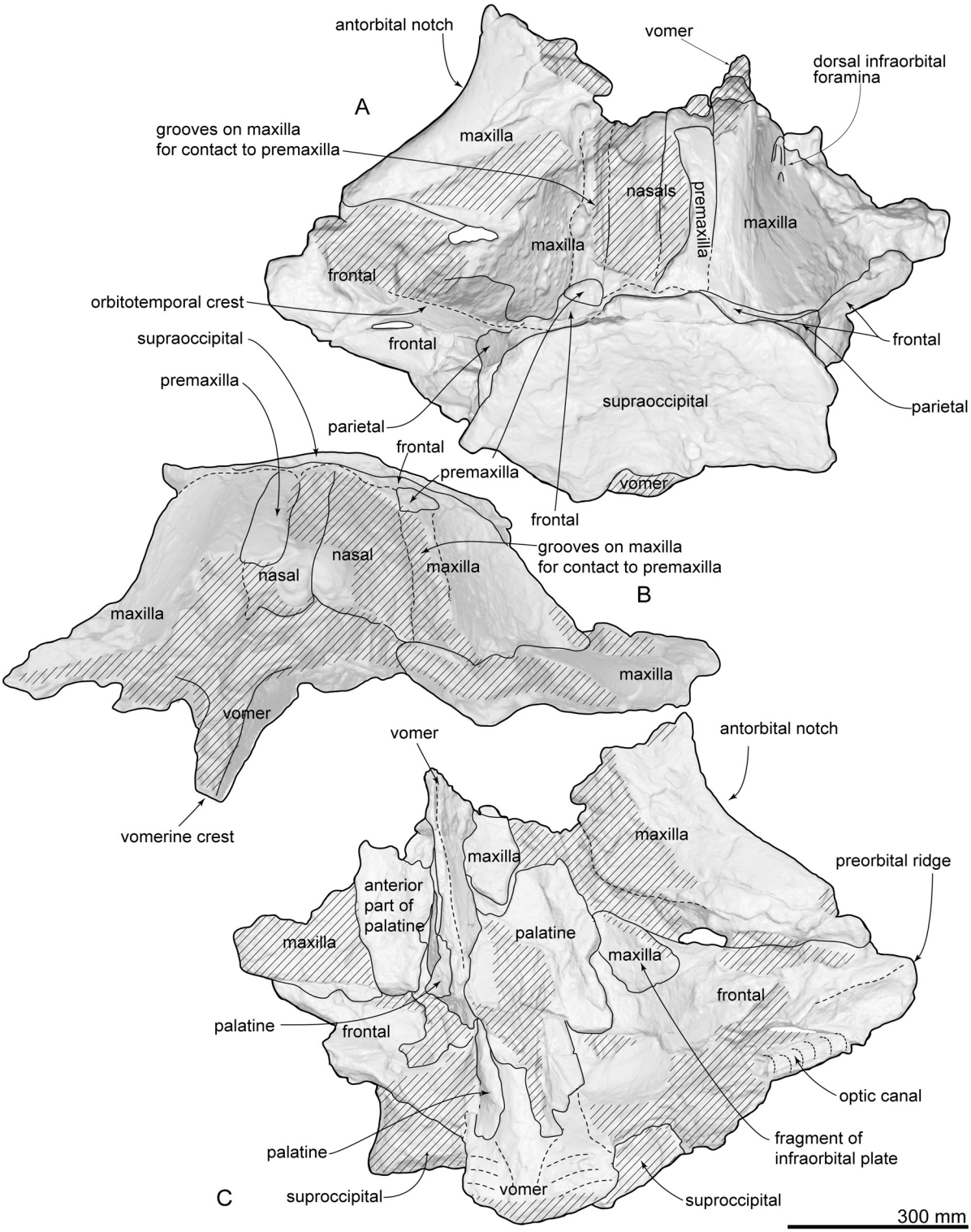

FIGURE 8. Key features on vertex area of skull, SMAC 2731, *Megabalaena sapporoensis* in dorsal view (A), anterior view (B), and ventral view (C). These images are based on a 3D model.

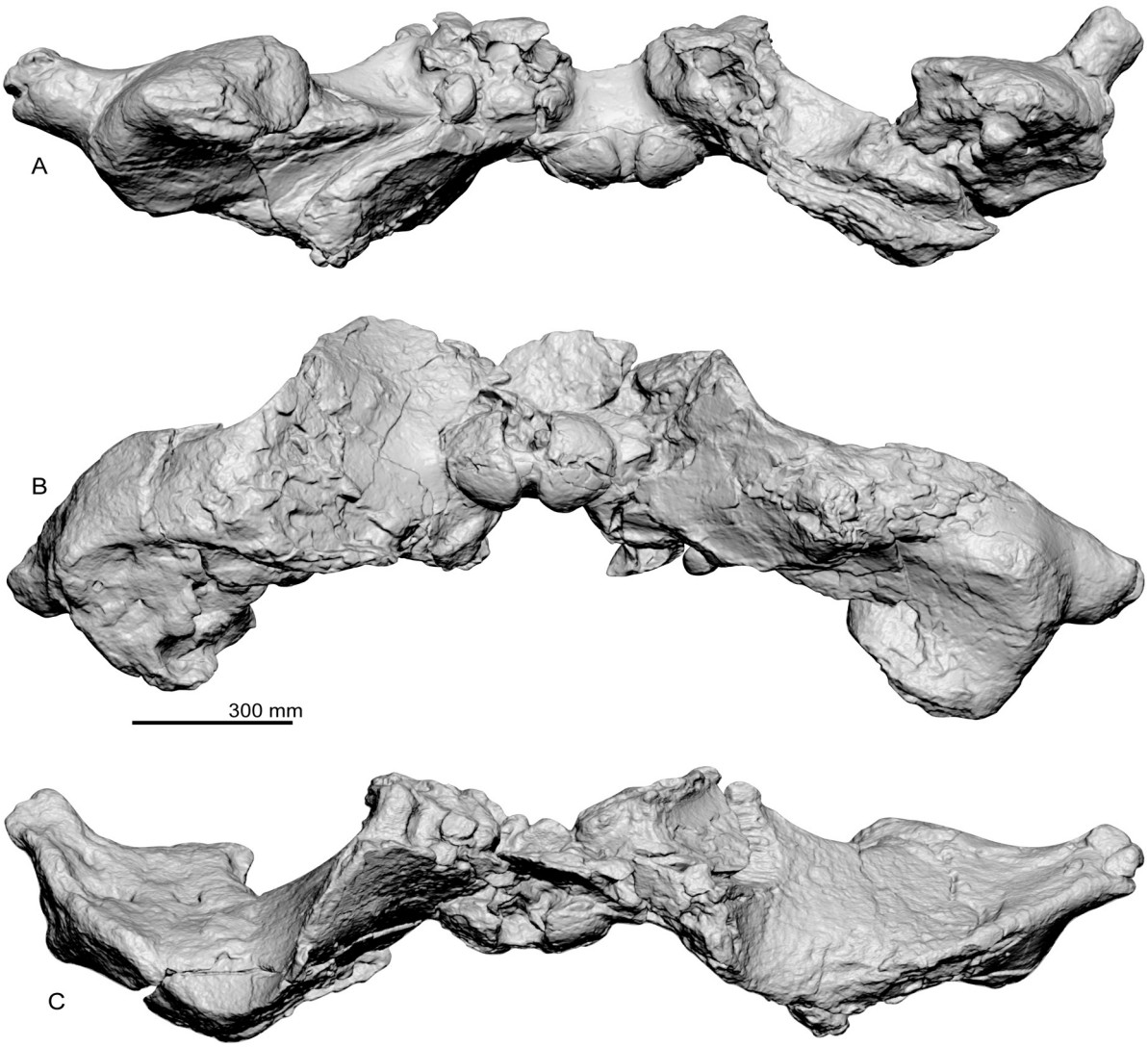

FIGURE 9. Basicranium, SMAC 2731, *Megabalaena sapporoensis* in ventral view (A), posterior view (B), and dorsal view (C). These images are based on a 3D model.

cesses. Compared with *Balaenotus insignis* and *Idiocetus gucciardinii* (Van Beneden 1880; Capellini 1905), *M. sapporoensis* can be differentiated by having a wider atlas with a dorsoventrally high transverse process. Compared with *Balaenotus insignis*, *M. sapporoensis* can be differentiated by having a dorsoventrally higher tympanic bulla in medial view, much wider fan-shaped scapula and much slenderer humerus (see more in discussion). Compared with *Idiocetus gucciardinii, M. sapporoensis* can be differentiated by having a wide anterior lobe of the tympanic bulla in dorsal view, and a mandible with a developed and more medially tilted coronoid process.

DESCRIPTION

Ontogenetic age. All preserved epiphyses of the vertebrae are fused. Through ontogeny, the order of vertebral fusion starts from the cervical and caudal regions to the middle (Flower, 1864; Ito and Miyazaki, 1990; Galatius and Kinze, 2003; Moran et al., 2015). Omura (1969) reported several *Eubalaena glacialis* including photos of physically mature males with ossified thoracic and lumbar

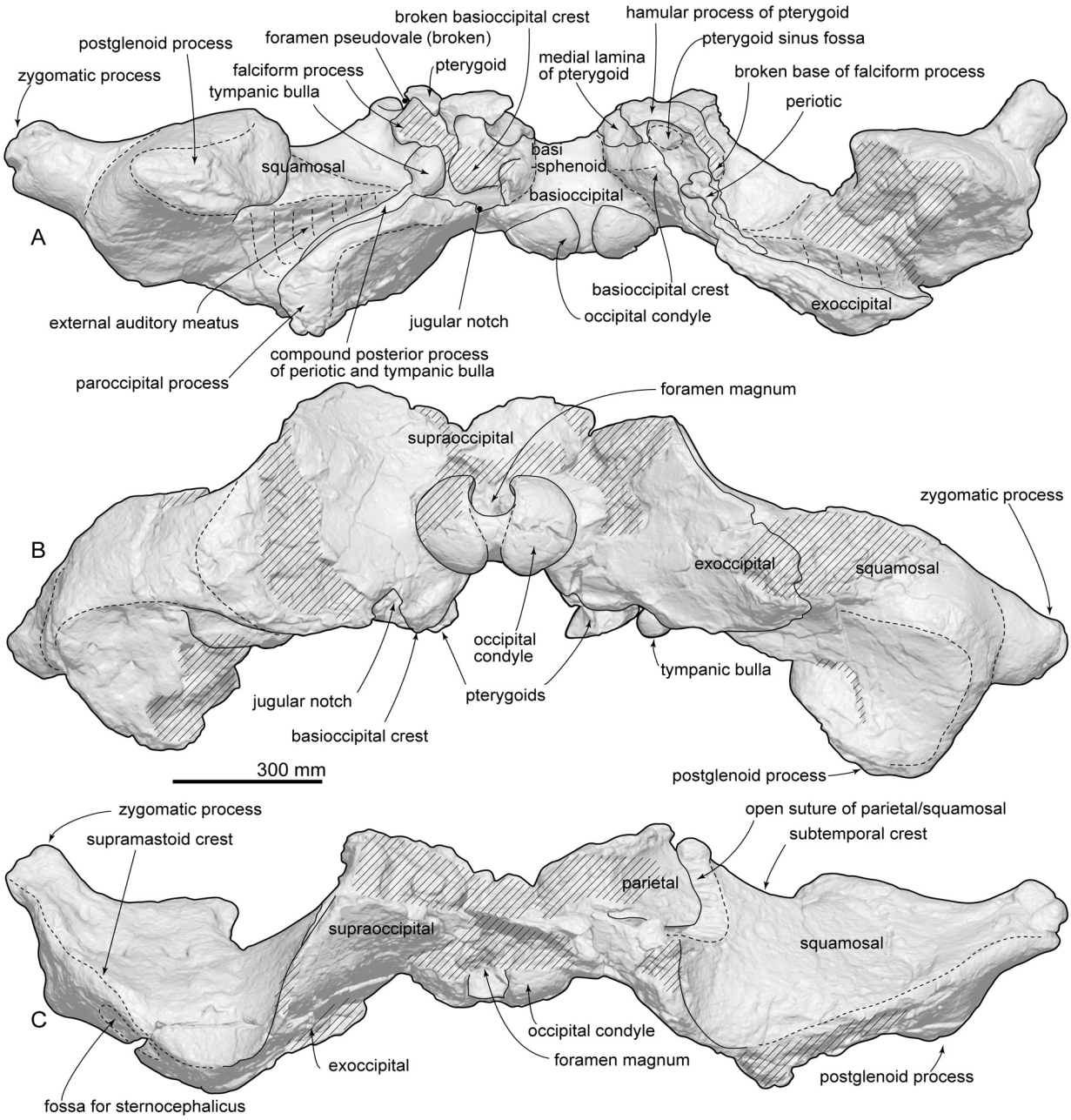

FIGURE 10. Key features on basicrania, SMAC 2731, *Megabalaena sapporoensis* in ventral view (A), posterior view (B), and dorsal view (C). These images are based on a 3D model.

vertebrae (IDs 61A (17.1 m long) and 61B (17.0 m long)). *Megabalaena sapporoensis* and the two individuals of *E. glacialis* have open suture of the parietal and squamosal at the temporal fossa, which might be not fused in adult balaenids. The observation and these previous studies suggest that SMAC 2731 is a physically matured adult.

Body size. The body size of the holotype of *Megabalaena sapporoensis* can be inferred from the Slater et al. (2017) formula for extinct mysticetes [log (TL) = 0.92 × (log (BZ) – 1.72) +2.68], which was originally established formula for stem mysticetes in Pyenson and Sponberg (2011), and the Bisconti et al. (2021) formula for the Balaenidae [log (TL) = 0.86303 × log (BZ) + 1.2125]. The bizy-

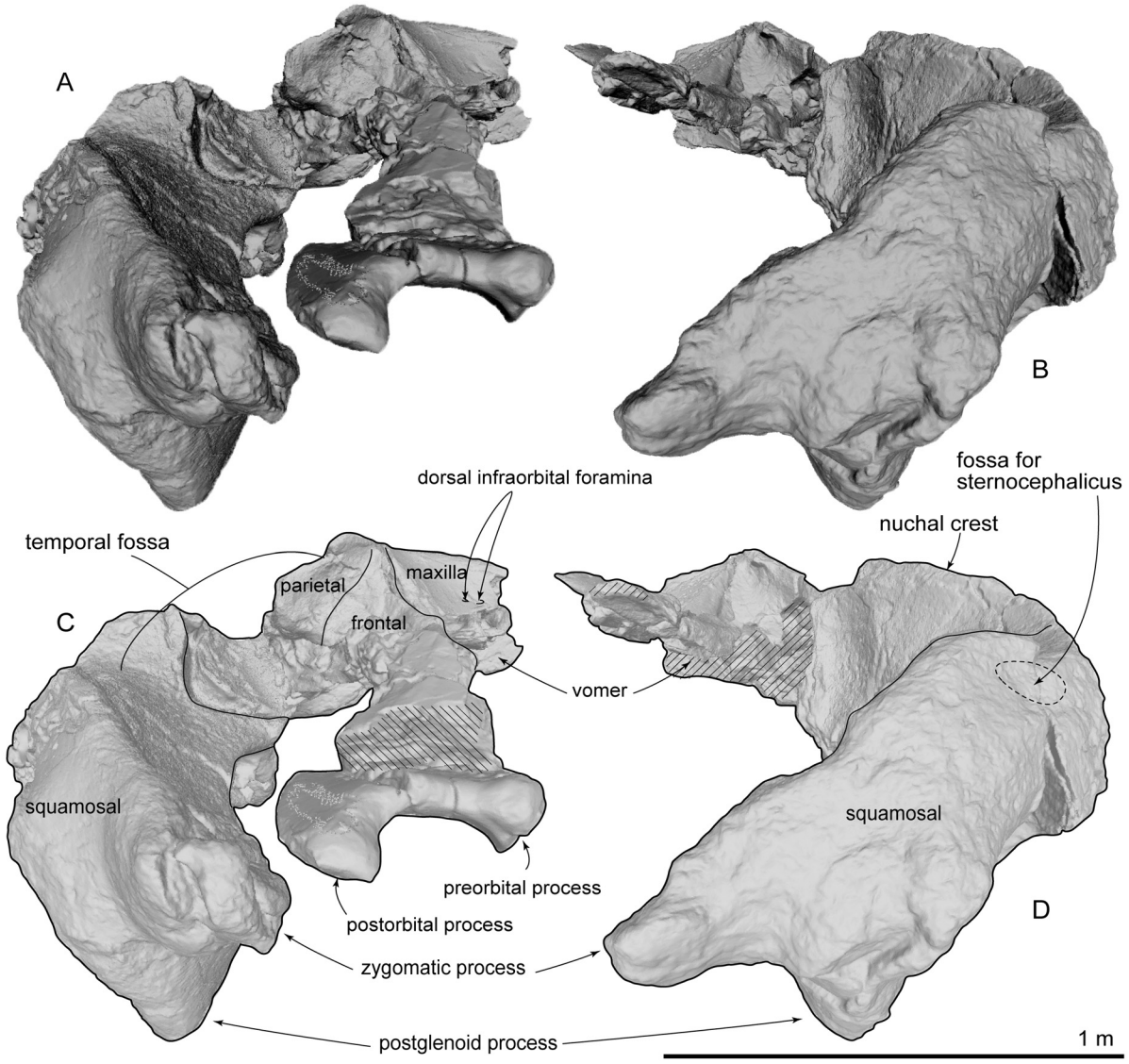

FIGURE 11. Skull, SMAC 2731, *Megabalaena sapporoensis* in right lateral view (A), left lateral view (B), and key features (C, D). These images are based on a 3D model.

gomatic width (BZ) of the holotype of *Megabalaena sapporoensis* is 2232 mm, giving reconstructed body length of 15.0 m and 12.7 m, respectively. We prefer 12.7 m, for the estimated total length of *M. sapporoensis*, because the formula of Bisconti et al. (2021) is specialized for the Balaenidae. We categorize balaenids by their total length as small (0–5.5 m), middle (5.6–8 m), large (10–13.5 m) and gigantic (>14 m) (Bisconti et al., 2021). Following the previous study, *M. sapporoensis* can be categorized as large balaenid (10–13.5 m), but it belongs to gigantic size (>14 m) if the result uses the formula from Slater et al. (2017).

General feature of the skull. The preserved right side of the skull (Figures 3–11) has a slender supraorbital process of the frontal with laterally strongly projected pre- and postorbital processes and robust zygomatic process. It has a wider base of the rostrum than those of modern balaenids (Figures 3–5). The skull is separated mainly into three parts (left frontal + jugals (Figure 6), a vertex area (Figures 7 and 8), and a basicranial area (Figures 9 and 10).

Premaxilla. The ascending process of the right premaxilla is removed to the midline and covers the nasal dorsally. Its lateral border is straight, but its medial border is damaged. The preserved right

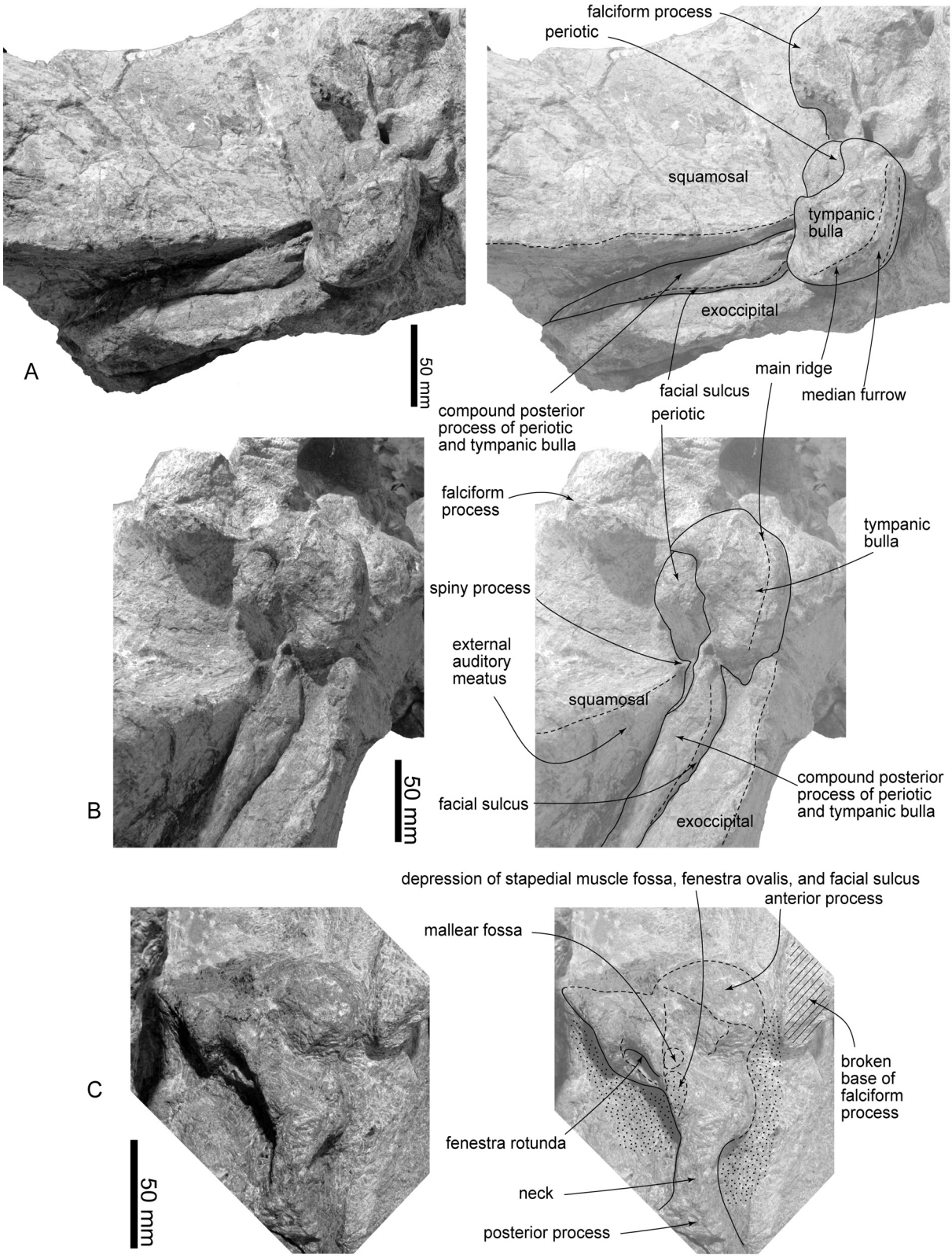

FIGURE 12. Ear bones in situ of SMAC 2731, *Megabalaena sapporoensis,* right periotic and tympanic bulla in ventral view (A), lateral view (B), and left periotic in ventral view (C).

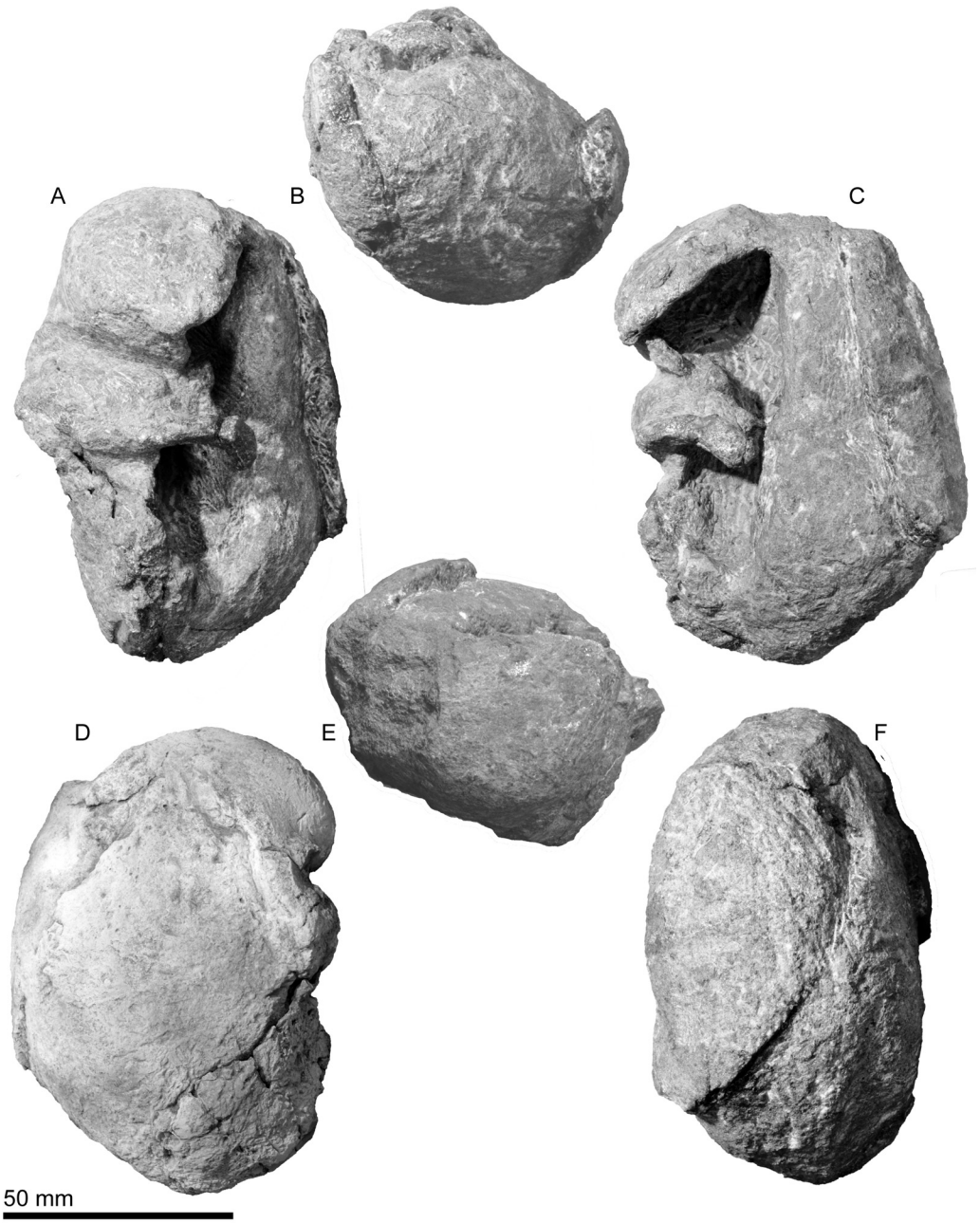

FIGURE 13. Left tympanic bulla of SMAC 2731, *Megabalaena sapporoensis* in lateral view (A), anterior view (B), dorsal view (C), ventral view (D), posterior view (E), and medial view (F).'

premaxilla is about 50 mm wide and 270 mm long. The posterior end of the premaxilla contacts the frontals.

Maxilla. The left maxilla exhibits a strongly curved lateral margin at the rostrum base in dorsal and ventral view (Figure 8A and C). This area is the posterior part of the antorbital notch. The ascending process of the maxilla forms a gradual slope from the vertex to the lateral end. Three dorsal infraorbital foramina are preserved on the right maxilla (about 10 mm wide) (Figure 8A). At the vertex, a parasagittally oriented medial border of the ascending process contacts the premaxilla. In ventral view (Figure 8C), the maxilla contacts the vomer medially and frontal posteriorly. There is a triangular, smooth, and thin bony plate preserved ventral to the frontal, which is a displaced fragment of the left infraorbital plate of the maxilla.

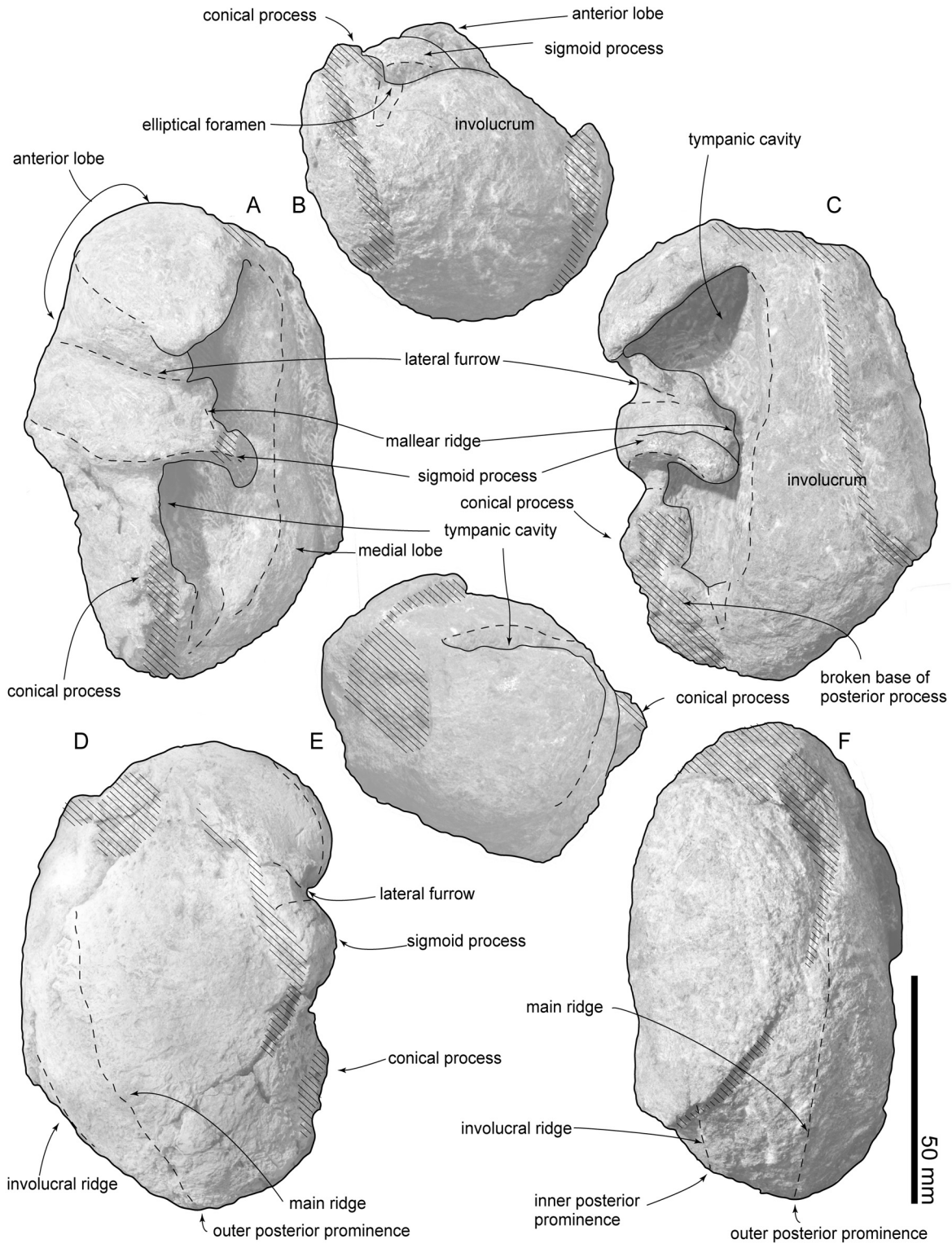

FIGURE 14. Key features of left tympanic bulla of SMAC 2731, *Megabalaena sapporoensis* in lateral view (A), anterior view (B), dorsal view (C), ventral view (D), posterior view (E), and medial view (F).

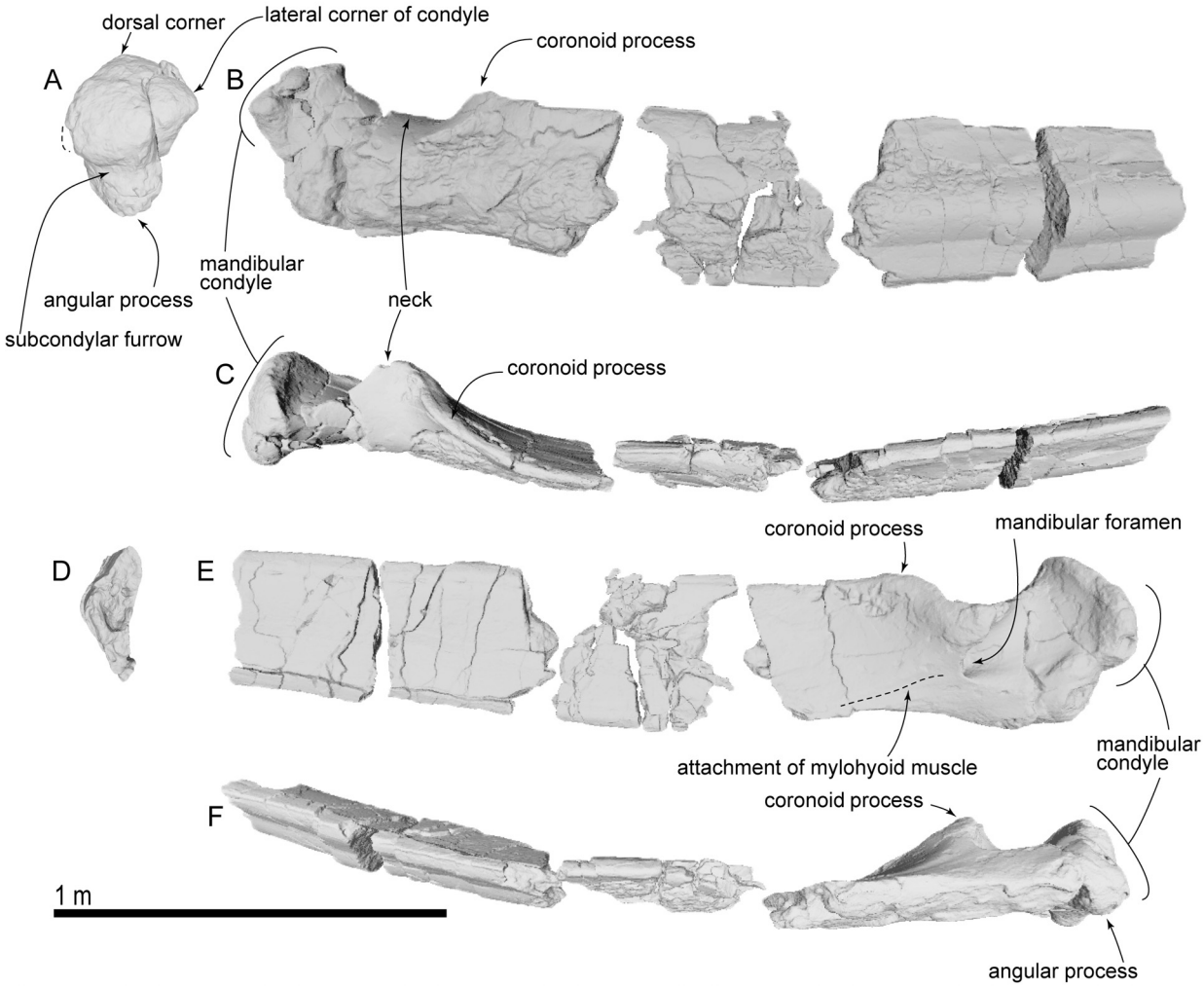

FIGURE 15. Right mandible of SMAC 2731, *Megabalaena sapporoensis* in posterior view (A), lateral view (B), dorsal view (C), anterior view (D), medial view (E), and ventral view (F). These images are based on a 3D model.

Nasal. Nasals are long and dorsoventrally high (left nasal is about 95 mm wide, 75 mm high, 310 mm long) and have a damaged dorsal surface. There are rounded anteriorly projected processes at the midline on the right and left nasals.

Frontal. At the vertex, the frontal exhibits a transversally wide and anteroposteriorly short exposure between the supraoccipital and maxilla. The supraorbital process is anteroposteriorly narrow with laterally well-projected pre- and postorbital processes (Figure 6A to C). The preorbital process is triangular with rounded anterior border in dorsal and ventral view. The postorbital process is robust and projects laterally well. These processes are dorsoventrally high. Between the pre- and postorbital processes, the orbital margin of the frontal is strongly concave. In lateral view, the orbit is rounded, and its anteroposterior length is 170 mm. In ventral view, the preorbital ridge is blunt, and the postorbital ridge is sharp. Between the ridges, the optic canal opens ventrally and laterally widely and continues to the lateral edge of the orbit. On the dorsal surface of the supraorbital process, the orbitotemporal crest is sharp and strongly developed medially (Figure 8B) and faint laterally on the supraorbital process (Figure 6A). The medial part of the frontal contacts with the vomer medially and is covered by the maxilla and palatine anteromedially and medially (respectively; Figures 7 and 8C). At the vertex, the frontal has an anteroposteriorly short exposure, and it contacts the nasal and premaxilla anteriorly, and the parietal and supraoccipital posteriorly.

Jugal. The jugal is an anteroposteriorly long (220 mm) and dorsoventrally thin (maximum height is 47 mm) bone (Figure 6). The maxillary border has a

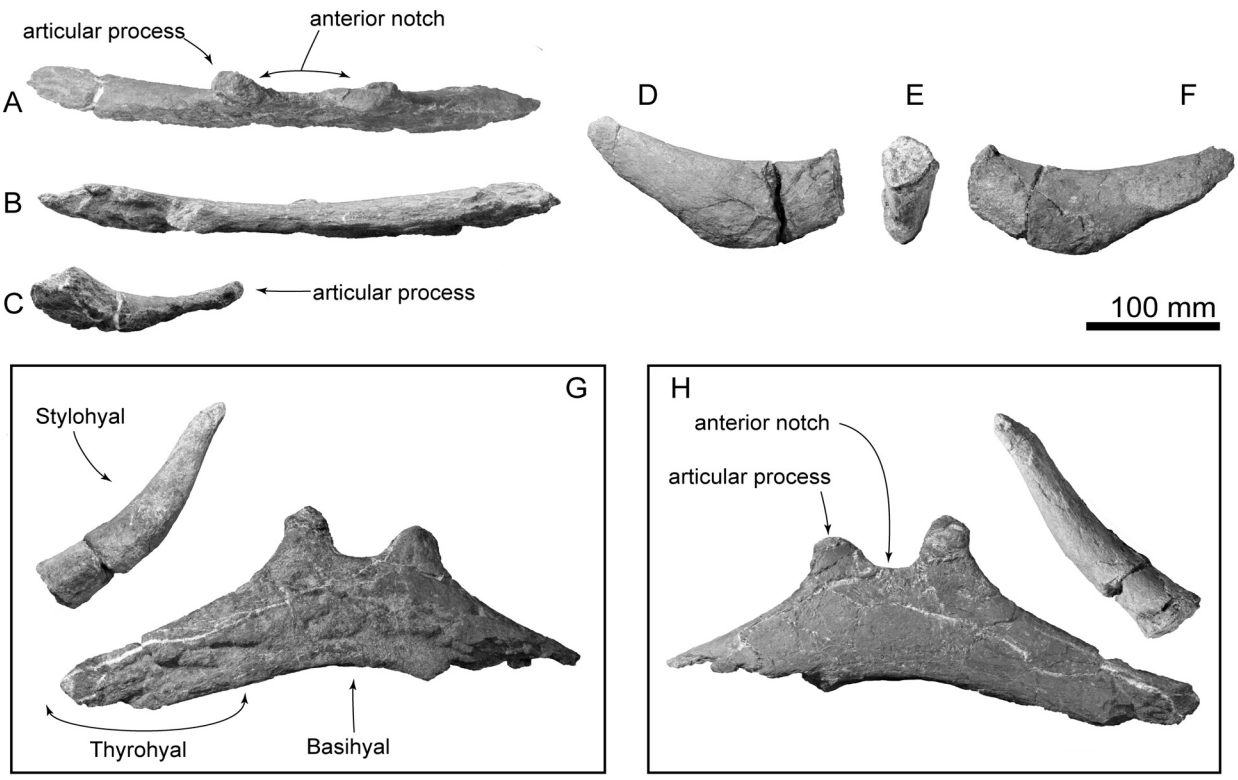

FIGURE 16. Hyoid bones of SMAC 2731, *Megabalaena sapporoensis.* Basihyal and thyrohyal in anterior view (A), posterior view (B), and right lateral view (D). Right stylohyal in medial view (D), posterior end (E), and lateral view (F). Hyoid bones in dorsal view (G) and ventral view (H).

TABLE 3. Measurements in mm of *Megabalaena sapporoensis* (SMAC 2731) left periotic and tympanic bulla. Dimensions follow Tsai and Fordyce (2015). Distances are either horizontal or vertical, unless identified as point to point. + shows an incomplete measurement, because of erosion. Measurements are rounded to the nearest 0.5 mm.

Periotic	
Length of anterior process of periotic (right side)	45.5
Maximum transverse width of the body of periotic	86.5+
Length of pars cochlearis	29.0+
Width of pars cochlearis	48.0+
Dorsoventral diameter of fenestra rotunda	7.5
Width of fenestra rotunda	11.5
Length of the posterior process of the periotic	343.5
Bulla	
Greatest length, in lateral view	108.5
Greatest length of tympanic cavity	71.5
Greatest width, in lateral view	54.0
Length of anterior lobe, from lateral furrow to anterior tip of tympanic bulla	35.5

deep and smooth excavation on the dorsal surface, which contacts the maxilla. Medial to the maxillary border, the frontal process projects anteriorly, which is dorsoventrally thin and squared in dorsal and ventral view. The jugal is weakly curved and ventrally convex and forms the ventral border of the orbit. The temporal border forms a flat surface dorsally, which contacts the zygomatic process of the squamosal.

Parietal. The parietal is broadly exposed laterally, between the frontal and supraoccipital in lateral view (Figure 11A and C) and forms the lateral part of the vertex. The lateral exposure of the parietal forms the anteromedial surface of the temporal fossa.

Palatine. The palatine is an anteroposteriorly long and dorsoventrally thin plate just medial to the posterior end of the maxilla (Figure 8C). The shape of the maxillopalatine suture is unclear, but the anterior part of the palatine invades into the posterior border of the maxilla. The preserved anterior part of the palatine is smooth ventrally.

Vomer. The anterior part of the vomer has a sharp vomerine crest in anterior view (Figure 8B). The preserved posterior part of the vomer has a low

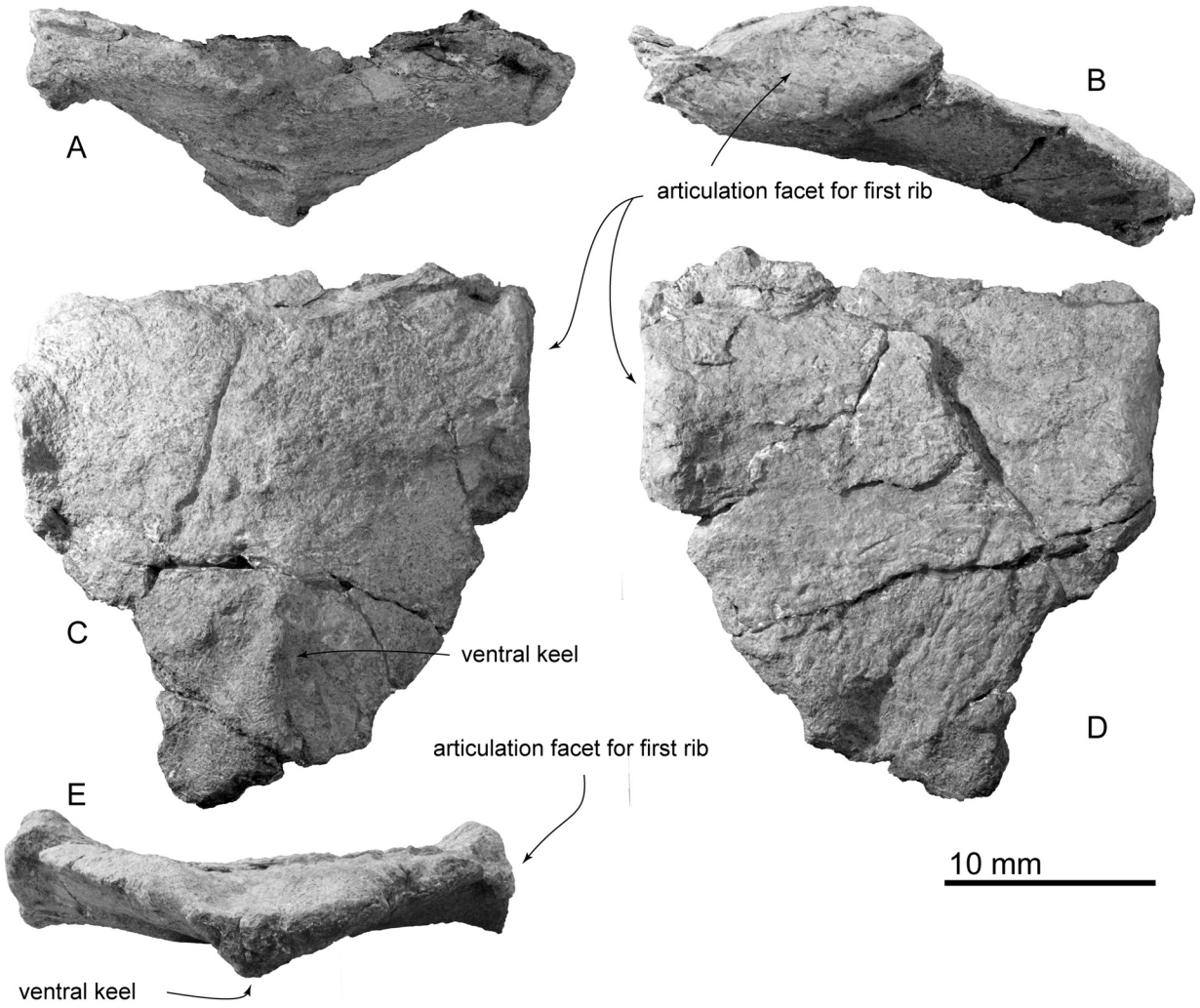

FIGURE 17. Sternum of SMAC 2731, *Megabalaena sapporoensis* in anterior view (A), left lateral view (B), ventral view (C), dorsal view (D), posterior view (E).

posterior end of the vomerine crest in ventral view (Figure 8B). There are two weak depressions on the right and left sides of the end of the vomerine crest, which correspond to the posterior internal choanae.

Pterygoid. The pterygoid continues posteriorly to overlap the basioccipital crest (Figure 10A). The hamular process is a dorsoventrally thick and transversely wide bony plate forming the anterior border of the pterygoid sinus fossa.

Squamosal. In ventral view (Figure 10A), between the squamosal and pterygoid, there is a notch, which might be a broken foramen pseudovale. The falciform is broken but thick posterior to the foramen pseudovale. Posterior to the falciform process, a sharp spiny process projects medially (Figure 12B). The posterior border of the squamosal contacts to the exoccipital laterally. Just anterior to the border, there is a long and laterally widely open external auditory meatus. Anterolateral to the external auditory meatus, a huge postglenoid process projects ventrally. The anterior surface of the postglenoid process is a weakly swollen articular surface for the mandible. The posterior surface of the postglenoid process is strongly excavated. In dorsal view, the right squamosal exhibits the open suture of the squamosal and parietal (Figure 10C). The squamosal has a slender zygomatic process projecting ventrolaterally. The anterior part of the zygomatic process is squared in dorsal and ventral view. The supramastoid crest is blunt and runs on the dorsal surface of the zygomatic process and reaches the posterior part of the nuchal crest. The sternocephalicus fossa on the posterolateral surface of the zygomatic process is shallow.

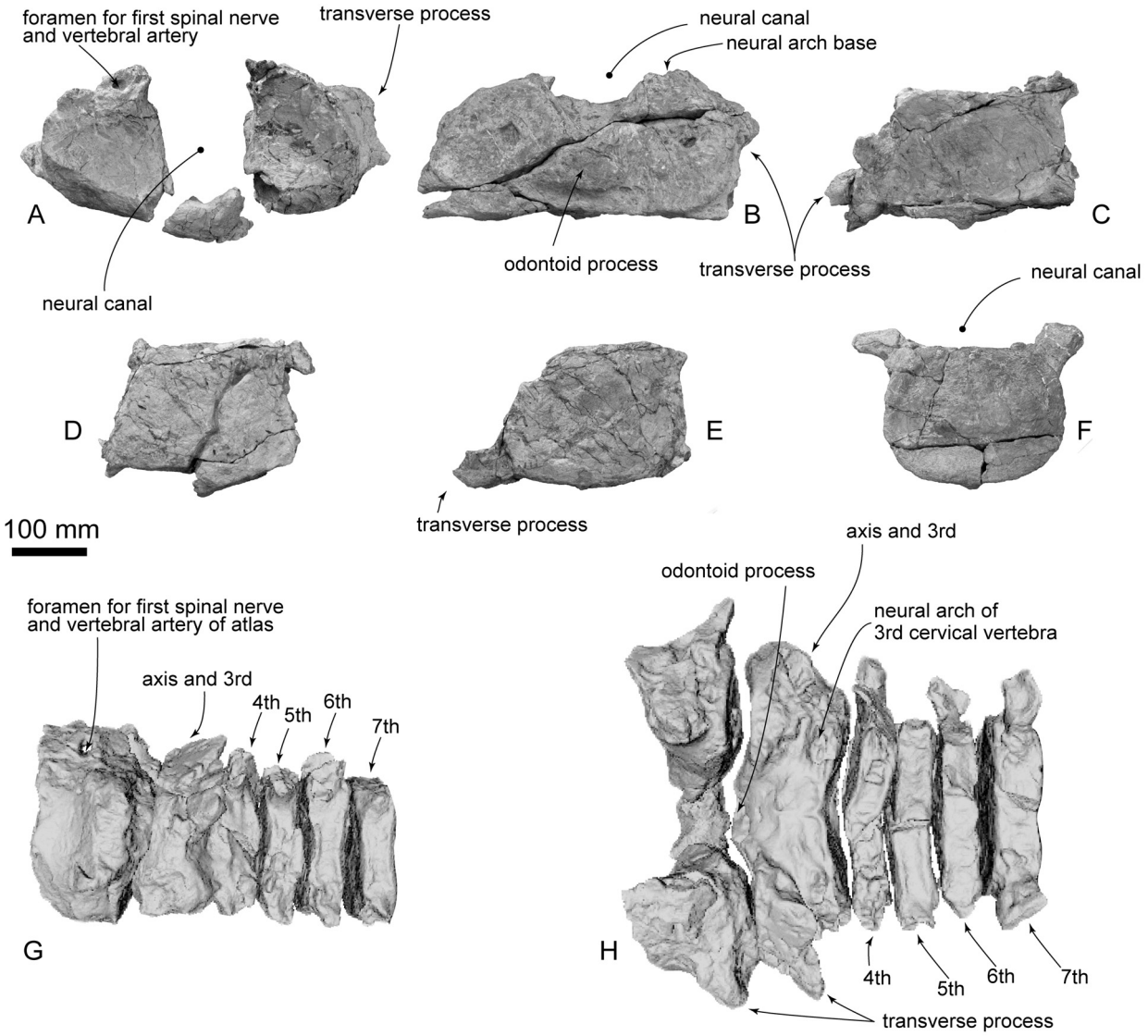

FIGURE 18. Cervical vertebrae of SMAC 2731, *Megabalaena sapporoensis.* In anterior view, atlas (A), axis and third cervical vertebra (B), fourth cervical vertebra (C), fifth cervical vertebra (D), sixth cervical vertebra (E), seventh cervical vertebra (F). Whole cervical vertebrae in left lateral view (G) and dorsal view (H). (G) and (H) are based on a 3D model.

Exoccipital and supraoccipital. In dorsal views (Figure 8A), the supraoccipital has an anteriorly projected part at the center and curved lateral part of the nuchal crest. The supraoccipital apex is convex anteriorly and it covers the frontals anteriorly.

In posterior view (Figure 9B), the exoccipital and supraoccipital are fused. In ventral view (Figure 9A), the lateral end of the exoccipital is anteroposteriorly thickened. The occipital condyle is globular and projects distinctly posteriorly. A wide elliptical foramen magnum is located at a dorsal half of the occipital condyle.

Basioccipital and basisphenoid. In ventral view (Figure 9A), basioccipital and basisphenoid are fused. A transversely thick and flat basioccipital crest projects ventrally strongly. There is a weak transverse ridge on the ventral surface of the basioccipital crest.

Periotic. The periotics (Figure 12 and Table 3) are in situ, and only the left one is visible (Figure 12C). The anterior process is mediolaterally wide and is still partly covered by the squamosal. The lateral tuberosity is invisible because of the matrix. Posteriorly, a transversely wide elliptical fenestra rotunda is visible. Lateral to the fenestra rotunda, there is a

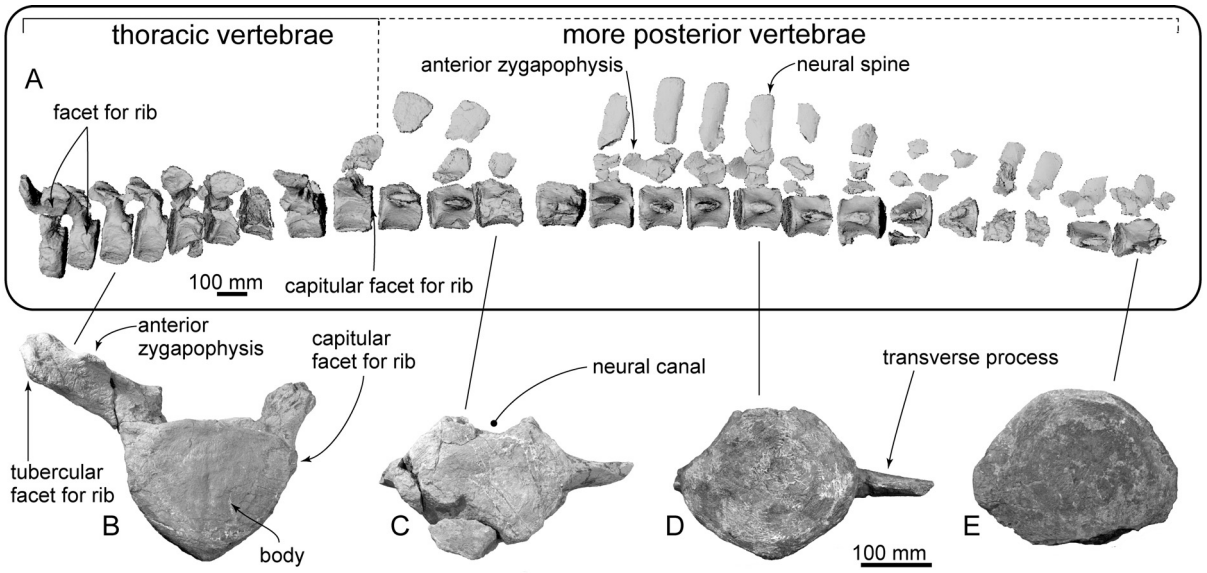

FIGURE 19. Thoracic and more posterior vertebrae of SMAC 2731, *Megabalaena sapporoensis,* in left lateral view based on a 3D model (A). Third thoracic vertebra in anterior view (B), more posterior vertebrae in anterior view (C and D), third most posterior vertebra in posterior view (E).

shallow and circular mallear fossa anteriorly and a long depression covered by the matrix including the stapedial muscle fossa, fenestra ovalis and facial sulcus posteriorly. The compound posterior process of the periotic and tympanic bulla extends posterolaterally (Figure 12A and B) and bears a shallow facial sulcus near its posterior border.

Tympanic bulla. The tympanic bullae (Figures 12 to 14, Table 3) is broad bean shape in ventral view, which are anteroposteriorly longer than the width. The involucrum is dorsoventrally high with a weakly swollen medial lobe at the level of the conical process. The anterior lobe of the tympanic bulla is swollen medially and has a weak ridge running transversely on the anterior lobe. There is a large sigmoid process posterior to the anterior lobe, which is diagenetically displaced into the tympanic cavity. The lateral border of the sigmoid process is gradually rounded in posterior view (Figure 13B), and the medial margin of the sigmoid process is thick (approximately 9 mm long). Anteriorly, the lateral furrow runs transversely and separates the sigmoid process from the anterior lobe. There is an anteroposteriorly long mallear ridge just anterior to the sigmoid process. There is an anteroposteriorly long and mediolaterally thin conical process posterior to the sigmoid process. The broken base of the posterior process is located posterior to the conical process. Posterior to the conical process, the outer posterior prominence is a larger projection compared to the inner posterior prominence. The main ridge runs anteroposteriorly on the lateral surface of the tympanic bulla from the outer posterior prominence. The inner posterior prominence is weakly projected posteriorly dorsal to the outer posterior prominence (Figure 13F). Between the prominences, a clear median furrow is not developed.

Mandible. An incomplete right mandible is preserved as five separated fragment parts including the most posterior part (Figure 15, Table 2). The mandible in Figure 3 has been digitally re-inflated to resemble the proportions of other balaenids. The most anterior part (Figure 15D) is the body of the mandible. It is dorsoventrally high and mediolaterally narrow, but its medial surface is mediolaterally crushed during fossilization (Shinmura et al., 2024). The posterior part of the mandible has a relatively low high coronoid process as a balaenid. In dorsal view (Figure 15C), between the coronoid process and mandibular condyle, a low neck expands medially strongly. The mandibular foramen opens posterodorsally largely (80 mm in diameter) and the mandibular foramen is expanded. The mylohyoid groove is developed as a shallow longitudinal groove anterior to the mandibular foramen along the ventromedial side of the mandible. The angular process is transversely narrow and weakly projected posteriorly. The mandibular condyle is separated from the angular process by a transversely long subcondylar furrow on the medial and posterior sides. The subcondylar furrow is deeper than those of extant balaenids. The man-

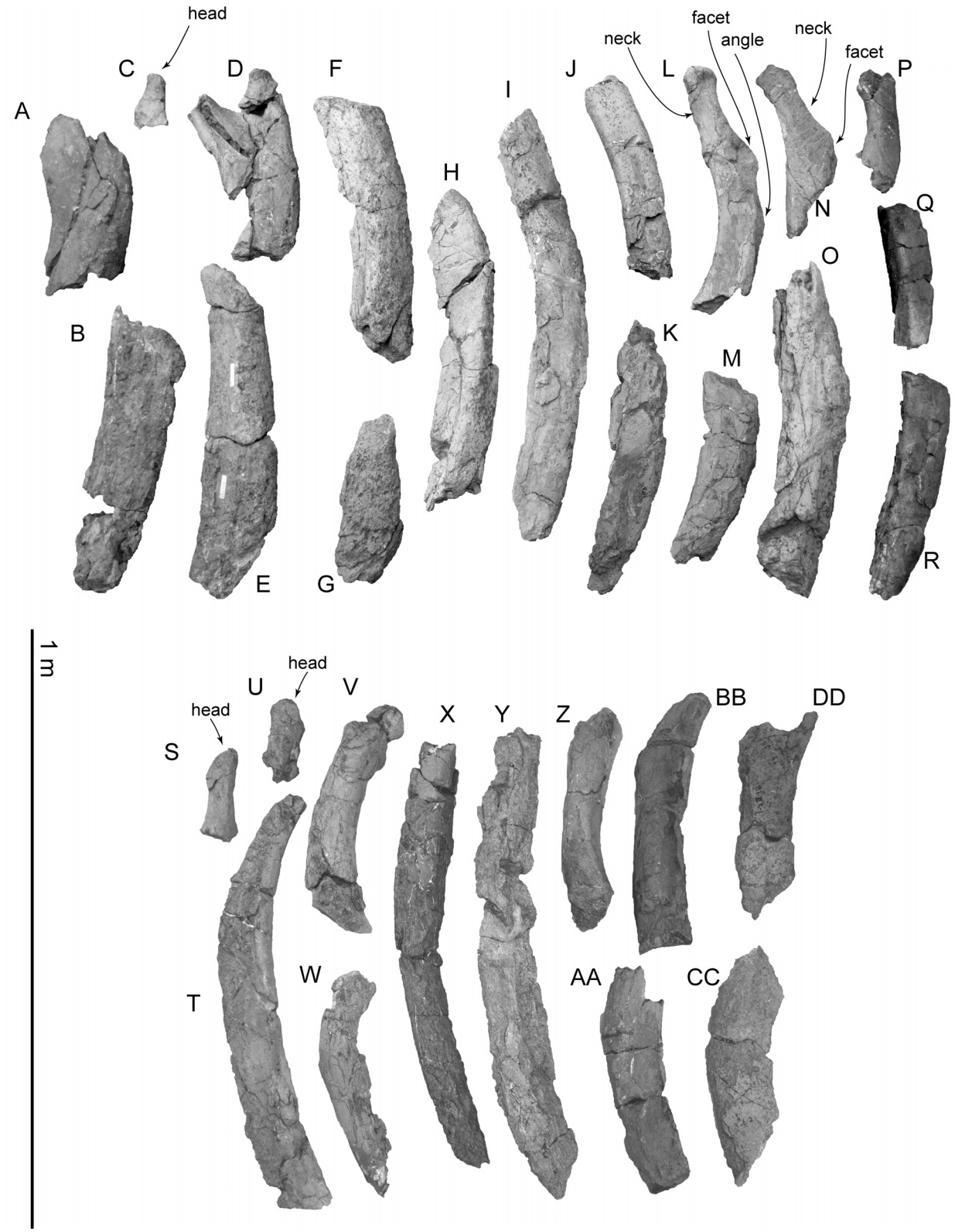

FIGURE 20. Ribs of SMAC 2731, *Megabalaena sapporoensis*. Ribs interpreted as from the left side (A to R), and right side (S to DD).

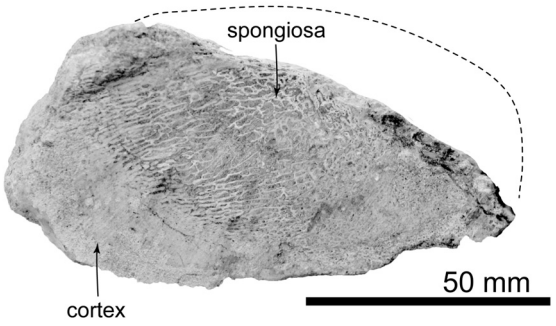

FIGURE 21. A cross-section photo of the distal end of a rib T in Figure 20.

dibular condyle is oriented posterodorsally. The shape of the mandibular condyle is elliptical and is nearly elliptical in shape and transversely wider dorsally, forming blunt dorsolateral and dorsal corners in articular/posterior view (Figure 15A). In dorsal view, the condyle is subtriangular (Figure 15C). The lateral corner of the mandibular condyle (Tanaka and Taruno 2024) is dorsally elevated, at the same level as the dorsal border of the mandibular ramus.

Hyoid bones. The right stylohyal and a single fused element of the basihyal-thyrohyal are preserved (Figure 16G and H). The basihyal-thyrohyal

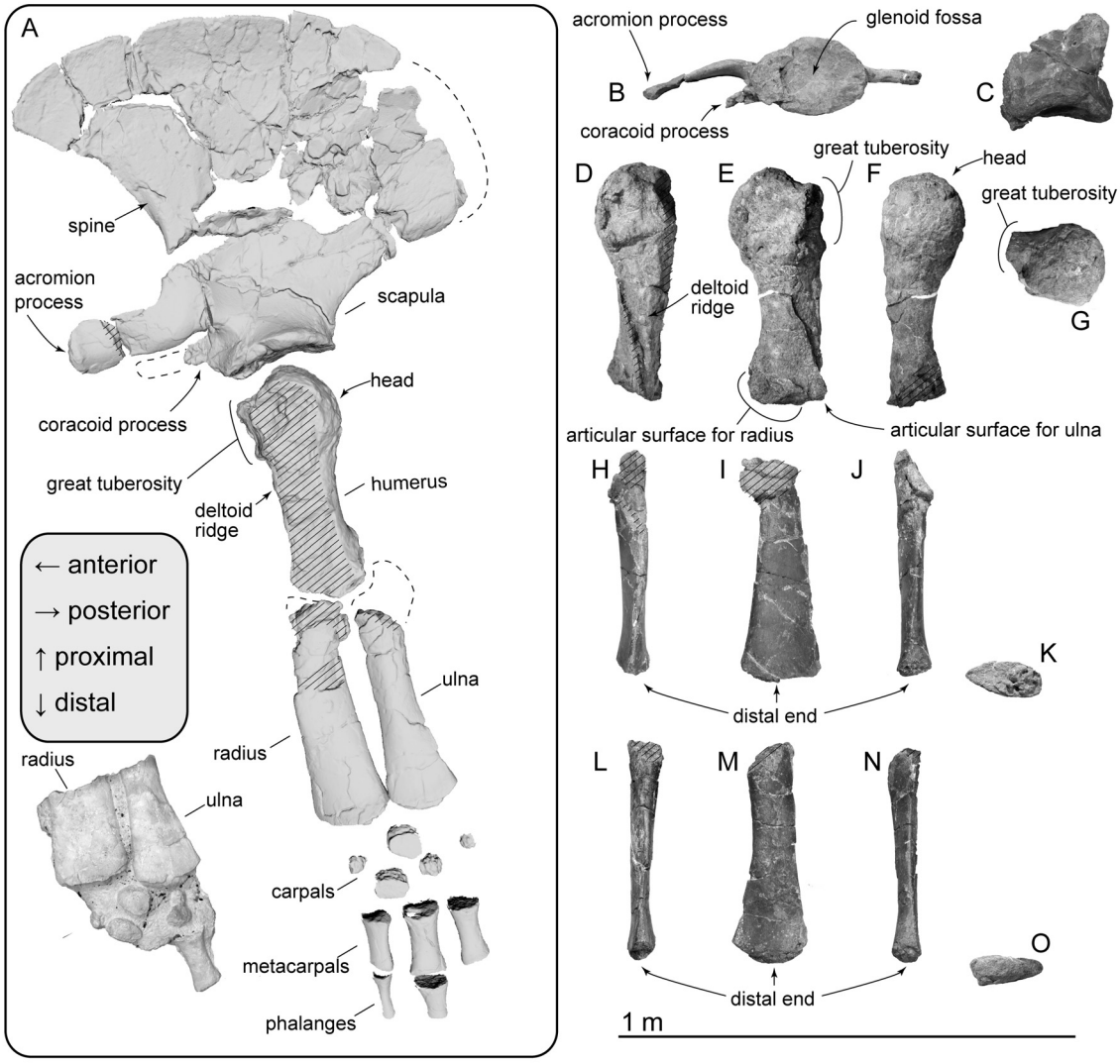

FIGURE 22. Forelimb elements of SMAC 2731, *Megabalaena sapporoensis*. All preserved left side elements in lateral view and a cast showing original deposited position of the ulna, radius, carpals and a metacarpal based on a 3D model (A). Left scapula in ventral view (B). Right scapula in lateral view (C). Humerus in anterior view (D), medial view (E), posterior view (F), and proximal view (G). Radius in anterior view (H), medial view (I), posterior view (J), and distal view (K). Ulna in anterior view (L), medial view (M), posterior view (N), and distal view (O).

TABLE 4. Measurements in mm of *Megabalaena sapporoensis* (SMAC 2731) vertebrae. Distances are either horizontal or vertical, unless identified as point to point. + shows an incomplete measurement, because of erosion.

	length of body	width of body	height of body	maximum preserved height	maximum preserved width	neural spine height	neural spine length
Atlas	140	-	-	260	-	-	-
Axis and 3rd cervical vertebra	100	-	-	-	490	-	-
Axis	-	390	90	-	-	-	-
3rd cervical vertebra	260	150	-	-	-	-	-
4th cervical vertebra	50	250	190	-	370	-	-
5th cervical vertebra	45	255	220	-	290	-	-
6th cervical vertebra	50	240	190	-	230	-	-
7th cervical vertebra	50	245	195	-	320	-	-
1st thoracic vertebra	70	230	200	-	300	-	-
2nd thoracic vertebra	80	240	200	-	310	-	-
3rd thoracic vertebra	90	237	190	-	301	-	-
4th thoracic vertebra	100	240	190	-	435	-	-
5th thoracic vertebra	110	235	190	-	410	-	-
6th thoracic vertebra	110	240	190	-	440	-	-
7th thoracic vertebra	126	219	194+	-	-	-	-
8th thoracic vertebra	135	275	181+	-	475	-	-
9th thoracic vertebra	135	246	190	-	445	-	-
more posterior vertebra 1	155	252	209	-	345	-	-
more posterior vertebra 2	178	241	196	-	360	-	-
more posterior vertebra 3	185	280	191	-	406	-	-
more posterior vertebra 4	187	248+	185	-	349	-	-
more posterior vertebra 5	202	233	185	-	313	-	-
more posterior vertebra 6	197	250	228	-	429	-	-
more posterior vertebra 7	203	244	220	-	439	-	-
more posterior vertebra 8	214	254	221	-	405	440	192
more posterior vertebra 9	210	270	231	-	304	-	-
more posterior vertebra 10	220	243	230	-	278	-	-
more posterior vertebra 11	238	-	-	-	-	-	-
more posterior vertebra 12	245	-	235	-	-	-	-
more posterior vertebra 13	250	-	-	-	-	-	-
more posterior vertebra 14	285	-	-	-	-	-	-

is dorsoventrally thin (about 22 mm with at the center) plate with posterolaterally projected lateral portions (preserved maximum dimensions are 410 mm wide, 145 mm long). Its ventral surface and the right end and left lateral portion are broken. There are two anteriorly well-projected articular processes for the ceratohyal on the anterior margin of the basihyal-thyrohyal. Between the articular processes, there is a widely open anterior notch. The posterior processes on the posterior margin seem absent. The right stylohyal (Figure 16D-F) is a transversely thin bar and is anteriorly slender and posteriorly thick (preserved maximum dimensions are 210 mm long, 45 mm wide, and 70 mm high). Its anterior end is broken. Its posterior end is dorsoventrally higher elliptical and flat (45 mm wide and 60 mm high) (Figure 16E).

Sternum. The sternum is shield-like and symmetrical, and the posterior part is broken (Figure 17) (preserved maximum dimensions are 260 mm long, 240 mm wide, and 70 mm high). The anterior part is wider due to the presence of the articulation facet for the first rib on the lateral margins. The articulation facet for the first rib is anteroposteriorly

TABLE 5. Measurements in mm of *Megabalaena sapporoensis* (SMAC 2731) forelimb. Distances are either horizontal or vertical, unless identified as point to point. + shows an incomplete measurement, because of erosion.

Scapula		
	length of glenoid fossa	280
	width of glenoid fossa	200
Humerus		
	proximodistal length	560
	maximum anteroposterior length at proximal end	255
	maximum width of proximal end	199
	minimum length at shaft	135
	maximum length of distal end	180
	maximum width of distal end	145
Ulna		
	proximodistal length	490+
	minimam length at shaft	95
	maximum length of distal end	170
	maximum width of distal end	65
Radius		
	proximodistal length	545
	minimum length at shaft	140
	maximum length of distal end	195
	maximum width of distal end	85

long elliptical and flat surface (110 mm long, 55 mm high) (Figure 17B). The ventral side of the sternum is convex and has an anteroposteriorly long ventral keel (Figure 17C).

Vertebra. The vertebrae were found in articulation. The proposed sequence of vertebrae is based on the sequence observed during the excavation and/or preparation. All cervical vertebrae are preserved as six bones (Figure 18). The axis and third cervical vertebra are fused firmly at the bodies (Figure 18H). At least nine thoracic vertebrae have existed, and16 more posterior vertebrae cannot be identified thoracic or lumbar vertebrae because of damages.

The atlas is rounded in anterior view with a concave anterior articular surface for the skull and convex posterior articular surface for the axis (Figure 18A, G, and H). The laterally projected transverse process is anteroposteriorly thick, and dorsoventrally high at its base (there is no evidence of the transverse foramen preserved). The neural canal is a dorsoventrally high foramen formed also by the socket for the odontoid process. On the broken base of the neural arch, there is a dorsoventrally high elliptical and large foramen for the first spinal nerve and vertebral artery (15–20 mm in diameter).

The fused axis and third cervical vertebra are very wide because of a large transverse process (490 mm wide). The anterior articular surface for the atlas is weakly concave. Between the articular surfaces, a blunt odontoid process projects anteriorly weakly. The posterior articular surface for the fourth cervical vertebra is laterally wider than high circle and is strongly excavated in the mid line (Figure 18R).

The fourth to sixth cervical vertebrae have transversely wide and anteroposteriorly thin bodies. There are thin bodies and process ventral median ridges.

The seventh cervical vertebra has slightly thicker body than the fourth to sixth cervical vertebrae. The body shape in anteroposterior view is more rounded elliptic than the other cervical vertebrae.

The first thoracic vertebra can be articulated to the seventh cervical vertebra. The anterior thoracic vertebrae such as the second to fourth thoracic vertebrae have anteriorly projected anterior zygapophyses (Figure 19A and B). There is a large capitular facet for the rib facing ventrolaterally at the lateral end of the transverse process. The transverse process projects dorsolaterally in more anterior thoracic vertebrae and laterally in more posterior thoracic vertebrae. There is also a smaller facet for the rib at the posterolateral edge of the body. This feature can be examined from the first to ninth thoracic vertebrae. However, none of the more posterior preserved vertebrae preserves the facet for rib.

Here, we tentatively identify the thoracic-lumbar vertebrae posterior to the ninth thoracic vertebra, because identifying the limits on boundaries between thoracic, lumbar, and caudal regions. The thoracic vertebrae are distinguishable from the lumbar vertebrae by having articular facets for the ribs on the end of the transverse process. Rib facets on vertebrae posterior to the ninth thoracic vertebra are not adequately preserved. The caudal vertebrae are distinguishable from the lumbar vertebrae by having the haemal facets. The most posterior vertebra cannot be identified as a lumbar or caudal vertebra, because it does not preserve the ventral border including the base of the haemal facets.

Vertebrae posterior to the ninth thoracic vertebra have bodies that are anteroposteriorly 1.15–2.1 times longer than more anterior vertebrae. Their

transverse processes are dorsoventrally thin. All preserved neural spines are separated from the bodies. The neural arch of one of the more posterior vertebrae has anteriorly well-projected and dorsoventrally high anterior zygopophyses at the anterior edge of the neural spine in lateral view. The neural spine is about 400 mm high, and it has a squared dorsal end in lateral view.

Ribs. There are over 100 rib fragments, which do not have contact with other fragments. The ribs number 1 to 18 and 19 to 30 in Figure 20 are proposed to be the left and right, respectively. The ribs are transversely wide and anteroposteriorly thin, which are probably the middle part of the ribs among the series of the thoracic. Figure 20 shows relatively well-preserved rib fragments. Rib number 1 in Figure 20 is wide, which might be the dorsal part of the most anterior rib. Its width is about 160 mm. Maximum preserved length of rib number 9 in Figure 20 is about 650 mm. Rib number 12 has a rounded top and a long neck. The distance between the head and angle of rib number 12 is about 190 mm. The longest preserved rib is number 25 in Figure 20, which is about 760 mm long. The distal end of rib number 20 in Figure 20 was cut by a saw possibly during excavation (Figure 21). It has about a 2 cm thick dense cortex and spongiosa at the medullary zone of the rib.

Scapula. The scapula is anteroposteriorly longer than wide and triangular, with a convex curved dorsal border (Figure 22A). On the lateral surface, there is a weak scapular spine running dorsoventrally near the anterior edge of the scapula. Ventral to the spine, there is an anteriorly well-projected and mediolaterally thin acromion process. Ventral to the acromion process, much smaller coracoid process projects anteriorly. The acromion and coracoid processes of extant balaenids are much weaker than these of *Megabalaena sapporoensis.* The glenoid fossa is an anteroposteriorly long ellipse in ventral view and is weakly depressed (Figure 22B).

Humerus. The humerus has a slender shaft and semi globular head (Figure 22A, D to G). The shaft is mediolaterally thinner than anteroposteriorly long. A dorsoventrally long and rugose great tuberosity projects anteriorly at the proximal end of the shaft. The deltoid ridge is low and proximodistally short. The damaged distal end is posteriorly flat, which is the articular surface for the ulna.

Ulna and radius. The proximodistal length of the ulna and radius are slightly longer than that of the humerus. The ulna (Figure 22A and H to K) is proximodistally shorter than the radius (Figure 22A and I to O). Both bones are mediolaterally flat and distally anteroposteriorly widened. At the distal ends, the anterior surface of the radius and the posterior surface of the ulna are transversely thin.

Carpal, metacarpal, and phalanges. A cast exhibits the original position of the ulna, radius, carpals, and a metacarpal (Figure 22A). The preserved metacarpals and phalanges might be belonged to the 2nd to 4th fingers based on relative position against the ulna and radius, examined in the extant species (Cooper et al., 2007). The larger preserved carpal was discovered next to the posterior end of the radius and the anterior end of the ulna, thus this might be the intermedium (90 mm long, 85 mm high, 70 mm wide). It has rugose surfaces except lateral surfaces, which are flat and smooth. The smallest carpal is about 50 mm in diameter, and all its surfaces are rugose.

The metacarpals are spool-shaped with a waist in the middle, which is an approximately cylindrical in cross-section. The metacarpals have anteroposteriorly longer and shorter ends, which possibly are the proximal and distal ends respectively. The largest preserved metacarpal is 170 mm long, 98 mm in proximal length, 64 mm in proximal width, 97 mm in distal length, 47 mm in distal width. The smallest preserved metacarpal is 132 mm long, 82 mm in proximal length, 55 mm in proximal width, 66 mm in distal length, 49 mm in distal width.

The phalanges have anteroposteriorly much shorter distal ends than the proximal ends. The largest preserved phalanx is 101 mm long, 88 mm in proximal length, 51 in proximal width, 54 mm in distal length, 29 mm in distal width. The smallest preserved phalanx is 124 mm long, 57 mm in proximal length, 46 mm in proximal width, 42 mm in distal length, 28 mm in distal width.

Comparisons. Compared to the oldest known balaenid *M. parvus* with a weaker lateral projection of the zygomatic process, the exoccipital width of *M. sapporoensis* measures 60% of the bizygomatic width, which is a common ratio for the Balaenidae. Between the pre- and postorbital processes, the orbital margin of the frontal is strongly concave, differing from the straight lateral margin in other balaenids *(M. parvus, B. brachyrhynus, Eubalaena ianitrix, A. dosanko, B. astensis, B. mysticetus,* and *E. glacialis). Balaenula balaenopsis* has excavated orbit in dorsal and ventral view, but its posterior orbital process does not project laterally well like that of *M. sapporoensis.* Regarding the cervical vertebrae fusion, *M. sapporoensis* has only the axis and 3rd cervical vertebra are fused, which is a minimal degree of vertebra fusion condition in the

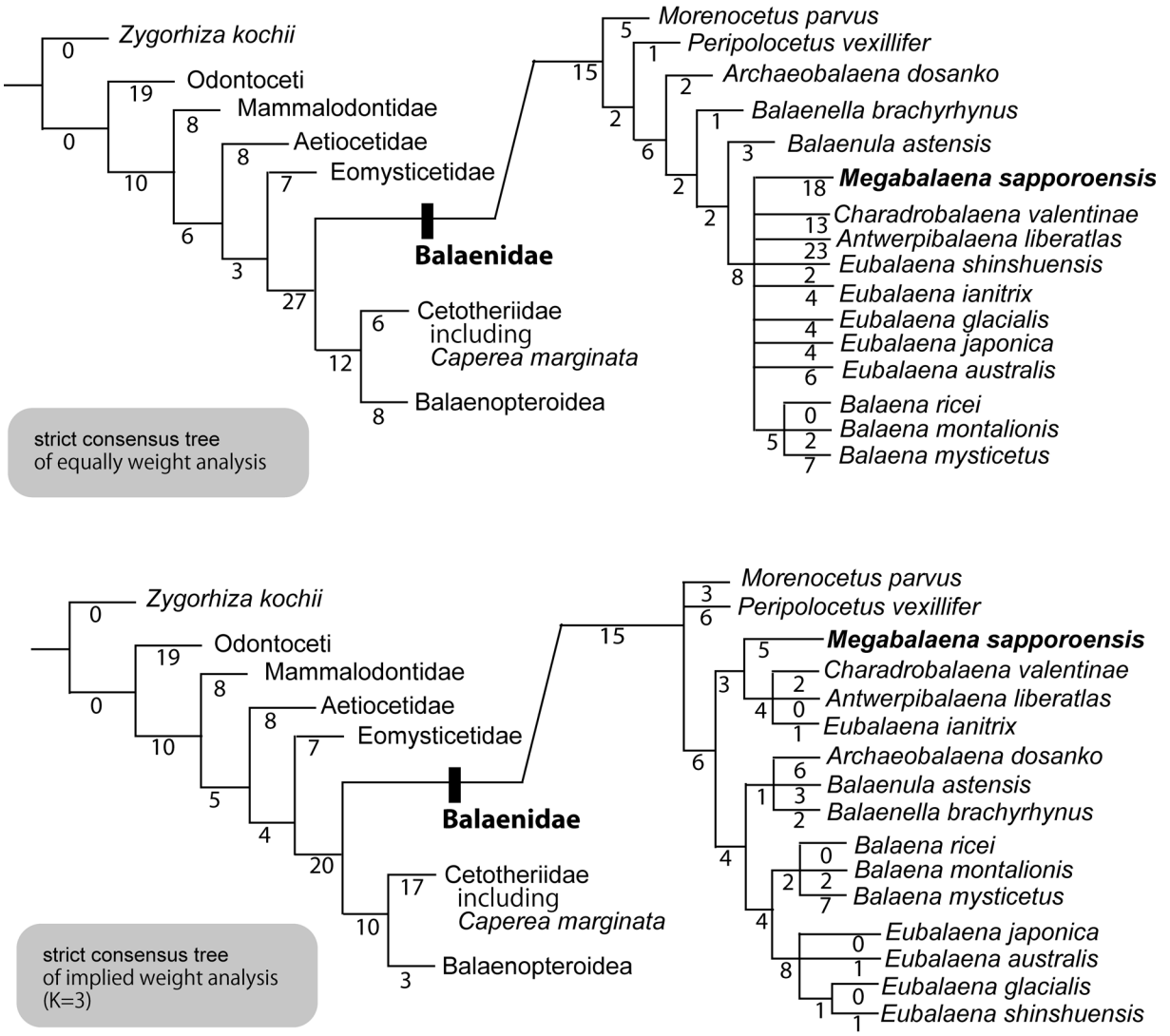

FIGURE 23. 50% majority (top) and strict (bottom) consensus trees of 53 most parsimonious trees showing the phylogenetic position of *Megabalaena sapporoensis* gen. et sp. nov. with branch length. The most parsimonious trees were 1003 steps. The clades Aetiocetidae, Eomysticetidae, Balaenidae, Cetotheriidae and a clade comprising *Isanacetus, Parietobalaena* and related taxa are collapsed. (See Appendix 5 for cladogram with all taxa shown.)

Balaenidae (see more in discussion). However, this condition can be seen in some Miocene non-balaenid baleen whales such as *Thinocetus arthritus, Uranocetus gramensis* and *Pelocetus calvertensis* (Kellogg, 1965, 1969; Steeman, 2009).

Phylogenetic results. The phylogenetic analyses present 70 shortest trees of 870 steps each for unweighted, and 10 shortest tree with a tree bisection reconnection score of 84.00321. Strict consensus trees of the equal and implied weight analyses are similar in having a clade of the *Balaena,* and recognizing *Morenocetus parvus* and *Peripolocetus vexillifer* as the most basal clades among the Balaenidae (Figure 23). However, only the strict consensus tree of implied weight analysis formed a clade of *Megabalaena sapporoensis* with *Charadrobalaena valentinae* + *Antwerpibalaena liberatlas* + *Eubalaena ianitrix.*

The topology of the 50% majority consensus and strict consensus trees of implied weighting analysis are the same (Appendix 5). Their branching patterns (Figure 23) are similar in forming clades of *Balaena, Eubalaena* and also a clade of the *Balaena* + *Eubalaena* from that of the analysis of Tanaka et al. (2020), except *Eubalaena ianitrix* excluded from the *Eubalaena* clade and was placed in a clade with *M. sapporoensis.*

The 50% majority consensus and strict consensus trees of equally weighted analysis (Figure 23; Appendix 5) are slightly different from that of

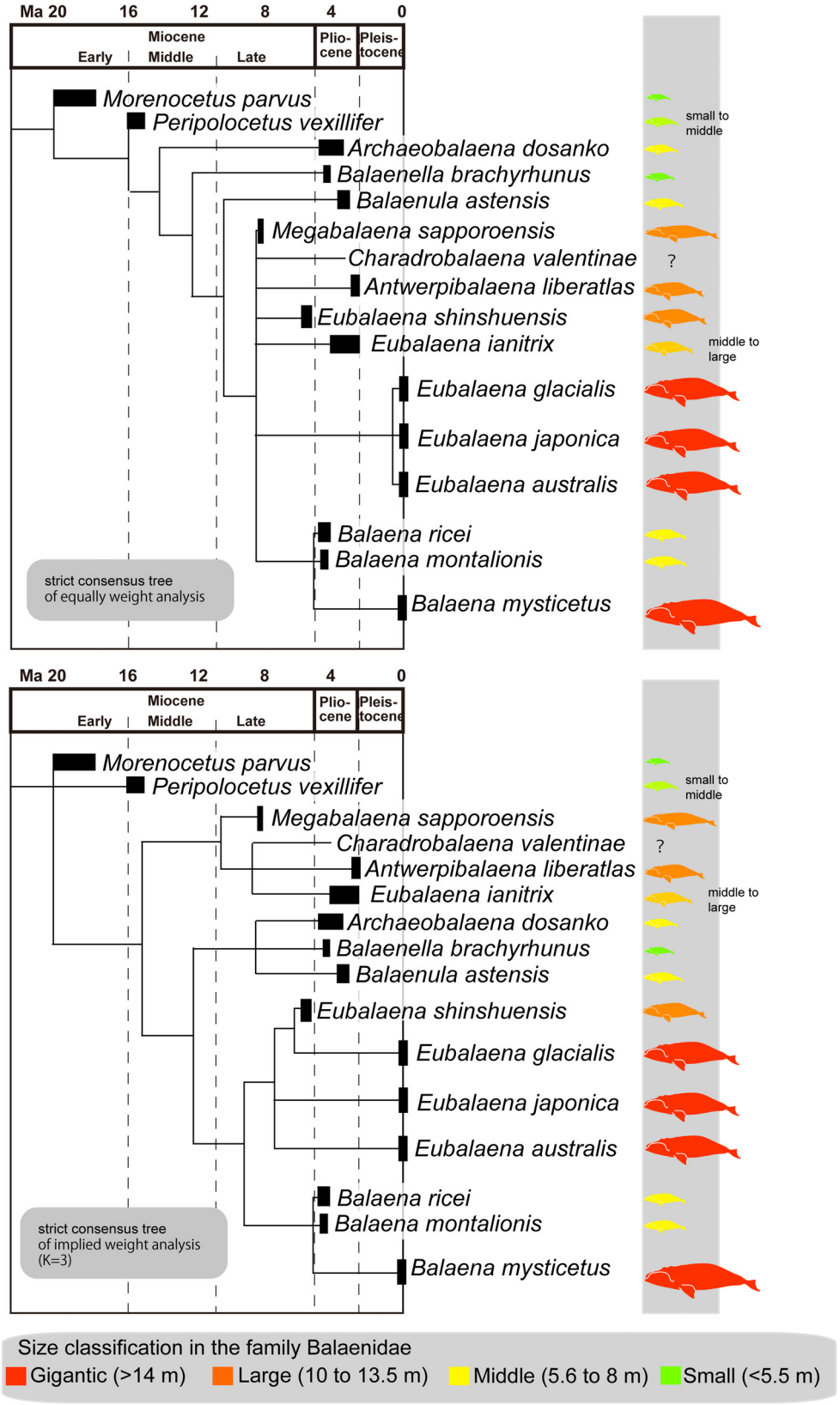

FIGURE 24. Size distribution of the Balaenidae. The topology adopted the 50% majority consensus tree in this study (top in Figure 22). Total length of balaenids were taken from Table 6.

TABLE 6. Estimated total length and size classifications of balaenids. Estimated total length of extinct balaenids except *Megabalaena sapporoensis* were taken from Bisconti et al. (2021). Modern adult total length taken from Jefferson et al. (2008). Age of *Balaena ricei, Balaenella brachyrhynus, Balaenula astensis* and *Balaena montalionis* were taken from supplementary file of Marx and Fordyce (2015).

Species	Specimen	total length in meters	size	age	epoch		locality	reference
Morenocetus parvus	MPL 5-11	4.2	small	Early Miocene	Burdigalian	19.8–18.2	Trelew, Argentina	Bisconti et al., 2021
Peripolocetus vexillifer	CAS 905	5.9	middle	early Middle Miocene	Langhian	16.0–15.2	Sharktooth Hill, California	Bisconti et al., 2021
Peripolocetus vexillifer	SDSNH 99766	4.5	small	early Middle Miocene	Langhian	16.0–15.2	-	Bisconti et al., 2021
Megabalaena sapporoensis	SMAC 2731	12.7	large	early Late Miocene	Tortonian	9.4-8.6	Hokkaido, Japan	This study
Eubalaena shinshuensis	SFMCV-0024	At least 12.0 to 10.8	large	late Late Miocene	Messinian	6.1–5.9	Shinshishinmachi, Nagano, Japan	Bisconti et al., 2021; this study
Archaeobalaena dosanko	FCCP 1049	5.8	middle	Early Pliocene	Zanclean	5.2-3.5	Hokkaido, Japan	Bisconti et al., 2021
Balaenella brachyrhynus	NMB 42001	5.2	small	Early Pliocene	Zanclean	5.0–4.4	Kallo, Belgium	Bisconti et al., 2021
Balaena ricei	USNM 22553	7.1	middle	Early Pliocene	Zanclean	4.9–4.4	Rice's Pit, Virginia	Bisconti et al., 2021
Balaena montalionis	MSNTUP I-12357	7.3	middle	Early Pliocene	Zanclean	4.8–4.4	Casina, Italy	Bisconti et al., 2021
Charadrobalaena valentinae	MCRE 232834	-	large?	Early Pliocene	Zanclean	3.8-3.6	Emilia Romagna, Italy	This study
Balaenula astensis	MSNTUP I-12555	6.5	middle	Early Pliocene	Zanclean	4.0–3.0	Portacomaro, Italy	Bisconti et al., 2021
Balaenidae sp.	MCRE 232834	10.8	large	Early Pliocene	Zanclean	3.81–3.6	-	Bisconti et al., 2021
Eubalaena sp.	MCMV M_PAL_002-005	14.3	gigantic	Late Pliocene	Piacenzian	3.6–2.6	Tuscany, Italy	Bisconti et al., 2021
Antwerpibalaena liberatlas	IRSNB M 2325	10.7 to 9.5	large	Late Pliocene	Piacenzian	3.21–2.76	Belgium	Bisconti et al., 2021
Eubalaena ianitrix	IRSNB M. 879	8.2	middle to large	latest Early to Late Pliocene	-	-	Antwerp, Belgium	Bisconti et al., 2021
Balaena mysticetus	-	20 female, 18 male	gigantic	modern	Holocene	0	-	Jefferson et al., 2008
Eubalaena glacialis	-	17	gigantic	modern	Holocene	0	-	Jefferson et al., 2008
Eubalaena australis	-	17	gigantic	modern	Holocene	0	-	Jefferson et al., 2008
Eubalaena japonica	-	Over 17	gigantic	modern	Holocene	0	-	Jefferson et al., 2008

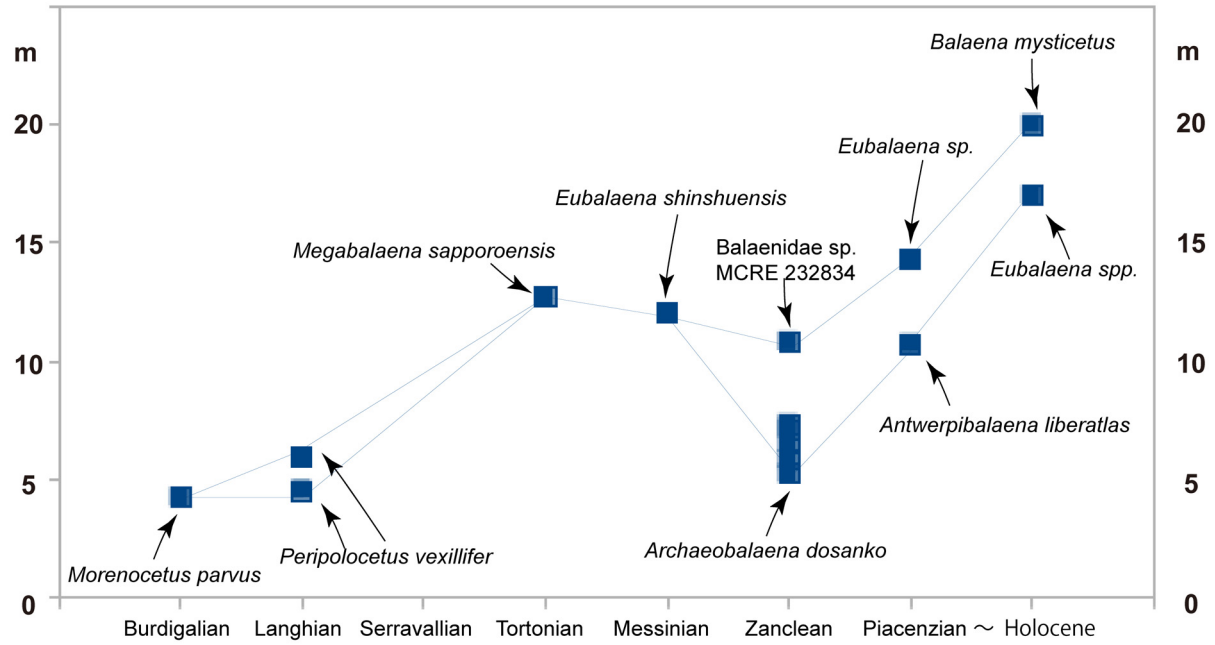

FIGURE 25. Balaenidae diversity with maximum and minimum body size of the Balaenidae over time. Total length of balaenids were taken from Table 6. Some epochs have only one record of balaenid, which can be used for body size estimation. *Eubalaena ianitrix* estimated as 8.2 m of body length is omitted because it has a wide range from latest Early to Late Pliocene.

the analysis of Tanaka et al (2020) in that there is a large unresolved polytomy of *Charadrobalaena valentinae* + *Antwerpibalaena liberatlas* + *Eubalaena shinshuensis* + *Eubalaena ianitrix* and two clades of crown balaenids. *M. sapporoensis* was placed among the unresolved polytomy in the Balaenidae with a long branch length (Figure 23).

Our phylogenetic analysis results were different from one of the latest balaenid study by Bisconti et al. (2021) in a branching pattern of *Peripolocetus vexillifer* and *Caperea marginata*. In their study, *C. marginata* forms a clade with the Balaenidae, and *P. vexillifer* was the most basal taxon among the large group Balaenomorpha. In our analysis, *C. marginata* was placed in the Cetotheriidae and forms a clade with the Balaenopteridae (Figure 23).

DISCUSSION

Gigantism. Body size variations among the Balaenidae are presented here (Figures 24 and 25) using the result of phylogenetic analysis (Figure 23) and estimated body size of extinct species (Table 6). The estimated total lengths of balaenids excluding *Megabalaena sapporoensis* were obtained from Bisconti et al. (2021). Notably, the previously determined total length of *Eubalaena shinshuensis* based on the bizygomatic width (Buono et al., 2017; Slater et al., 2017; Bisconti et al., 2021) about 12.0 to 10.8 m is slightly underestimated, as the specimen lacks the anterior part of the zygomatic process. Thus, the estimated body length is unknown, however it is over 12.0 to 10.8 m. Modern maximum adult total length was taken from Jefferson et al. (2008).

Our phylogenetic analyses results revealed that the earliest balaenids, such as *M. parvus* and *Peripolocetus vexillifer* known from the Early to Middle Miocene respectively are placed as earlier branching taxa. The two earliest balaenids suggest that the total lengths of Balaenidae were originally about 4 to 6 m, which are much smaller than those of modern balaenids reaching 17 to 20 m.

An approximately 9 million years long gap in the Miocene record of balaenids exists after *Peripolocetus vexillifer* (16.0-15.2 Ma) and prior to *Eubalaena shinshuensis* (6.1-5.9 Ma) (Marx and Fordyce 2015). From the late and latest Miocene (approximately 9-6 Ma), *M. sapporoensis* at 12.7 m and *E. shinshuensis at* over 12.0-10.8 m (Bisconti et al., 2021; this study) in length. Currently, *M. sapporoensis* partly fills the Miocene gap of balaenids, and emphasizes that the origin of gigantism is chronologically deeper than previously considered.

TABLE 7. Ratio of the humerus and radius in the Balaenidae. Larger number indicates more slender humerus.

	Humerus; Proximodistal length/minimum anteroposterior length	Humerus; Proximodistal length/ maximum anteroposterior length	Radius; Proximodistal length/minimum anteroposterior length	Radius; Proximodistal length/ maximum anteroposterior length	specimen numbers	Reference
Yamatocetus canaliculatus	3.9	2.4	4.6	3.6	KMNH VP 000,017	Okazaki, 2012
Megabalaena sapporoensis	4.1	2.2	4.2	2.9	SMAC 2731	This study
Antwerpibalaena liberatlas	2.6	1.9	3.5	1.6	IRSNB M2325	Duboys de Lavigerie et al., 2020
Charadrobalaena valentinae	-	-	4.0	2.7	MCRE 232834	Bisconti
Balaena ricei	2.6	1.7	2.8	2.3	USNM 22553	Duboys de Lavigerie et al., 2020
Balaena mysticetus	2.7	1.6	3.5	2.5	ZMUC 1596	Duboys de Lavigerie et al., 2020
Eubalaena australis	2.8	1.7	2.5	1.7	MNHNP A2929	Benke 1993
Eubalaena australis	2.1	1.4	2.7	1.7	NMNZ MM002239	Duboys de Lavigerie et al., 2020

We do not have enough numbers of balaenid fossils from the Late Miocene, thus can not justify are *M. sapporoensis* and *E. shinshuensis* represent a standard size of balaenids at that epochs or not. However, at least the first gigantism in the Balaenidae linage was happened before the Tortonian.

From the Zanclean to Quaternary, the maximum size of balaenids increased dramatically and size disparity of the balaenids were declined (Figure 25). Our phylogenetic hypotheses showed that the extant and largest member of the family *Balaena mysticetus* has two middle-sized extinct relatives. It suggests that the linage leading to *Balaena mysticetus* became gigantic during the late Pliocene to Pleistocene or later. During the Pliocene, small balaenids were thought to have declined as a result of the onset of Northern Hemisphere glaciation and more patchy prey distribution (Marx and Fordyce, 2015; Slater et al., 2017). There are several balaenid fossils from the Pleistocene (e.g., Boessenecker, 2013). Adding named and phylogenetically examined Pleistocene balaenids will help to illuminate how extant large balaenids emerged and such small fossil balaenids disappeared.

Thus, we still cannot conclude that the body size of the Balaenidae increased over geological time (Duboys de Lavigerie et al., 2020). In terms of body size diversity, *M. sapporoensis* enhances our understanding of balaenid diversity, which was seems have expanded at least before the Late Miocene. In addition, a recent study of Nagasawa et al (2024) reported three large mandibles of mysticetes from the middle Miocene (about 13 to 12 Ma), which were revealed as cross-sections in huge concretion at the coast in Oga Peninsula, Akita, Japan. These mandibles were identified as balaenids and estimated their body sizes as 16 to 23 meters based on the cross-section shapes of the mandibles. We hope that these fossils at the site to be preserved and provided more detailed studies of these fossils to understand the origin of the first gigantism among the Balaenidae before the Late Miocene.

As fossil records of the Late Miocene balaenids are still limited, more balaenid records from this period and earlier in the Miocene are needed to develop a more detailed understanding of body size evolution including the origin(s) of gigantism.

Filling a part of morphological gap of the Balaenidae. The early balaenids are poorly known due to the scarce fossil record, *M. sapporoensis* helps fill a part of 9-million-year gap in the fossil

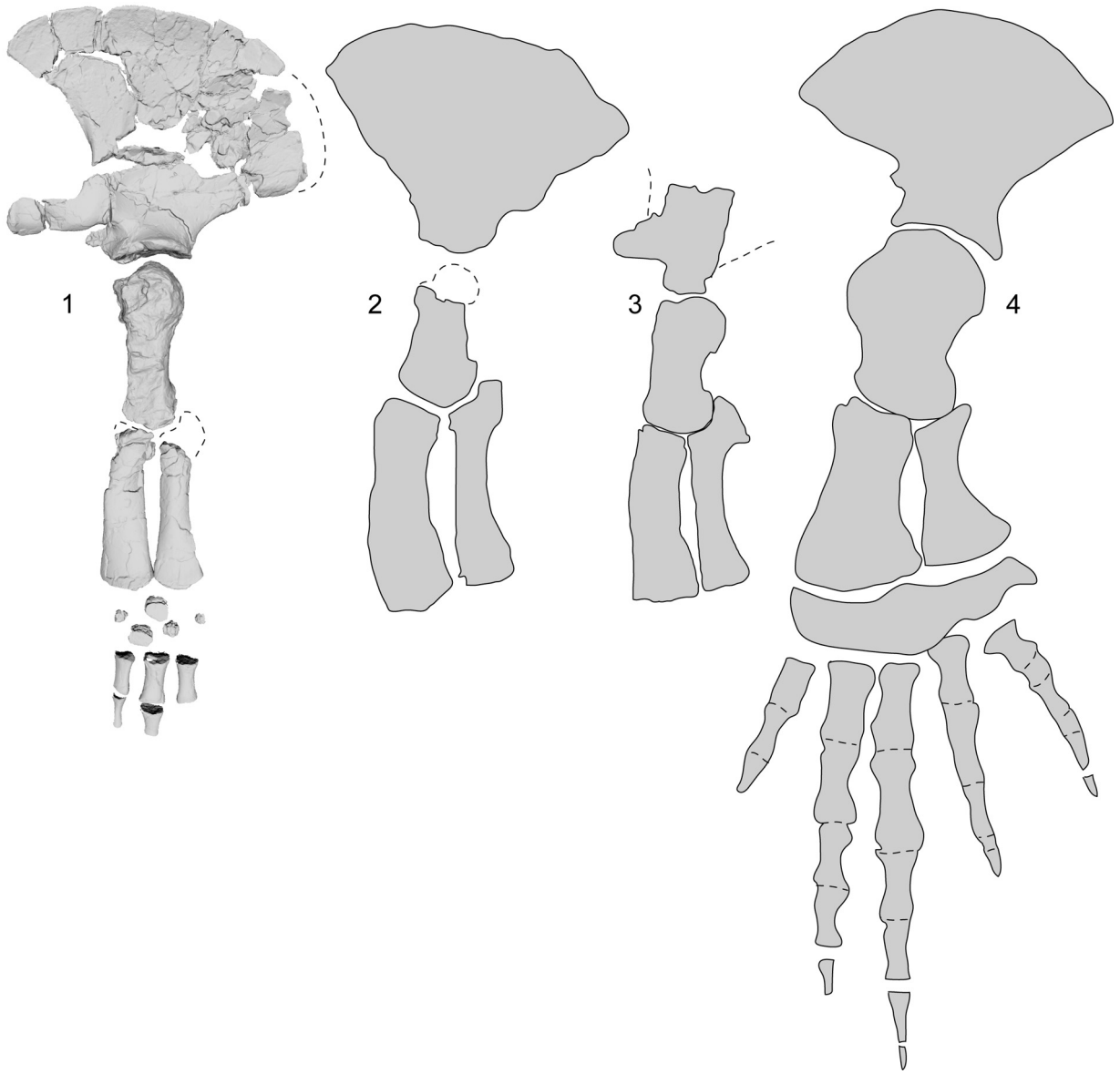

FIGURE 26. Forelimb elements of balaends. *Megabalaena sapporoensis* (A), *Charadrobalaena valentinae,* outline taken from Bisconti et al. (2023) and is a mirror image (B), *Antwerpibalaena liberatlas*, outline taken from Duboys de Lavigerie et al. (2020) and is a mirror image (C), *Eubalaena japonica*, outline taken from Omura (1958) (D), and are not to scale.

record, connecting primitive conditions to specialized modern balaenids. A brief trend of the flipper shape of Miocene to modern balaenids is changed from slender to robust.

The flipper shape of modern balaenids are broad and paddle-like, aiding in low-speed maneuverability (Figure 26) (Benke, 1993; Cooper et al., 2007; DuBoys de Lavigerie et al., 2020). Previously, the Pliocene balaenid *Antwerpibalaena liberatlas* was documented a "previously unseen variability in balaenid flipper shape," with more slender forelimb long bones (Duboys de Lavigerie et al., 2020). Notably, the preserved humerus and radius of *M. sapporoensis* display even more slender (Table 7), resembling those of the eomysticetid *Yamatocetus canaliculatus* (Okazaki, 2012). Compared with *Y. canaliculatus*, *M. sapporoensis* has a lower deltoid ridge on the humerus and an anteroposteriorly longer distal end of both the ulna and radius. Compared with *A. liberatlas, M. sapporoensis* has a semi globular humerus head and anteroposteriorly shorter distal ends of the ulna and

TABLE 8. Comparison of the conditions of cervical vertebra fusion among the family Balaenidae. “Sep” means separated. “Fu” means fused.

Species	age		Specimen number	Ontogenetic state	Atlas	Axis	C3	C4	C5	C6	C7	reference
Morenocetus parvus	Early Miocene	19.8–18.2	MLP 5–11	subadult	?	?	?	?	?	?	?	Cabrera 1926, Buono et al., 2017
Megabalaena sapporoensis	Early Late Miocene	9.4-8.6	SMAC 2731	adult	Sep	Fu	Fu	Sep	Sep	Sep	Sep	This study
Balaena ricei	Early Pliocene	4.9–4.4	USNM 22553	physically immature	Fu	Fu	Fu	Fu	Fu	Fu	Fu	Westgate and Whitmore 2002
Charadrobalaena valentinae	Early Pliocene	3.8-3.6	MCRE 232834	older than juvenile	Fu	Fu	Fu	Fu	Fu	Fu	Fu	Bisconti et al., 2023
Antwerpibalaena liberatlas	Late Pliocene	3.21–2.76	IRSNB M2325	adult	Sep	Fu	Fu	Fu	Fu	Fu	Fu	Duboys de Lavigerie et al., 2020
Balaenula balaenopsis	Zanclean/ Piacenzian	?	-	young	Sep	Fu	Fu	Fu	Fu	Fu	Sep	Van Beneden 1872
Balaenotus insignis	Zanclean/ Piacenzian	?	-	-	Sep	Fu	Fu	Fu	Fu	Fu	Sep	Van Beneden 1872, Abel 1941
Balaena mysticetus	modern		-	adult	Fu	Fu	Fu	Fu	Fu	Fu	Fu	Jefferson et al., 2008
Balaena mysticetus	modern		-	young	Fu	Fu	Fu	Fu	Fu	Fu	Sep	Nishiwaki and Kasuya 1970
Eubalaena glacialis	modern		-	adult	Fu	Fu	Fu	Fu	Fu	Fu	Fu	Jefferson et al., 2008
Eubalaena australis	modern		-	adult	Fu	Fu	Fu	Fu	Fu	Fu	Fu	Jefferson et al., 2008
Eubalaena japonica	modern		-	adult	Fu	Fu	Fu	Fu	Fu	Fu	Fu	Jefferson et al., 2008

radius. A proportion of the humerus such as proximodistal length/anteroposterior maximum length of the humerus are 2.2 *(M. sapporoensis),* 1.9 *(A. liberatlas),* 1.3 *(Eubalaena japonica),* which suggests that the humerus of balaenids became robust. A proportion of the radius such as proximodistal length/anteroposterior length of the distal end of the radius are 2.8 *(M. sapporoensis),* 2.8 *(C. valentinae),* 2.6 *(A. liberatlas),* 1.6 *(Eubalaena japonica),* which also suggests that the radius of balaenids became robust. We could not use the ulna, because its proximal end is not preserved in *M. sapporoensis*, however most likely the ulna might had the same trend to these of the humerus and radius. In addition, a ratio of the upper and lower arms such as proximodistal length of the humerus and radius are 1.0 *(M. sapporoensis),* 0.8 *(A. liberatlas),* 1.0 *(E. japonica),* which suggests that the ratio of the upper and lower arm length is not so changed from Miocene to modern balaenids.

Thus, from early members to modern balaenids, the forelimb elements were changed from longer and narrower flippers to more robust ones (Figure 27, Table 7) These morphological changes suggest different forelimb usage among these species.

Unlike many modern toothed whales, baleen whales generally have unfused and separated neck vertebrae. However, modern adult balaenids exhibit seven completely fused cervical vertebrae. These differences of cervical vertebra fusion had been hypothesized because of difference in feeding behavior such as the size of prey and locomotion styles that may impose varied forces on the neck (VanBuren and Evans, 2017). Here, we compare cervical vertebra fusion in the Balaenidae (Table 8). Notably, the neck vertebra fusion progresses possibly through ontogeny, as the vertebraterial epiphyses fuse through ontogeny (Moran et al., 2015). A young extant *Balaena mysticetus* has a fused 1st to 6th cervical vertebrae and separate 7th cervical vertebra (Nishiwaki and Kasuya 1970). Thus, Table 8 includes suggested ontogenetic stage of compared specimens.

The Late Pliocene balaenid *Antwerpibalaena liberatlas* also has fused 2nd to 7th cervical vertebrae, however the atlas is separated (Duboys de Lavigerie et al., 2020). Two other Early Pliocene

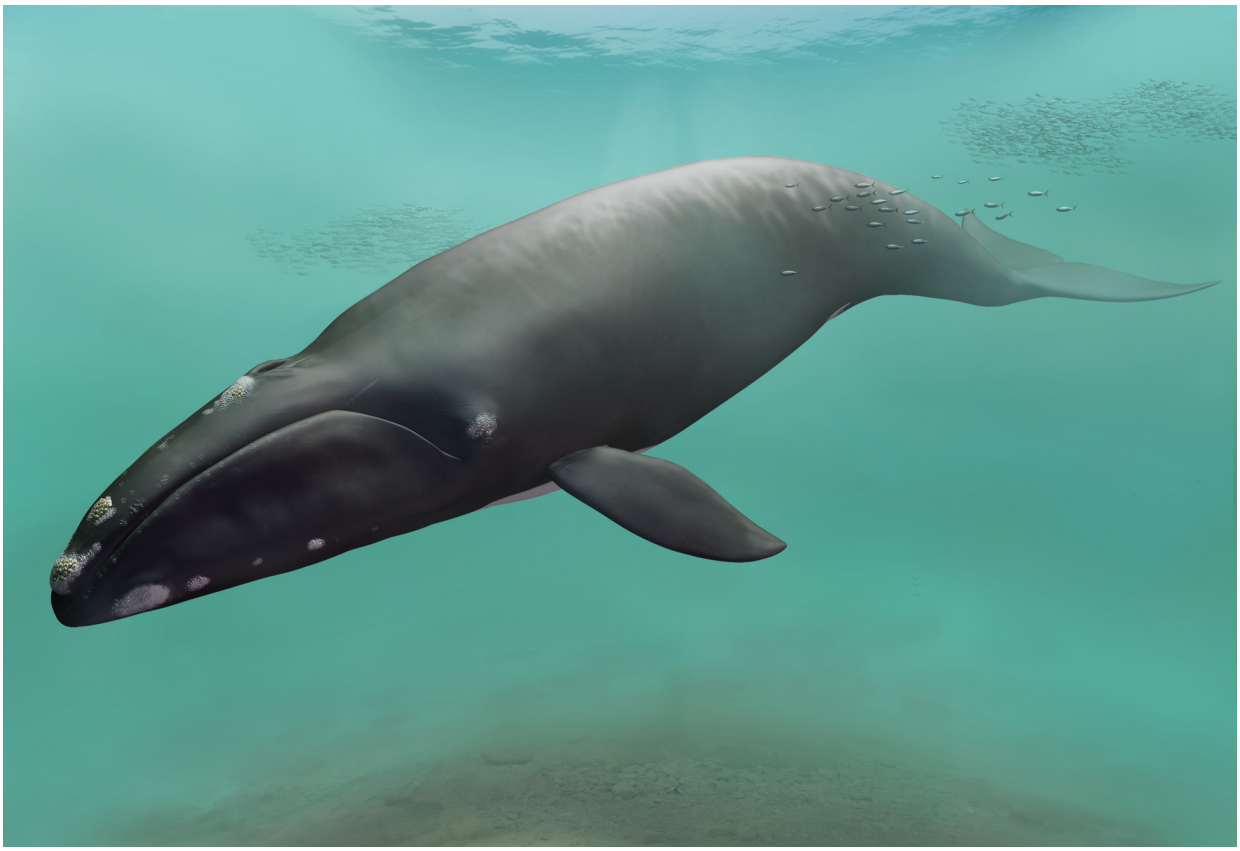

FIGURE 27. Restoration of *Megabalaena sapporoensis* by Tatsuya Shinmura (Ashoro Museum of Paleontology).

balaenids, *Balaena ricei* (adult) and *Charadrobalaena valentinae* (older than juvenile) display completely fused cervical vertebrae (Westgate and Whitmore 2002; Bisconti et al., 2023). Descriptions of Van Beneden (1872) state that the holotype of *Balaenula balaenopsis*, which is a young individual has a separated atlas and seventh cervical vertebra. However, *B. balaenopsis* elements reported in Van Beneden (1872) are possibly not belonging to one individual (Buono et al., 2017). *Balaenotus insignis* has a separated atlas (with fused fifth and sixth cervical vertebrae are fused [Abel, 1941]).

The earliest known balaenid *Morenocetus parvus,* was initially reported to have fused second to fifth cervical vertebrae (Cabrera 1926). However, a later study noted that these vertebrae are currently missing, and a previously identified mandible attributed to *M. parvus* actually dates from the Pleistocene or later, making it unrelated to the original individual (Buono et al., 2017). Thus, the original description of the cervical vertebrae of *M. parvus* is doubtful.

Megabalaena sapporoensis provides the oldest and reliable morphological data on the cervical evolution of the Balaenidae. It has partially fused cervical vertebrae, and separated the axis and third cervical vertebra (Figure 18). There is possibility that the atlas and axis were fused via the broken and lost neural arch of the atlas and the neural spine of the axis. Therefore, in adult individuals of the Balaenidae, cervical vertebral fusion possibly began with the axis and third cervical vertebra during the Late Miocene, then vertebral fusion was followed by the fourth to sixth cervical vertebra. Finally, all cervical vertebrae were fused by the Early Pliocene, over a span of 4 million years.

CONCLUSION

Megabalaena sapporoensis gen. et sp. nov. (SMAC 2731) represents an archaic balaenid from the Late Miocene (9.0 ± 0.4 Ma), discovered in the upper part of the Toyama Formation, Sapporo, Hokkaido, Japan. It is distinguishable from other balaenids by its unfused cervical vertebrae, except the axis and third cervical vertebra, and its slender forelimb long bones, including the humerus, radius, and ulna. These features are considered primitive among the Balaenidae. *M. sapporoensis* partly fills

a 9-million-years gap in the fossil record, bridging the transition from primitive states to specialized modern balaenids. Phylogenetic analyses place *M. sapporoensis* as more derived than *Balaenula astensis* within a large unresolved polytomy that includes *Eubalaena shinshuensis*, extant species of *Eubalaena* and others (equally weight analysis), and place *M. sapporoensis* in a clade with *Charadrobalaena valentinae* + *Antwerpibalaena liberatlas* + *Eubalaena ianitrix* (implied weight analysis). The estimated body length of *M. sapporoensis* is 12.7 m, which is three times longer than the oldest known balaenid, *Morenocetus parvus*. Overall, *M. sapporoensis* expands our understanding of early balaenid body size diversity during the Miocene.

AUTHORS' CONTRIBUTIONS

Authors' contributions. H.F. originally started the study and provided ideas of discussion. H.F. was passed away in 2023 during this research project running. T.K. carried out the first phylogenetic analysis. Y.T. wrote the first draft and carried out the phylogenetic analysis presented in this manuscript. T.K. prepared some figures, and provided some ideas on discussion. T.S. created 3D restorations. H.O. examined geologic age by fission track dating. T.K., T.S. and H.O. revised manuscript.

Funding. This work was partly supported by Japan Society for the Promotion of Science [KAKENHI Grant Numbers JP18K01110] to TK.

ACKNOWLEDGEMENTS

Thanks go to K. Mori to discover the study material. Citizens and staffs of Sapporo Museum Activity Center for digging up the specimen, and Construction management department of Hokkaido for their advice between 2008 and 2012. J. Kagemoto (Matsunoyu, Kogakeyu Onsen) provided permission to dig up the specimen. I. Sato and others for help in digging up the specimen in 2014. T. Kato and T. Oka (Earthscience Co.) helped for geological survey at the locality. H. Takanashi, Y. Tachi, T. Hiyoriyama, S. Amano, N. Morishita, M. Yoshii (all Sapporo Natural History Research Group), K. Arayama, I. Kawamata, S. Kimura, N. Nagase, T. Okano, Y. Onoe, M. Ozaki, M. Usuda (all volunteers at Hokkaido University Museum), M. Kimura, R. Sasaki, M. Takahashi, staff of SMAC and others for preparation of the specimen. We thank N. Kohno, Y. Tajima and T.K. Yamada (all NMNS) and G. Nakamura (MTUF) for their permissions to examine comparative specimens. We thank O. Lambert (Institut royal des Sciences naturelles de Belgique), R.W. Boessenecker (University of California Museum of Paleontology) and an anonymous referee for their constructive comments on this manuscript. Also, H. F. thanks to H. Ichishima (Fukui Prefectural Dinosaur Museum) for his advice on baleen whale fossils. Neutron irradiation in fission-track dating was partially supported by the Joint Usage/Research of the Institute for Integrated Radiation and Nuclear Science, Kyoto University (KURNS).

REFERENCES

Abel, O. 1941. Vorläufige mitteilungen uber die revision der fossilen Mystacoceten aus dem Tertiär Belgiens (Zweiter Bericht). Bulletin du Musée royal d'Histoire naturelle de Belgique, 17:1-29.

Allen, J.A. 1908. The North Atlantic right whale and its near allies. Bulletin of the AMNH; v. 24, article 18. New York: Published by order of the Trustees, American Museum of Natural History.

Benke, H. 1993. Investigations on the osteology and the functional morphology of the flipper of whales and dolphins (Cetacea). Investigations on Cetacea, 24:9-252.

Bisconti, M. 2003. Evolutionary history of Balaenidae. Cranium, 20:9-50.

Bisconti, M. 2005. Skull morphology and phylogenetic relationships of a new diminutive balaenid from the Lower Pliocene of Belgium. Palaeontology, 48:793-816.

Bisconti, M., Chicchi, S., Monegatti, P., Scacchetti, M., Campanini, M., Marsili, S., and Carnevale, G. 2023. Taphonomy, osteology and functional morphology of a partially articulated skeleton of an archaic Pliocene right whale from Emilia Romagna (NW Italy). Bollettino della Società Paleontologica Italiana, 62:1-22.

Bisconti, M., Pellegrino, L., and Carnevale, G. 2021. Evolution of gigantism in right and bowhead whales (Cetacea: Mysticeti: Balaenidae). Biological Journal of the Linnean Society, XX: 1-27.

Boessenecker, R.W. 2013. A new marine vertebrate assemblage from the Late Neogene Purisima Formation in Central California, part II: pinnipeds and cetaceans. Geodiversitas, 35:815-940. https://doi.org/10.5252/g2013n4a5

Buono, M.R., Fernández, M.S., Cozzuol, M.A., Cuitiño, J.I., and Fitzgerald, E.M.G. 2017. The early Miocene balaenid *Morenocetus parvus* from Patagonia (Argentina) and the evolution of right whales. PeerJ, 5:e4148. https://doi.org/10.7717/peerj.4148

Cabrera, Á. 1926. Cetáceos fósiles del Museo de la Plata. Revista del Museo de la Plata, 29:363-411.

Capellini, G. 1905. Balene fossili toscane. III. *Idiocetus guicciardinii*. Memorie della Regia accademia delle Scienze dell'Istituto di Bologna, 6: 71-80.

Committee on Taxonomy. 2022. Retrieved February 27, 2023, from https://marinemammalscience.org/science-and-publications/list-marine-mammal-species-subspecies/

Cooper, L.N., Berta, A., Dawson, S.D., and Reidenberg, J.S. 2007. Evolution of hyperphalangy and digit reduction in the cetacean manus. The Anatomical Record, 290:654-672.

Duboys de Lavigerie, G.D., Bosselaers, M., Goolaerts, S., Park, T., Lambert, O., and Marx, F.G. 2020. New Pliocene right whale from Belgium informs balaenid phylogeny and function. Journal of Systematic Palaeontology, 18:1141-1166.

Flower, W.H. 1864. Notes on the skeletons of whales in the principal museums of Holland and Belgium, with descriptions of two species apparently new to science. Proceedings of the Zoological Society of London, 1864: 384-420.

Flower, W.H. 1885. An Introduction to the Osteology of the Mammalia. 3 ed. Macmillan and Co., London.

Furusawa, H. 2007. Sirenian fossils, p. 60-68. In Sapporo Museum Activity Center (ed.), A comprehensive survey of mammal fossils from Sapporo. Sapporo Museum Activity Center, Hokkaido.

Galbraith, R.F. 1981. On statistical models for fission track counts. Journal of the International Association for Mathematical Geology, 13:471-488.

Galatius, A. and Kinze, C.C. 2003. Ankylosis patterns in the postcranial skeleton and hyoid bones of the harbour porpoise *(Phocoena phocoena)* in the Baltic and North Sea. Canadian Journal of Zoology, 81:1851-1861. https://doi.org/10.1139/z03-181

Goloboff, P.A. and Catalano, S.A. 2016. TNT version 1.5, including a full implementation of phylogenetic morphometrics. Cladistics, 32:221-238. https://doi.org/10.1111/cla.12160.

Ito, H. and Miyazaki, N. 1990. Skeletal development of the striped dolphin *(Stenella coeruleoalba)* in Japanese waters. Journal of the Mammalogical Society of Japan, 14:79-96. https://doi.org/10.11238/jmammsocjapan1987.14.79

Jefferson, T.A., Webber, M.A., and Pitman, R.L. 2008. Marine Mammals of the World: a Comprehensive Guide to their Identification. Academic Press, Oxford, UK.

Kellogg, R. 1931. Pelagic mammals from the Temblor Formation of the Kern River region, California. Proceedings of the California Academy of Sciences, 19:217-397.

Kimura, T. 2009. Review of the fossil balaenids from Japan with a re-description of *Eubalaena shinshuensis* (Mammalia, Cetacea, Mysticeti). Quaderni del Museo di Storia Naturale di Livorno, 22:3-21.

Kimura, T., Narita, K., Fujita, T., and Hasegawa, Y. 2007. A new species of *Eubalaena* (Cetacea: Mysticeti: Balaenidae) from the Gonda Formation (latest Miocene-Early Pliocene) of Japan. Bulletin of Gunma Museum of Natural History, 11:15-27.

Maddison, W.P. and Maddison, D.R. 2021. Mesquite: a modular system for evolutionary analysis. Available at http://mesquiteproject.org

Marx, F.G. and Fordyce, R.E. 2015. Baleen boom and bust: a synthesis of mysticete phylogeny, diversity and disparity. Royal Society Open Science, 2:140434. https://doi.org/10.1098/rsos.140434

Marx, F.G. and Lambert, O. 2021. Fossil record, p. 11-17. The Bowhead Whale. Elsevier.

McGowen, M.R., Spaulding, M., and Gatesy, J. 2009. Divergence date estimation and a comprehensive molecular tree of extant cetaceans. Molecular Phylogenetics and Evolution,

53:891-906.
https://doi.org/10.1016/j.ympev.2009.08.018
Mead, J.G. and Fordyce, R.E. 2009. The therian skull: a lexicon with emphasis on the odontocetes. Smithsonian Contributions to Zoology, 627:1-248.
https://doi.org/10.5479/si.00810282.627
Moran, M.M., Bajpai, S., George, J.C., Suydam, R., Usip, S., and Thewissen, J.G.M. 2015. Intervertebral and epiphyseal fusion in the postnatal ontogeny of cetaceans and terrestrial mammals. Journal of Mammalian Evolution, 22:93-109.
https://doi.org/10.1007/s10914-014-9256-7
Nagasawa, K., Watanabe, A., Sawaki, H., Watanabe, H., and Kawabe, T. 2024. Fossil mandibles of baleen whales in huge concretions of the Middle Miocene, Oga Peninsula, Akita Prefecture, Northeast Japan. Journal of Fossil Research, 57:15-25.
Ohira, H. 2004. Fission track ages of zircons from Miocene tuffs in the Hiki Hills and the Arakawa River, Saitama Prefecture, central Japan. Monograph of Association for the Geological Collaboration in Japan. 52:51-65.
Okazaki, Y. 2012. A new mysticete from the upper Oligocene Ashiya Group, Kyushu, Japan and its significance to mysticete evolution. Bulletin of the Kitakyushu Museum of Natural History and Human History, Series A (Natural History), 10:129-152.
Omura, H. 1958. North Pacific right whale. Scientific Reports of the Whales Research Institute, 13:1-52.
Omura, H., Ohsumi, S., Nemoto, T., Nasu, K., and Kasuya, T. 1969. Black right whales in the North Pacific. Scientific Reports of the Whales Research Institute, 21:1-78.
Ozaki, M. and Komatsubara, T. 2014. 1:200,000 Land geological map in the Ishikari Depression and its surrounding area with explanatory note, p. 1-28. S-4. Seamless Geoinformation of Coastal Zone “Southern Coastal Zone of the Ishikari Depression.” Geological Survey of Japan.
Pyenson, N.D. and Sponberg, S.N. 2011. Reconstructing body size in extinct crown Cetacea (Neoceti) using allometry, phylogenetic methods and tests from the fossil record. Journal of Mammalian Evolution, 18:269-288.
Shinmura, T., Tanaka, Y., and Furusawa, H. 2024. Using 3D CG technology for the reconstruction of whale fossils. Journal of Fossil Research, 57(1/2): 44-49.
Slater, G.J., Goldbogen, J.A., and Pyenson, N.D. 2017. Independent evolution of baleen whale gigantism linked to Plio-Pleistocene ocean dynamics. Proceedings of the Royal Society B: Biological Sciences, 284:1-8.
https://doi.org/10.1098/rspb.2017.0546
Suzuki, A. 2007. Molluskan fossils, p. 69-75. A comprehensive survey of mammal fossils from Sapporo. Sapporo Museum Activity Center.
Tanaka, Y. 2024. A feeding organ the basihyal and thyrohyal tells which size of prey do true baleen whales (Cetacea, Chaeomysticeti) eat. Palaeontologia Electronica, 27:a8.
https://doi.org/10.26879/1311
Tanaka, Y., Furusawa, H., and Kimura, M. 2020. A new member of fossil balaenid (Mysticeti, Cetacea) from the early Pliocene of Hokkaido, Japan. Royal Society Open Science, 7:1-20.
Tanaka, Y. and Kohno, N. 2015. A new late Miocene odobenid (Mammalia: Carnivora) from Hokkaido, Japan suggests rapid diversification of basal Miocene odobenids. PLoS ONE, 1-25.
https://doi.org/10.1371/journal.pone.0131856
Tanaka, Y. and Taruno, H. 2019. The First Cetacean Record from the Osaka Group (Middle Pleistocene, Quaternary) in Osaka, Japan. Paleontological Research, 23:166-173.
https://doi.org/10.2517/2018PR016
Tanaka, Y. and Taruno, H. 2022. First record of a right whale fossil from the pre-historic period of Japan. Aquatic Mammals, 48:255-261.
Tanaka, Y. and Taruno, H. 2024. Remains of a fin whale from Osaka, Japan, and comparison of baleen whale cases in the past and present of Osaka Bay (Seto Inland Sea). Mammal Study, 49:217-228.
https://doi.org/10.3106/ms2023-0041
Tsai, C.H. and Fordyce, R.E. 2015. The earliest gulp-feeding mysticete (Cetacea: Mysticeti) from the Oligocene of New Zealand. Journal of Mammalian Evolution, 22:1-26.
Van Beneden, P.J. 1872. Les baleines fossiles d’Anvers. Bulletins de L’Academie Royale des Sciences, des Lettres et des Beaux-arts, 2:6-20.

Van Beneden, P.J. 1880. Description des ossements fossiles des environs d'anvers: Cétacés Genre *Balaenula, Balaena* et *Balaenotus*. Annales du Musée Royal d'Histoire Naturelle de Belgique. Série Paléontologique. Hayez.

VanBuren, C.S. and Evans, D.C. 2017. Evolution and function of anterior cervical vertebral fusion in tetrapods. Biological Reviews, 92:608-626. Wiley Online Library.

Westgate, J.W. and Whitmore, F.C. 2002. *Balaena ricei*, a new species of bowhead whale from the Yorktown Formation (Pliocene) of Hampton, Virginia. Smithsonian Contributions to Paleobiology, 93:295-312.

Woodward, B.L., Winn, J.P., and Fish, F.E. 2006. Morphological specializations of baleen whales associated with hydrodynamic performance and ecological niche. Journal of Morphology, 267:1284-1294.

APPENDIX 1.

Datamatrix in NEXUS format.
(Download file at https://palaeo-electronica.org/content/2025/5581-archaic-balaenid-from-japan)

APPENDIX 2.

Datamatrix in TNT format.
Download file at https://palaeo-electronica.org/content/2025/5581-archaic-balaenid-from-japan)

APPENDIX 3.

Character list. The all characters are cited from Tanaka et al (2020), which was derived from Buono et al. (2017).

Skull

1. Length of rostral portion of maxilla anterior to antorbital notch: less than bizygomatic width (0); equal to or greater than bizygomatic width (1); more than one and a half times the bizygomatic width (2).

2. Portion of rostrum anterior to nasals in lateral view: below the level of the supraoccipital (0); raised to the level of the supraoccipital (1); raised above the level of the supraoccipital (2)

3. Lateral edge of maxilla in cross section: forms an angle of more than 45 degrees (0); lateral edge is flattened with an angle of less than 45 degrees (1).

4. Lateral border of maxilla anterior to antorbital notch (or homologous point on rostrum) in dorsal view: concave (0); straight or slightly convex (1); broadly convex (2).

5. Transverse width of maxilla at midpoint: distinctly less than that of the premaxilla (0); roughly equal to or up to twice the width of the premaxilla (1); more than twice the width of the premaxilla (2).

6. Premaxilla in dorsal view: widens at anterior end (0); portion anterior to nasal opening narrows or remains the same width anteriorly (1).

7. Premaxilla adjacent to and anterior to narial fossa: elevated above the maxilla and forming a distinct lateral face (0); continuous or nearly continuous with the maxilla (1).

8. Premaxilla adjacent to and at posterior edge of nasal opening: does not clearly overhang maxilla (0); premaxilla overhangs maxilla (1).

9. Anterior portions of premaxillae: firmly contact each other (0); premaxillae are separated or only loosely contact along their entire length (1).

10. Suture between maxilla and premaxilla on rostrum: firmly articulated (0); loose (1).

11. Antorbital process: absent (0); present and defined by a steep face clearly separating the posterolateral corner of the maxilla from its more anterior rostral portion (1); present as a distinct anterior projection lateral to antorbital notch (2).

12. Anterior border of supraorbital process lateral to ascending process of the maxilla: b by lacrimal and maxilla (0); b by lacrimal only (1); as state 0, but with the antorbital process of the maxilla and the anterior border of the supraorbital process separated by a basin (2); as state 0 but with maxilla overriding the anteriormost border of the supraorbital process (3).

13. Distinct pocket between the ascending process of the maxilla dorsally and the supraorbital process ventrally: absent (0); present (1).

14. Lateral process of maxilla (*sensu* Marx, Lambert & Uhen, 2016): absent (0); present and clearly distinct from ascending process of maxilla (1); present and confluent with ascending process of maxilla (2).

15. Lateral process of the maxilla: directed posterolaterally at an oblique angle to the anteroposterior axis of the cranium (0); directed laterally, nearly perpendicular to the anteroposterior axis of the cranium (1).

16. Posterior portion of palatal surface of maxilla: flattened or slightly concave (0); medial portion of maxilla forms a longitudinal keel b laterally by a shallow longitudinal trough (1); medial portion forms a keel without any adjacent trough (2).

17. Palatal surface of anterior part of rostrum: flat or gently concave (0); bears pronounced longitudinal keel formed by the vomer and the medial edges of the maxillae (1).

18. Exposure of premaxilla on palate: exposed along at least one third of the medial border of the maxilla (0); limited in extent to less than one third of the medial border of the maxilla (1).

19. Palatal window exposing vomer: absent (0); present (1); narrow and variable exposure of vomer along most or all of the midline of the rostrum (2); vomer broadly exposed along the midline of the rostrum (3).

20. Palatal nutrient foramina and sulci: absent (0); present (1).

21. Outline of suture between maxillae, vomer and palatines: roughly straight transversely or bowed anteriorly (0); forms a posteriorly pointing V shape (1); anterior margins of palatines form two separate and posteriorly pointing U shapes (2).

22. Anteriormost point of palatine: located in line with or posterior to the level of the antorbital notch or equivalent point on rostrum (0); located anterior to the level of the antorbital notch (1).

23. Anterior portion of palatine distinctly concave transversely and forming a sharp median crest: absent (0); present (1).

24. Anterior edge of nasal fossa: located in posterior three quarters of rostrum (0); located in anterior quarter of rostrum (1).

25. Facial portion of rostrum in lateral view: step-like (0); straight (1); concave (2).

26. Rostrum shape: width at antorbital notches or equivalent point on rostrum less than 80% the length of the rostrum, as measured from its tip to the antorbital notches (0); width at antorbital notches or equivalent point more than 80% the length of the rostrum (1).

27. Teeth in adult individuals: present (0); absent or vestigial (1).

28. Skull length about one third or more of total body length: absent (0); present (1).

29. Cranial asymmetry: present (0); absent (1).

30. Diameter of orbit as measured between the distalmost points of the preorbital and postorbital processes: less than 25% of bizygomatic width (0); 25% or more (1).

31. Anterior edge of supraorbital process lateral to ascending process of maxilla with the skull in dorsal view: oriented transversely or pointing anteriorly (0); pointing posteriorly (1); linguiform and tapering to a point (2).

32. Outline of anterior edge of supraorbital process in dorsal view: roughly straight or concave (0); distinctly sinusoidal (1).

33. Transverse width of anterior edge of supraorbital process lateral to ascending process of maxilla: longer than or equal to the combined transverse width of the adjacent rostral bones, as measured from the sagittal plane to the lateral border of the ascending process of the maxilla (0); shorter than the combined transverse width of the adjacent rostral bones (1).

34. Posterior border of supraorbital process in dorsal view: concave (0); straight (1).

35. Supraorbital process of frontal in anterior view: horizontal or nearly horizontal (0); gradually slopes away lateroventrally from the skull vertex (1); as state 1 but with the lateral portion of the supraorbital being nearly horizontal, thus causing the latter to appear concave in anterior view (2); abruptly depressed to a level noticeably below the vertex, with the lateral skull wall above the supraorbital formed by both parietal and frontal (3).

36. Anterior and posterior borders of supraorbital process in dorsal view: roughly parallel or converging medially (0); converging laterally (1).

37. Width of supraorbital process as measured in a straight line from the lateralmost point of the postorbital process to the intertemporal constriction: equal to or shorter than the anteroposterior length of the supraorbital process above the orbit (0); up to twice the length above the orbit (1); more than twice the length above the orbit (2).

38. Postorbital process in dorsal view: oriented posteriorly (0); oriented laterally (1); oriented posterolaterally (2); short and not markedly projecting in any direction (3).

39. Postorbital process in lateral view: pointed or rounded (0); forms and anteroposteriorly elongate triangle with a flattened posterior face (1).

40. Orbital rim of supraorbital process of frontal in lateral view: dorsoventrally thin (0); thickened with a flat lateral surface (1); thickened with a rounded lateral surface (2).

41. Position of anteriormost point of supraorbital process in dorsal view: in line with the posterior extremity of the nasals or passing through the nasals (0); at the same level as the anterior extremity of the nasals (1); anterior to the anterior extremity of the nasals (2).

42. Position of the dorsal margin of the orbit (in lateral view, with skull resting on a horizontal surface): above or in line with the vertex of the skull (0); located roughly a half of distance between the vertex of the skull and the ventral surface of the postglenoid process (1) located a 2/3 the vertical distance between the vertex of the skull and the ventral surface of the postglenoid process (2); located a 1/3 the vertical distance between the vertex of the skull and the ventral surface of the postglenoid process (3)

43. Lacrimal in dorsal view: situated entirely lateral to the ascending process of the maxilla (0); lacrimal extends medially and separates the lateral corner of the ascending process from the more anterior portion of the maxilla (1).

44. Contact of jugal with zygomatic process of squamosal: the two bones overlap dorsoventrally (0); little or no overlap (1).

45. Anteriormost portion of jugal broadly underlapped by maxilla: absent (0); present (1).

46. Optic canal in ventral view: ventrally open (0); medial portion is enclosed by anterior and/or posterior bony laminae (1).

47. Postorbital ridge along medial portion of optic canal: absent or anteroposteriorly thin, with the optic canal running adjacent to the posterior border of the supraorbital process (0); well developed and thickened, thus resulting in the displacement of the optic canal away from the posterior border of the supraorbital process (1).

48. Maxillary infraorbital plate (sensu Marx, Lambert & Uhen, 2016): absent (0); present (1).

49. Maxillary window (sensu Marx, Lambert & Uhen, 2016) originating from posterior border of infraorbital plate: absent (0); present (1).

50. Anteromedial corner of supraorbital process extending to a point medial to antorbital notch: absent (0); present (1).

51. Preorbital region of frontal in lateral view: thickened compared to more central portions of the orbit (0); dorsoventrally flat (1).

52. Enlarged dorsal infraorbital foramen on ascending process of maxilla, opening into a posterodorsally directed sulcus: absent (0); present (1).

53. Premaxillary sac fossa: absent (0); present (1).

54. Premaxillary foramen: absent (0); present (1).

55. Suture between maxilla and frontal: contact between the bones is straight or maxilla overrides anteromedial corner of the frontal (0); maxilla overrides half or more of the frontal (1).

56. Lateral borders of ascending process of maxilla: lateral edges convergent with the process tapering to a point (0); lateral edges parallel or divergent posteriorly (1).

57. Triangular wedge of frontal separating ascending process of maxilla from nasal orpremaxilla: absent (0); present (1).

58. Posterior ends of ascending processes of maxillae in dorsal view: separated by either frontals or both nasals and premaxillae (0); converging towards the midline and separated by nasals only (1); contact each other medially (2).

59. Relative position of posteriormost edge of ascending process of maxilla in dorsal view: approximately in transverse line with, or posterior to, posterior edge of nasal (0); anterior to posterior edge of nasal (1).

60. Shape of posterior border of ascending process of maxilla: pointed or rounded (0); squared off (1).

61. Lateral profile of cranium along exposure of parietals on vertex: dorsal edge of parietal ascends steeply towards posterior edge of skull at an angle of 10 degrees or more, measured relative to the lateral edge of rostrum (0); dorsal edge of parietal is low to flat with an angle of less than 10 degrees (1).

62. Length of nasal relative to bizygomatic width: less than 50% of bizygomatic width (0); more than 50% of bizygomatic width (1).

63. Lateral margins of nasal: parallel (0); posteriorly convergent (1).

64. Anterior margins of nasals: roughly straight or U-shaped (0); form a distinct, posteriorly pointing W-shape (1); with point on midline and a gap on each side between premaxilla and nasal (2);

65. Dorsal surface of nasals: flattened (0); developed into a sagittal keel (1).

66. Separation of posterior portions of nasals along sagittal plane by narial process of frontal: present (0); absent (1).

67. Zygomatic process of squamosal and exoccipital in dorsal view: clearly separated by an angle (0); posterior border of zygomatic process and lateral edge of exoccipital are confluent, forming a continuous or nearly continuous lateral skull border (1).

68. Orbitotemporal crest: positioned along posterior border of supraorbital process, with the origin of the temporal muscle facing posteriorly or posteroventrally (0); absent or positioned on the dorsal surface of the supraorbital process, with the origin of the temporal muscle facing posterodorsally or dorsally (1).

69. Area enclosed by orbitotemporal crest on supraorbital process of frontal: forms less than half of the dorsal surface of the supraorbital process (0); covers half or more of the dorsal surface of the supraorbital process (1).

70. Outline and orientation of orbitotemporal crest: subparallel to posterior border of supraorbital process (0); distal half oriented distinctly posterolaterally and approaching the posterolateral corner of the supraorbital process (1); as state 1, but with the crest terminating halfway along the posterior border of the supraorbital process (2); as state 2, but with the crest being distinctly U-shaped (3).

71. Shape of temporal fossa: longer anteroposteriorly than wide transversely, or as wide as long (0); wider than long (1).

72. Intertemporal constriction: longer anteroposteriorly than wide transversely (0); as state 1, but with the temporal fossa forming a large parasagittal oval (1); wider transversely than long anteroposteriorly (2).

73. Exposure of frontal on skull vertex: broadly exposed (0); anteroposteriorly compressed or absent (1).

74. Parietal and interparietal: anteriormost point located no further forward than postorbital process (0); anteriormost point in line with supraorbital process (1).

75. Outline of fronto-parietal suture: straight or lobate (0); frontals projects posteriorly along the sagittal plane and separate the left and right parietal anteriorly (1); highly irregular (2).

76. Parietal in lateral view: as long or longer anteroposteriorly than high dorsoventrally (0); higher dorsoventrally than long anteroposteriorly (1).

77. Spreading of anterolateral portion of parietal on to posteromedial corner of supraorbital process of frontal: absent (0); present (1).

78. Anteriormost point of parietal and interparietal: more posterior than the posterior border of the ascending process of the maxilla (0); more anterior than or in line with the posterior border of the ascending process of the maxilla (1).

79. Anteriormost point of supraoccipital in dorsal view: located posterior to or in line with the anterior border of the squamosal fossa (0); in line with temporal fossa, but posterior to the apex of the zygomatic process of the squamosal (1); in line with or located anterior to the level of the apex of the zygomatic process of the squamosal (2); in line with the anterior half or anterior edge of the supraorbital process (3).

80. Anteroposterior position of posterior apex of nuchal crest: posterior to the occipital condyle (0); anterior to or in line with the posteriormost point of the occipital condyle (1).

81. Mediolateral position of posterior apex of nuchal crest: aligned with the medial half or halfway point of the temporal fossa (0); approaching the level of the lateral border of the temporal fossa (1).

82. Distinct tubercle at junction of parieto-squamosal suture and supraoccipital: absent (0); present (1).

83. Exposure of alisphenoid within or at ventral border of temporal fossa: exposed on temporal wall of skull and contributing to orbital fissure (0); alisphenoid separated from orbital fissure or not exposed on temporal skull wall (1).

84. Postparietal foramen located at junction of parietal and squamosal: absent (0); present (1).

85. Zygomatic process of squamosal dorsoventrally expanded in lateral view: absent (0); present, with the zygomatic process being distinctly higher dorsoventrally than wide transversely (1).

86. Orientation of zygomatic process of squamosal in dorsal view: directed anteromedially (0); directed anteriorly or slightly anterolaterally (1); directed anterolaterally (2).

87. Zygomatic process of squamosal in lateral or ventral view: tapering anteriorly (0);expanded anteriorly, thus forming a central constriction (1).

88. Twisting of zygomatic process of squamosal: absent (0); present, with the zygomatic process being partially twisted clockwise on the left and anticlockwise on the right (1); as state 1, but with the process twisted almost 90 degrees (2).

89. Position of apex of zygomatic process of squamosal: situated entirely posterior to the postorbital process (0); closely apposed to the postorbital process, or situated ventral to the latter (1).

90. Apex of zygomatic process of squamosal deflected anteroventrally: absent (0); present (1).

91. Supramastoid crest of zygomatic process of squamosal (skull in lateral view): present (0); absent (1).

92. Size of squamosal including zygomatic and postglenoid processes: longer anteroposteriorly than high dorsoventrally, or about as high as long (0); distinctly higher than long (1).

93. Parieto-squamosal suture shaped like a crest or ridge: absent or low (0); present and distinctly elevated (1).

94. Squamosal prominence (*sensu* Fordyce & Marx, 2013): present as a projection on the crest delimiting the lateral or posterolateral edge of the squamosal fossa (0); absent (1).

95. Transverse width of squamosal lateral to exoccipital: width equal to or greater than 15% of the distance between the sagittal plane and the lateral edge of the exoccipital (0); exposed portion of squamosal is less than 15% of that distance (1).

96. Length of squamosal fossa relative to maximum transverse width of temporal fossa, as measured in a straight line from the posteriormost point of the temporal fossa to the posteriormost point of the nuchal crest: length of squamosal fossa is three quarters the width of the temporal fossa or longer (0); length of squamosal fossa is less than three quarters the width of the temporal fossa (1).

97. Squamosal cleft (*sensu* Marx, Lambert & Uhen, 2016): absent (0); present (1).

98. Squamosal crease: absent (0); present (1).

99. Paired tubercles on supraoccipital: absent (0); limited to low ridges forming the lateral edges of a medial fossa (1); present (2).

100. Lateral edge of supraoccipital in dorsal view: convex (0); straight (1); concave (2); sigmoidal (3).

101. Anterior border of supraoccipital shield: rounded or pointed (0); squared (1).

102. Overall outline of supraoccipital in dorsal view: rounded (0); triangular (1).

103. Anterior half of dorsal surface of supraoccipital: concave (0); flat or convex (1).

104. External occipital crest: absent or faint (0); restricted to anterior half of supraoccipital shield (1); present and running all the way along the supraoccipital shield (2).

105. Tip of postglenoid process in lateral view: curving anteriorly (0); pointing ventrally (1); pointing posteriorly (2).

106. Ventral edge of postglenoid process in lateral view: approximately in line with or dorsal to the ventral edge of the exoccipital (0); extending well ventral to the ventral edge of the exoccipital (1).

107. Orientation of postglenoid process in posterior view: ventrolateral (0); ventral (1); ventromedial (2).

108. Outline of postglenoid process in anterior or posterior view: parabolic (0); as state 0, but with lateral and medial edges parallel or concave (1); as state 1, but distinctly wider transversely than high dorsoventrally (2); triangular (3); trapezoidal, with a ventrally directed medial border (4).

109. Twisting of postglenoid process in ventral view: absent (0); twisted clockwise on the left side and anticlockwise on the right side so that the glenoid cavity faces anteromedially (1).

110. Position of base of postglenoid process in ventral or posterior view: in line with the lateral edge of the skull (0); shifted away medially from the lateral edge of the skull (1).

111. Medial border of postglenoid process in ventral view: confluent with more medial portion of squamosal (0); offset from remainder of squamosal by a distinct ridge (1).

112. Choanal margin of palatine in ventral view: absent (0); straight or convex (1); concave (2); forms a longitudinal notch (3).

113. Pterygoid in ventral view: partially or entirely exposed (0); palatine almost completely covers pterygoid and extends on to the hamular process (1).

114. Anteriormost point of pterygoid sinus fossa: located anterior to foramen pseudovale (0); approximately in line with anterior edge of foramen pseudovale (1); located posterior to anterior edge of foramen pseudovale (2).

115. Dorsal lamina of pterygoid: absent or restricted to anteromedial quarter of pterygoid sinus fossa (0); present and covering half or more of ventral exposure of alisphenoid within pterygoid sinus fossa (1).

116. Shape of pterygoid hamulus: finger-like (0); expanded into a dorsoventrally flattened plate flooring the pterygoid sinus fossa (1); triangular and wing-like (2); reduced in size or almost absent (3).

117. Position of pterygoid hamulus in ventral view: located directly adjacent to the sagittal plane and almost contacting each other (0); well separated from each other (1).

118. Position of foramen pseudovale: foramen located within squamosal or between squamosal and pterygoid, and opening anterolaterally or laterally (0); as state 0, but with foramen opening posteriorly (1); foramen lies within pterygoid (2).

119. Foramen pseudovale raised above more lateral portions of squamosal in ventral view: absent (0); present (1).

120. Fossa on squamosal for reception of sigmoid process of tympanic bulla: present (0); absent or poorly defined (1).

121. Base of postglenoid process in ventral view: in transverse line with or located posterior to the posterior half of the tympanic bulla (0); in transverse line with or located anterior to the anterior half of the tympanic bulla (1); in transverse line with the anteroposterior centre of the tympanic bulla (2).

122. Ventral border of sagittal part of vomer (nasals septum) in ventral view: posteriormost portion projects beyond the posterior border of the palatines and is visible in ventral view (0); completely covered by palatines (1).

123. Basioccipital crest: narrow transversely (0); wide and bulbous (1).

124. Lateral border of basioccipital crest in ventral view: straight (0); concave (1).

125. Orientation of basioccipital crests in ventral view: diverging posteriorly (0); parallel or subparallel (1).

126. Ventromedial corner of paroccipital process in posterior view: located more ventrally than the basioccipital crest (0); level with or more dorsal than the basioccipital crest (1).

127. Posteriormost point of exoccipital in dorsal view: located more anteriorly than posterior edge of occipital condyle (0); level with or posterior to posterior edge of condyle (1).

Hyoid

128. Outline of stylohyal in cross section: cylindrical (0); flattened (1).

129. Orientation of thyrohyal in dorsal or ventral view: oriented posteriorly (0); oriented laterally (1).

130. Shape of thyrohyal: cylindrical (0); flattened and wing-like (1); plate-like (2).

131. Ankylosed basihyal and thyrohyals: absent (0); present (1).

Periotic

132. Dorsal and medial elongation of pars cochlearis towards cranial cavity: absent (0); present (1); as state 1, but with only the anterior side of the pars cochlearis being elongated (2).

133. Attachment of anterior process to pars cochlearis: absent (0); present (1).

134. Anterior process of periotic in lateral view: squared off or rounded (0); triangular (1); anterior border of process is two-bladed and L-shaped (2).

135. Shape of anteroventral angle of anterior process of periotic in medial or lateral view: rounded or forms a relatively blunt angle (0); slender and tapering to a point (1).

136. Ventral edge of anterior process of periotic in medial view: at the same level or dorsal to ventral edge of pars cochlearis (0); ventral to ventral profile of pars cochlearis (1).

137. Dorsal deflection of anterodorsal corner of anterior process: absent (0); present (1).

138. Anterior process transversely compressed and blade-like: absent (0); present (1).

139. Length of anterior process of periotic: shorter than the anteroposterior length of the pars cochlearis, as measured from the anterior border of the pars cochlearis to the medial border of the fenestra rotunda (0); same length or longer than the pars cochlearis (1).

140. Anteroexternal sulcus: forms an oblique or vertical groove on lateral side of anterior process, immediately anterior to lateral tuberosity (0); absent (1).

141. Pyramidal process: absent (0); present (1).

142. Articulation of anterior process of periotic and tympanic bulla: no contact, or contact with accessory ossicle via fovea epitubaria on the anterior process of the periotic (0); accessory ossicle or homologous region on periotic fused to bulla (1).

143. Anterior bullar facet: present (0); absent (1).

144. Lateral tuberosity of anterior process: absent or relatively small and rounded (0); well developed and distinctly triangular (1); hypertrophied and blade-like (2); forms a distinct shelf (3).

145. Position of lateral tuberosity: situated posterolateral to anterior pedicle of tympanic bulla or fovea epitubaria (0); situated lateral or anterolateral to anterior pedicle of tympanic bulla or fovea epitubaria (1).

146. Body of periotic lateral to pars cochlearis hypertrophied: absent (0); present laterally and ventrally (1); present laterally only (2).

147. Mallear fossa: well excavated and possessing a clearly defined rim (0); present only as a depression with diffuse edges (1).

148. Distinct ridge delimiting insertion surface of tensor tympani on medial side of anterior process: absent (0); absent, but insertion surface distinctly excavated (1); present (2).

149. Dorsal extension of attachment area for tensor tympani on medial side of anterior process: absent or indistinct (0); present as a deeply excavated canal (1).

150. Anteromedial corner of pars cochlearis in ventral view: developed as a rounded, anteroposterior ridge (0); angular and projecting medially, resulting in a flattened ventral surface of the pars cochlearis (1); smooth and rounded (2).

151. Promontorial groove on medial side of pars cochlearis: present, but relatively shallow (0); present and deeply excavated (1); present and forming a distinct constriction, separating a smooth and rounded ventral portion of the pars cochlearis from a flattened and striated dorsal one (2); absent (3).

152. Caudal tympanic process in posteromedial view: well separated from crista parotica (=facial crest) (0); narrow separation or contact (1).

153. Posteromedial corner of pars cochlearis medial to fenestra rotunda: rounded and level with fenestra rotunda (0); inflated and projecting posteriorly beyond fenestra rotunda (1).

154. Morphology of caudal tympanic process: developed as a posteriorly extending triangular shelf (0); as state 0, but with the ventral border bulging ventrally (1); as state 0 but pointing posterodorsally (2); developed as a robust, ventrally directed projection (3); absent or poorly developed (4).

155. Anteroposterior alignment of proximal opening of facial canal, internal acoustic meatus and aperture for cochlear aqueduct: present (0); absent (1).

156. Anteroposterior alignment of aperture for cochlear aqueduct and aperture for vestibular aqueduct: absent (0); present (1).

157. Prominent septum dividing foramina for vestibular and cochlear nerves within internal acoustic meatus: present (0); absent (1).

158. Shape of aperture for cochlear aqueduct: round with sharply defined dorsal margins (0); slit-like (1).

159. Size of aperture for cochlear aqueduct: smaller than aperture for vestibular aqueduct (0); approximately the same size (1).

160. Aperture for cochlear aqueduct and fenestra rotunda: separate (0); confluent (1).

161. Superior process: present as a distinct crest forming the lateral wall of the suprameatal fossa (0); the lateral border of the suprameatal fossa is low and not clearly defined (1).

162. Suprameatal fossa hypertrophied: absent (0); present (1).

163. Development of crista transversa: depressed well below the rim of the internal acoustic meatus (0); well developed and reaching the cerebral surface of the pars cochlearis (1).

164. Hiatus Fallopii: absent or small opening located anterior or anteroventral to proximal opening of facial canal (0); as state 0, but with the hiatus Fallopii being well developed and large (1); anterior border of proximal opening of facial canal is continuous with the hiatus Fallopii and shaped like a fissure (2).

165. Size of proximal opening of facial canal: no more than half the size of the internal acoustic meatus (0); more than half the size of the internal acoustic meatus (1).

166. Squamosal flange located posterior to lateral tuberosity: absent (0); present (1).

167. Articulation surfaces on posterior processes of tympanic bulla and periotic: unfused (0); fused in adults to form compound posterior process (1).

168. Morphology of facial sulcus on distal half of compound posterior process: absent or relatively shallow sulcus with equally defined anterior and posterior borders (0); marked groove with an elevated anterior border (1); deeply incised canal (2); as state 2, but with the facial sulcus being partially or entirely floored, tubular and present along the entire ventral surface of the compound posterior process (3).

169. Position of facial sulcus on compound posterior process in ventral view: facial sulcus runs close to or along the posterior border of the compound posterior process (0); facial sulcus located centrally on the ventral surface of the compound posterior process (1).

170. Orientation of compound posterior process in ventral view, with periotic being in situ: oriented posterolaterally with respect to the longitudinal axis of the anterior process of the periotic (0); oriented at a right angle to the axis of the anterior process (1).

171. Shape of compound posterior process: cylindrical or slightly conical (0); short and stocky (1); flattened anteroposteriorly (2); forms a distinct plug (3).

172. Exposure of compound posterior process on lateral skull wall: external surface of compound posterior process is absent or poorly defined (0); external surface is present but distinct from lateral skull wall (1); lateral surface is expanded and firmly integrated into the posterior process being concave and defined by a distinct ridge separating it from the ventral surface (3).

173. Neck of compound posterior process markedly constricted: absent (0); present (1).

Tympanic bulla

174. Anterior border of bulla in dorsal or ventral view: obliquely truncated (0); squared (1); rounded (2); pointed (3).

175. Anterior portion of bulla transversely wider than posterior portion in ventral view: absent (0); present (1).

176. In situ orientation of main axes of tympanic bullae in ventral view: diverging posteriorly (0); parallel (1); diverging anteriorly (2).

177. Position of dorsal origin of lateral furrow: located along posterior two thirds of the anteroposterior length of the bulla (0); located at roughly one third of the anteroposterior length of the bulla (1).

178. Orientation of lateral furrow in lateral view: ventral (0); distinctly anteroventral (1).

179. Orientation of ventral keel of lateral lobe of bulla (*sensu* Boessenecker & Fordyce, 2015): faces ventrally (0); faces ventromedially or medially (1).

180. Anteroposterior outline of lateral lobe or main ridge of bulla: concave (0); straight or convex (1).

181 Position of involucral ridge in dorsal view: coincident with medial edge of the bulla (0); laterally retracted (1).

182. Sigmoid process deflected laterally in anterior or posterior view: absent (0); present (1); as state 1, but with the sigmoid process being nearly horizontal (2).

183. Dorsomedial corner of sigmoid process in anterior view: separated from the pedicle of the malleus (0); confluent with the pedicle of the malleus (1).

184. Ventral margin of sigmoid process in lateral view: present (0); absent, with the lateral margin of the sigmoid process turning smoothly into a sulcus on the lateral side of the bulla (1).

185. Shape of conical process in lateral view: well developed and dorsally convex (0); Reduced to a low ridge or absent (1).

186. Elliptical foramen: present (0); absent (1).

187. Medial lobe of tympanic bulla (*sensu* Boessenecker & Fordyce, 2015): present as distinct lobe and transversely wider than its lateral counterpart (0); present but subequal in width to the lateral lobe or smaller (1); absent or indistinct (2).

188. Crest connecting medial and lateral lobes of tympanic bulla in posterior view: present (0); absent (1).

189. Anteriormost point of involucral ridge: extends anteriorly to form the anteriormost point of the bulla (0); in line with or posterior to the anterior border of the bulla (1).

190. Dorsolateral surface of involucrum: divided into a low anterior and an elevated posterior portion, separated by a clearly defined step (0); forms a continuous rim (1).

191. Transverse creases on dorsal surface of involucrum: poorly developed or absent (0); well defined and deep (1).

192. Ridge on inside of bulla: extends laterally from involucrum and partially divides cavum tympani into anterior and posterior portions (0); absent (1).

193. Development of tympanic sulcus: developed as a faint line (0); forms a distinct crest or sulcus (1).

194. Outline and position of tympanic sulcus: forms a semicircular and ventrally curved line well separated from the intersection of the conical and sigmoid processes (0); forms a roughly horizontal line at or close to the level of the intersection of the conical and sigmoid processes (1).

195. Anteromedial portion of ventral surface of tympanic bulla: transversely convex (0); distinctly flattened or slightly concave (1).

196. Anterolateral corner of bulla: broadly rounded (0); inflated and forming a distinct lobe (1); flattened (2).

197. Anterolateral ridge or shelf: absent (0); present (1).

198. Position of posterior pedicle of tympanic bulla in dorsal view: situated at or near the posterior border of the bulla (0); located far anterior to the posterior end of the bulla (1).

Mandible

199. Posterior mandibular cheek teeth: oriented vertically or anteriorly (0); reclined posteriorly (1).

200. Medial surface of central part of mandible: similar to lateral surface (0); distinctly flattened relative to lateral surface (1).

201. Dorsomedial surface of posterior portion of mandibular body: flat or convex (0); distinctly excavated (1).

202. Mandibular symphysis: sutured or fused (0); unfused (1).

203. Outline of posterior portion of mandible in dorsal or ventral view: follows a straight line or simple curve (0); sigmoidal owing to a laterally reflexed neck and condyle (1).

204. Mandibular body in dorsal view: bowed medially (0); straight (1); bowed laterally, but with curvature mainly confined to anterior portion of mandible (2); evenly bowed laterally (3).

205. Anterior extremity of mandible: vertical or slightly twisted, with the ventral edge shifted medially (0); apex of mandible shifted to an almost horizontal position (1).

206. Mandibular body in medial or lateral view: height of ramus remains roughly constant throughout (0); arched dorsally (1); increases in height anteroposteriorly (2); dorsoventrally constricted near the centre (3); decreasing in height anteroposteriorly, with the anteriormost portion being distinctly expanded (4).

207. Height of mandibular foramen: dorsoventral height approximately that of the horizontal ramus, thus forming a mandibular fossa (0); dorsoventral height about half that of the horizontal ramus or less (1).

208. Anterior border of mandibular foramen: rounded (0); sharply triangular (1).

209. Dorsal border of mandibular foramen projected medially and developed into a roof: absent (0); present (1).

210. Satellite process (*sensu* Bisconti & Varola 2006): absent or limited to a low rugosity (0); present (1).

211. Relative position of anterior border of mandibular foramen: in line with coronoid process (0); posterior to coronoid process (1).

212. Subcondylar furrow (*sensu* Kimura, 2002): absent or extremely shallow (0); present as a well-defined groove medially only (1); as state 1, but with the dorsal border of the furrow being accentuated by a medially well-developed condyle (2); extends across the posterior surface of the condyle, separating it from the angular process both medially and laterally (3).

213. Coronoid process in lateral or medial view: forms a broad plate (0); distinctly triangular (1); shaped like a finger and pointing posteriorly (2).

214. Shape of coronoid process (if triangular) in lateral or medial view: sharply triangular and about as high dorsoventrally as long anteroposteriorly (0); bluntly triangular and considerably longer than high (1).

215. Anterior outline of coronoid process: vertical (0); bent laterally (1).

216. Postcoronoid elevation (*sensu* Struthers, 1889): absent (0); present (1).

217. Development of angular process in medial view: hollowed out (0); robust (1).

218. Anteroposterior position of angular process: located below the condyle, or slightly anterior (0); projects posteriorly beyond the condyle (1).

219. Angular process deflected ventrally: absent (0); present (1).

220. Fossa on medial side of angular process: absent (0); present (1).

221. Orientation of articular surface of mandibular condyle: posterior (0); posterodorsal (1); dorsal, with the condyle being confluent with a dorsoventrally expanded angular process (2); dorsal, with the condyle being larger than and clearly offset from the angular process (3).

222. Sulcus for attachment of mylohyoid muscle on ventromedial surface of mandible: absent (0); present (1).

Vertebral column

223. Height of transverse process of atlas at base: more than half the height of the articular surface (0); equal to half the height of the articular surface or less (1).

224. Foramen transversarium in axis: absent (0); present (1).

225. Development of parapophysis and diapophysis on axis in anterior or posterior view: parapophysis considerably more robust than diapophysis (0); parapophysis and diapophysis are similar in size (1).

226. Cervical vertebrae: separate (0); only axis and 3rd cervical vertebra fused (1); more than three vertebrae fused (2); completely fused (3).

227. Parapophysis on seventh cervical vertebra: present (0); absent (1).

228. Centra of cervical vertebrae in anterior or posterior view: rounded (0); squared (1).

229. Orientation of transverse processes of anterior lumbar vertebrae in anterior or posterior view: oriented distinctly ventrolaterally (0); oriented slightly ventrolaterally or subhorizontally (1); oriented laterally and horizontally (2).

230. Apices of neural spines of posterior thoracic and anterior lumbar vertebrae anteroposteriorly expanded and squared off: absent (0); present (1).

231. Number of lumbar vertebrae: more than 12 (0); 10 to 12 (1); fewer than 10 (2).

232. Metapophyses on posterior thoracic and anterior lumbar vertebrae in lateral view: oriented dorsally (0); oriented anterodorsally or anteriorly (1).

Ribs and sternum

233. Sternum: composed of several bones (0); composed of one bone (1).

234. Posterior ribs transversely expanded: absent (0); present (1).

Forelimb

235. Proportions of scapula: anteroposterior length of scapula approximately equals or is less than its maximum dorsoventral height (0); maximum anteroposterior length clearly exceeds its maximum dorsoventral height (1).

236. Coracoid process of scapula: present (0); absent (1).

237. Acromion process of scapula: present (0); absent (1).

238. Supraspinous fossa of scapula: present (0); absent or nearly absent, with acromion process located near anterior edge of scapula (1).

239. Deltoid crest of humerus: present as a distinct crest (0); absent or reduced to a variably developed rugosity (1).

240. Humerus: longer than or roughly the same length as radius and ulna (0); distinctly shorter than radius and ulna (1).

241. Orientation of humeral head in medial or lateral view: angled (0); vertical (1).

242. Distal portion of humerus in medial or lateral view: distal epiphysis narrower than shaft (0); distal epiphysis equal to or flared compared to shaft (1).

243. Articulation facet for radius on humerus in medial or lateral view: radial and ulnar facets are subequal in size (0); radial facet is distinctly larger than ulnar facet, excluding the olecranon (1).

244. Olecranon process: present as a distinct process (0); absent (1).

245. Manus: pentadactyl (0); tetradactyl (1).

Hind limb

246. Femur: present as a relatively well-developed bone (0); absent or reduced to a barely recognizable lump with an extremely rough surface texture (1).

247. Tibia: present (0); absent (1).

Soft tissue

248. Ventral throat grooves: absent (0); present and terminate well anterior to umbilicus (1); present and extend to umbilicus (2).

249. Ventral throat pouch: absent (0); present (1).

250. Tongue: muscular (0); reduced and predominantly connective tissue (1).

251. Temporomandibular joint: synovial (0); fibrocartilagenous mass originates in the glenoid fossa and envelopes the mandibular condyle (1).

252. Longitudinal ridges on rostrum: absent or indistinct (0); single median ridge (1); three longitudinal ridges (2).

253. Dorsal fin: present as fin or dorsal hump (0); absent (1).

254. Chromosome number: 42 (0); 44 (1).

255. Callosities: absent (0); present (1)

256. Coloration; dorsal blaze: absent (0); present (1)

257. Coloration ventral blaze: absent (0) present in <50% of the population (1) present in > 50% of the population (2)

APPENDIX 4.

Modifications from the character list of Tanaka et al (2020), which was derived from Buono et al. (2017).

226. Cervical vertebrae: separate (0); only axis and 3rd cervical vertebra fused (1); more than three vertebrae fused (2); completely fused (3).

A previous state “partially fused starting from the axis (1)” is divided into two: “only axis and 3rd cervical vertebra fused (1)” and “more than three vertebrae fused (2)”.

Physeter catodon 1 to 2

Balaena mysticetus 2 to 3

Balaena ricei 2 to 3

Eubalaena australis 2 to 3

Eubalaena glacialis 2 to 3

Eubalaena japonica 2 to 3

Caperea marginata 2 to 3

APPENDIX 5.

Full figures of the analysis.

Full figure of 50% majority consensus tree of equally weighted analysis with branch length.

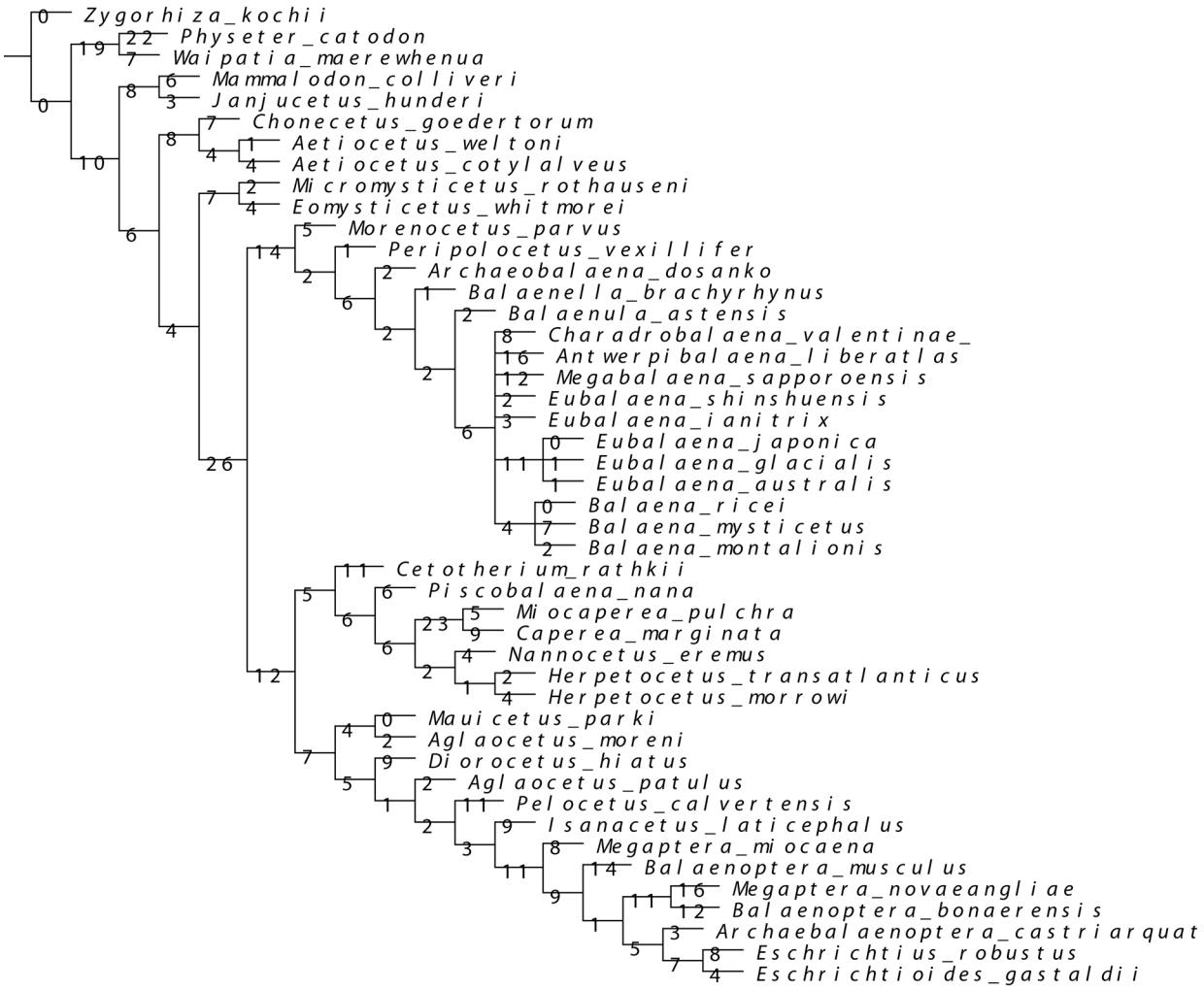

Full figure of strict consensus tree of equally weighted analysis with branch length.

Full figure of 50% majority consensus tree of implied weight analysis (K=3) with branch length.

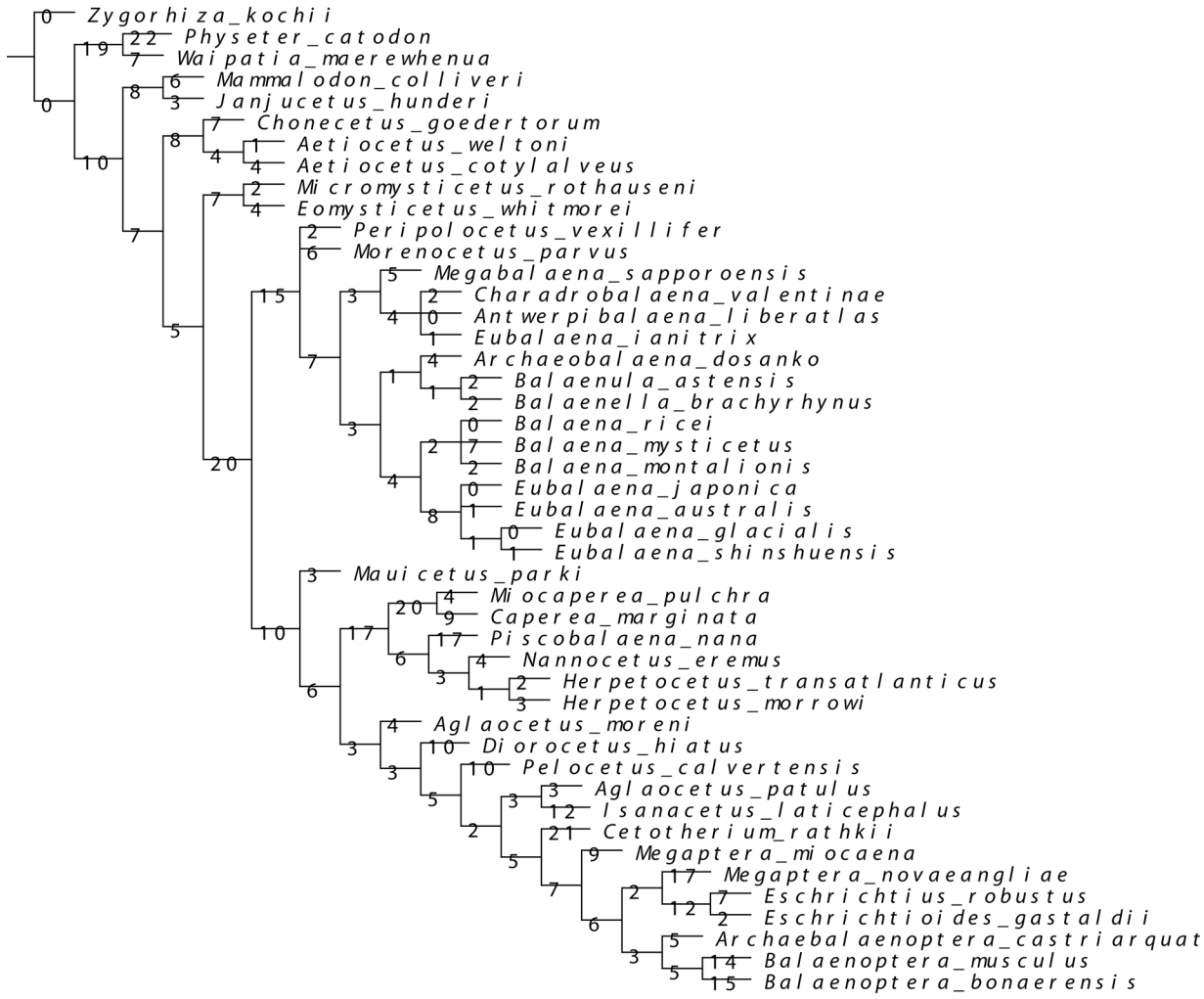

Full figure of 50% majority consensus tree of implied weight analysis (K=3) with branch length.

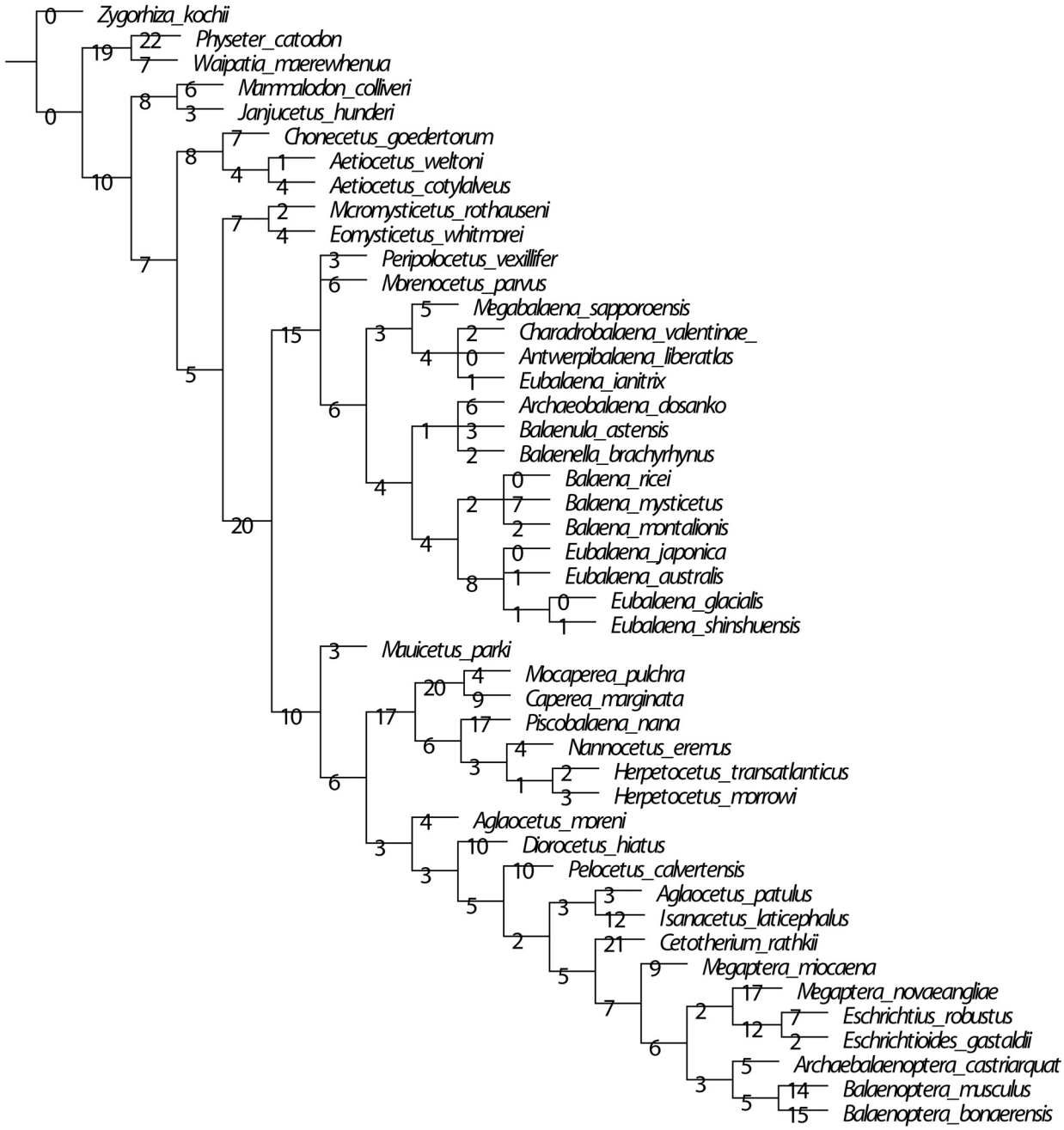

APPENDIX 6.

Tree file of 50% majority tree of equally weighted analysis.
Download file at https://palaeo-electronica.org/content/2025/5581-archaic-balaenid-from-japan)

APPENDIX 7.

Tree file of strict consensus tree of equally weighted analysis.
Download file at https://palaeo-electronica.org/content/2025/5581-archaic-balaenid-from-japan)

APPENDIX 8.

Tree file of 50% majority tree of implied weight analysis.
Download file at https://palaeo-electronica.org/content/2025/5581-archaic-balaenid-from-japan)

APPENDIX 9.

Tree file of strict consensus tree of implied weight analysis.
Download file at https://palaeo-electronica.org/content/2025/5581-archaic-balaenid-from-japan)